

AD-A189 603

CORROSION-WEAR PROCESS UNDER ROLLING-SLIDING MOTION(U)

1/2

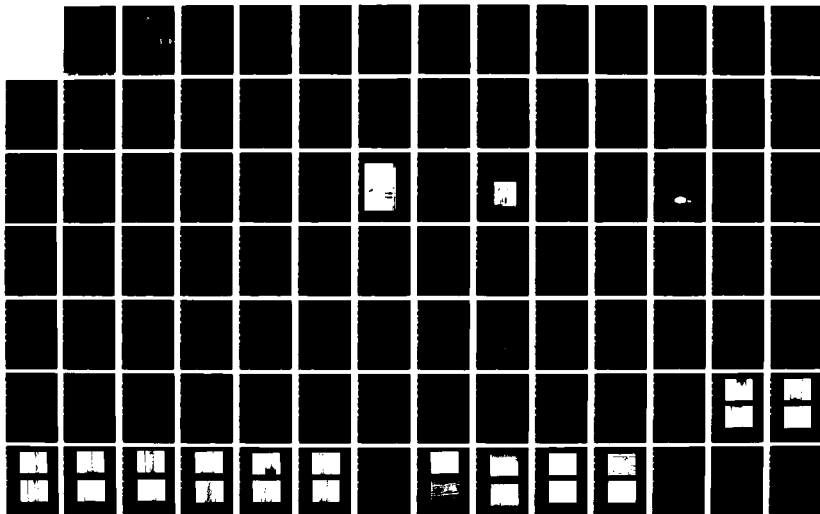
IIT RESEARCH INST CHICAGO IL 8 PANDA AUG 87

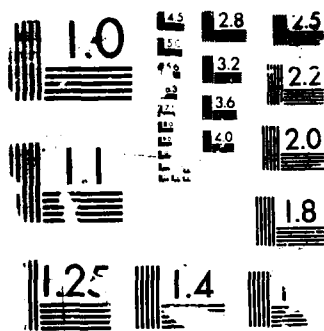
IITRI-M06140-6 NADC-87151-60 N62669-85-C-0265

UNCLASSIFIED

F/G 13/9

NL





RESOLUTION TEST CHART

DTIC FILE COPY

AD-A189 603



CORROSION-WEAR PROCESS UNDER ROLLING-SLIDING MOTION

Binayak Panda
IIT Research Institute
10 West 35th Street
Chicago, IL 60616-3799

AUGUST 1987

FINAL REPORT

NADC Contract No. N62269-85-C-0265

DTIC
ELECTE
JAN 05 1988
S D
CH

Approved for Public Release; Distribution is Unlimited

Prepared for
NAVAL AIR DEVELOPMENT CENTER
Department of the Navy
Warminster, PA 18974-5000

NOTICES

REPORT NUMBERING SYSTEM - The numbering of technical project reports issued by the Naval Air Development Center is arranged for specific identification purposes. Each number consists of the Center acronym, the calendar year in which the number was assigned, the sequence number of the report within the specific calendar year, and the official 2-digit correspondence code of the Command Office or the Functional Department responsible for the report. For example: Report No. NADC-86015-70 indicates the fifteenth Center report for the year 1986 and prepared by the Systems and Software Technology Department. The numerical codes are as follows:

CODE	OFFICE OR DEPARTMENT
00	Commander, Naval Air Development Center
01	Technical Director, Naval Air Development Center
02	Comptroller
05	Computer Department
07	Planning Assessment Resources Department
10	Anti-Submarine Warfare Systems Department
20	Tactical Air Systems Department
30	Battle Force Systems Department
40	Communication & Navigation Technology Department
50	Mission Avionics Technology Department
60	Air Vehicle & Crew Systems Technology Department
70	Systems & Software Technology Department
80	Engineering Support Group

PRODUCT ENDORSEMENT - The discussion or instructions concerning commercial products herein do not constitute an endorsement by the Government nor do they convey or imply the license or right to use such products.

REPORT DOCUMENTATION PAGE

1a. REPORT SECURITY CLASSIFICATION Unclassified			1b. RESTRICTIVE MARKINGS		
2a. SECURITY CLASSIFICATION AUTHORITY			3. DISTRIBUTION/AVAILABILITY OF REPORT Approved for public release; distribution unlimited.		
2b. DECLASSIFICATION/DOWNGRADING SCHEDULE					
4. PERFORMING ORGANIZATION REPORT NUMBER(S) IITRI-M06140-6			5. MONITORING ORGANIZATION REPORT NUMBER(S) NADC-87151-60		
6a. NAME OF PERFORMING ORGANIZATION IIT Research Institute		6b. OFFICE SYMBOL (If applicable)		7a. NAME OF MONITORING ORGANIZATION	
6c. ADDRESS (City, State, and ZIP Code) 10 West 35 Street Chicago, IL 60616-3799		7b. ADDRESS (City, State, and ZIP Code)			
8a. NAME OF FUNDING/SPONSORING ORGANIZATION Naval Air Development Center		8b. OFFICE SYMBOL (If applicable)		9. PROCUREMENT INSTRUMENT IDENTIFICATION NUMBER Contract N62269-85-C-0265	
8c. ADDRESS (City, State, and ZIP Code) Warminster, PA 18974-5000		10. SOURCE OF FUNDING NUMBERS			
		PROGRAM ELEMENT NO.		PROJECT NO.	TASK NO.
					WORK UNIT ACCESSION NO.
11. TITLE (Include Security Classification) Corrosion-Wear Process Under Rolling-Sliding Motion					
12. PERSONAL AUTHOR(S) Binayak Panda					
13a. TYPE OF REPORT Final		13b. TIME COVERED FROM 8/30/85 TO 2/28/87		14. DATE OF REPORT (Year, Month, Day) 1987 - 3 - 31	
15. PAGE COUNT					
16. SUPPLEMENTARY NOTATION					
17. COSATI CODES			18. SUBJECT TERMS (Continue on reverse if necessary and identify by block number)		
FIELD	GROUP	SUB-GROUP	Rubbing surfaces, wear, rolling and rolling-sliding motion, corrosion, electrochemical polarization, open-circuit potential, corrosion current density, friction coefficient (cont)		
19. ABSTRACT (Continue on reverse if necessary and identify by block number)					
<p>To advance the understanding of the corrosion-wear process under rolling and rolling-sliding motion, a dynamic corrosion-wear electrochemical cell was designed and constructed. This cell is capable of monitoring the electrochemical behavior under simultaneously occurring corrosion and wear processes simulating naval aircraft bearings. With this test apparatus, complete polarization diagrams were obtained for various rolling and rolling-sliding conditions along with the corrosion current density and open-circuit potential of the system.</p> <p>Even under pure rolling conditions, the effect of wear was significant in removing the passive film, as indicated by the increase in corrosion current and decrease in open-circuit potential. Increase in load and introduction of a few percent sliding generated more severe wear conditions, reflected in the results of electrochemical measurements.</p> <p>Results from the statistical analysis of the tests based on the Plackett-Burman test matrix indicated that more than one variable exerts significant influence on the electrochemical (cont)</p>					
20. DISTRIBUTION/AVAILABILITY OF ABSTRACT <input checked="" type="checkbox"/> UNCLASSIFIED/UNLIMITED <input type="checkbox"/> SAME AS RPT. <input type="checkbox"/> DTIC USERS			21. ABSTRACT SECURITY CLASSIFICATION		
22a. NAME OF RESPONSIBLE INDIVIDUAL Dr. Vinod S. Agarwala			22b. TELEPHONE (Include Area Code) (215) 441-1122		22c. OFFICE SYMBOL Code 6062

UNCLASSIFIED

SECURITY CLASSIFICATION OF THIS PAGE

18. Subject Terms (cont.)

active and passive metals, M50 steel, NaCl electrolyte; inhibitors $\text{Na}_2\text{Cr}_2\text{O}_7$, NaNO_2 , and Na_2MoO_4 .

19. ABSTRACT (cont.)

parameters. Addition of 500 ppm $\text{Na}_2\text{Cr}_2\text{O}_7$ into the electrolyte was the most significant factor statistically. A combination inhibitor consisting of 500 ppm NaNO_2 and 500 ppm $\text{Na}_2\text{Cr}_2\text{O}_7$ had the most dramatic effect in reducing corrosion in the absence of lubricating oil.

Optical microscopy and SEM evaluation of tested samples revealed many unique surface morphologies; smooth surfaces were seen under high corrosion current densities, whereas surface damage due to wear was retained under very low corrosion currents. Test conditions inducing intermediate corrosion current densities showed deposition of corrosion products on the surfaces and nucleation of pits. Nucleation of a large number of pits was observed even under a low applied load and a pure rolling motion.

UNCLASSIFIED

SECURITY CLASSIFICATION OF THIS PAGE

FOREWORD

This final report, "Corrosion-Wear Process Under Rolling-Sliding Motion," summarizes the studies conducted and the results obtained during the period 30 August 1985 to 28 February 1987, and is designated internally as Report No. IITRI-M06140-6.

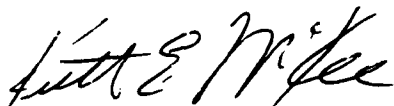
In this study, dynamic corrosion-wear equipment geared to conduct tribo-electrochemical studies under rolling and rolling-sliding motion was designed and used to study M50 bearing quality steels immersed in different electrolytes containing inhibitors and lubricants in 100 ppm NaCl solution. Of the 67 tests conducted, 24 were statistically designed and the data were statistically and phenomenologically analyzed. Optical and SEM studies were carried out, together with surface roughness measurements on the tested samples, and the findings were correlated with the electrochemical behavior.

The study indicated that it is possible to combat corrosion under rolling-sliding motion by using combination inhibitors. All the variables studied, including inhibitors and lubricant, interact in a complex manner resulting in very high and very low corrosion currents for a few combinations. While very high corrosion current resulted in smooth surfaces and very low corrosion current preserved the wear details, the combination variables resulting in intermediate corrosion currents nucleated pits. Thus recommendations were made for future investigation of the origin of these pits under the wear track.

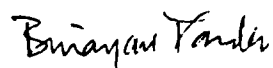


Accession For	
NTIS GRA&I	<input checked="" type="checkbox"/>
DTIC TAB	<input type="checkbox"/>
Unannounced	<input type="checkbox"/>
Justification	
By	
Distribution/	
Availability Codes	
Dist	Avail and/or Special
A-1	

We acknowledge with gratitude the support from NADC and the critical evaluation and suggestions offered by Dr. Vinod Agarwala at various stages of this program. At IITRI, technical contributions from E. Vesely and J. Moore are gratefully acknowledged.



Keith E. McKee, Director
Manufacturing Department



B. Panda
Associate Engineer



S. K. Verma, Director
Surface Engineering Center

TABLE OF CONTENTS

	<u>Page</u>
1. INTRODUCTION	1
2. PROGRAM OBJECTIVE AND TEST PARAMETERS.	3
2.1 Objective and Work Scope.	3
2.2 Test Parameters	3
3. THEORETICAL CONSIDERATIONS	4
3.1 Corroding Processes in Steel.	4
3.2 Electrolysis of NaCl Solution with Inert Electrodes	5
3.3 Important Inhibitors and Their Effects on Corrosion	6
3.4 Water-Soluble Lubricants.	7
3.5 Wear.	8
3.5.1 Types of Wear.	8
3.5.2 Sliding, Rolling, and Rolling-Sliding Motion and Their Associated Wear.	9
3.5.3 Friction During Rolling and Sliding.	10
3.5.4 Asperities and Their Interaction	13
3.6 Corrosion-Wear.	14
3.7 Previous IITRI Results on Corrosion-Wear.	16
4. TEST APPARATUS	19
4.1 Equipment Development	19
4.2 The Corrosion-Wear Test Apparatus for Rolling-Sliding Motion.	19
5. SAMPLE PREPARATION AND TEST PROCEDURES	24
5.1 Material.	24
5.2 Sample Preparation.	25
5.3 The Plackett-Burman Matrix.	26
5.4 Selection of Load	26
5.5 Selection of Inhibitors and Lubricant	28
5.6 Selection of Rolling-Sliding Ratio.	28
6. RESULTS AND DISCUSSION	30
6.1 Results with the First Group of Samples	30
6.1.1 Behavior of Open-Circuit Potential	31
6.1.2 Effect of Working Electrode Area on Polarization Behavior	36
6.1.3 Polarization Behavior Under Dynamic Corrosion-Wear Conditions	36
6.2 Results with the Second Group of Samples.	37
6.2.1 Statistically Designed Tests	37
6.2.2 Tests Under Pure Rolling Conditions.	48

TABLE OF CONTENTS (cont.)

	<u>Page</u>
6.3 Wear Loss Determined by Surface Roughness Measurements. . . .	58
6.4 Study of Wear Tracks.	65
6.4.1 Studies Under the Optical Microscope	65
6.4.2 Studies Under the Scanning Electron Microscope	65
7. CONCLUSIONS.	82
8. RECOMMENDATIONS FOR FUTURE RESEARCH.	84
References	86
Appendix: List of Variables and the Observed Open-Circuit Potential and Corrosion Current Density Values in Runs Performend . .	88

LIST OF TABLES

<u>Table</u>		<u>Page</u>
1	Capabilities of the Corrosion-Wear Test Equipment.	22
2	Sixteen-Test Statistical Design and Test Matrix.	27
3	Effect of Inhibitors and Contact Stress on the Open-Circuit Potential (OCP).	32
4	Results of Statistical Analysis for Open-Circuit Potential (OCP).	40
5	Results of Statistical Analysis for Corrosion Current Density (I_{corr}).	42
6	Effect of Load and of Sliding on the OCP and I_{corr} in the Presence of Nitrite Inhibitor.	54
7	Effect of Load and Sliding on OCP and I_{corr} in the Presence of Dichromate Inhibitor.	54
8	Effect of Load and Percent Sliding on the OCP and I_{corr} of M50 Steel in NaCl Solution in the Presence of a Lubricant.	56
9	Results of Optical Microscopy of Corroded Surfaces	66

LIST OF FIGURES

<u>Figure</u>		<u>Page</u>
1	Rolling under the action of a tangential force	11
2	Carter-Poritsky theory of driving wheel; tangential tractions, surface strains, and microslip in contact area	11
3	View of the assembled IITRI corrosion-wear test apparatus. . .	20
4	Side support device for the loading arm of the corrosion-wear test apparatus	22
5	Teflon-coated M50 sample and the loading disk.	25
6	Effect of velocity on the electrochemical behavior of a normal metal corroding with a diffusion-controlled cathodic process .	33
7	Schematic of the effects of passivating electrolyte and wear on anodic polarization of steel.	34
8	Effect of load on the polarization behavior of M50 steel in a solution containing 100 ppm NaCl and 500 ppm Na_2MoO_4	38
9	Polarization behavior of M50 steel with (run 33, trial 15 conditions in Table 2) and without (run 34, trial 16 conditions in Table 2) the addition of $\text{Na}_2\text{Cr}_2\text{O}_7$	44
10	Polarization behavior of M50 steel with (run 47, trial 12 conditions in Table 2) and without (run 37, trial 1 conditions in Table 2) the addition of $\text{Na}_2\text{Cr}_2\text{O}_7$	45
11	Polarization behavior of M50 steel with (run 41, trial 4 conditions in Table 2) and without (runs 38 and 42, trial 3 conditions in Table 2) dichromate addition	46
12	Polarization behavior of M50 steel with (run 43, trial 5 conditions in Table 2) and without (run 35, trial 10 conditions in Table 2) dichromate addition	47
13	Polarization behavior with (run 49, trial 9 conditions in Table 2) and without (run 40, trial 2 conditions in Table 2) dichromate addition.	49
14	Polarization behavior of M50 steel with (run 46, trial 11 conditions in Table 2) and without (run 45, trial 14 conditions in Table 2) dichromate addition	50

LIST OF FIGURES (cont.)

<u>Figure</u>		<u>Page</u>
15	Polarization behavior of M50 steel with (runs 50 and 51, trial 7 conditions in Table 2) and without (run 52, trial 13 conditions in Table 2) dichromate additions.	51
16	Polarization behavior of M50 steel with (run 48, trial 6 conditions in Table 2) and without (runs 53 and 54, trial 8 conditions in Table 2) dichromate additions.	52
17	Effect of load and sliding on the polarization behavior of M50 steel under pure rolling and rolling-sliding motion in electrolyte containing 100 ppm NaCl and 500 ppm NaNO ₂	53
18	Effect of load on the polarizaition behavior under rolling motion in electrolyte containing 100 ppm NaCl adn 500 ppm Na ₂ Cr ₂ O ₇	55
19	Effect of load and sliding on the polarization behavior under rolling and rolling-sliding motion in electrolyte containing 100 ppm NaCl and 10% lubricant	57
20	Difference between the surface profiles of the region around the wear track prior to and after the corrosion-wear tests . .	59
21	Difference between the surface profiles of the region around the wear track prior to and after the corrosion-wear test. . .	62
22	Appearance of the wear track when sample was tested under the trial 1 conditions in Table 2.	68
23	Appearance of the wear track when sample was tested under the trial 2 conditions in Table 2.	68
24	Appearnace of the wear track when sample was tested under the trial 3 conditions in Table 2.	69
25	Appearance of the wear track when sample was tested under the trial 4 conditions in Table 2.	69
26	Appearance of the wear track when sample was tested under the trial 5 conditions in Table 2.	70
27	Appearance of the wear track when sample was tested under the trial 6 conditions in Table 2.	70

LIST OF FIGURES (cont.)

<u>Figure</u>		<u>Page</u>
28	Appearance of the wear track when sample was tested under the trial 7 conditions in Table 2.	71
29	Appearance of the wear track when sample was tested under the trial 8 conditions in Table 2.	71
30	Appearance of the wear track when sample was tested under the trial 9 conditions in Table 2.	72
31	Appearance of the wear track when sample was tested under the trial 10 conditions in Table 2	72
32	Appearance of the wear track when sample was tested under the trial 11 conditions in Table 2	73
33	Appearance of the wear track when sample was tested under the trial 12 conditions in Table 2	73
34	Appearance of the wear track when sample was tested under the trial 13 conditions in Table 2	74
35	Surface appearance when sample was tested under the trial 14 conditions in Table 2.	74
36	Surface appearance when sample was tested under the trial 15 conditions in Table 2.	75
37	Surface appearance when sample was tested under the trial 16 conditions in Table 2 with no inhibitor in electrolyte	75
38	Surface morphology away from the wear track for a sample tested under corrosion-wear conditions of trial 10 in Table 2.	77
39	Sample surface when the sample was tested under the trial 3 conditions in Table 2.	77
40	Wear pattern of M50 steel under rolling-sliding conditions . .	78
41	Features on the wear track of a sample tested under the trial 14 conditions in Table 2	78
42	Features of area away from the wear track.	79

LIST OF FIGURES (cont.)

<u>Figure</u>		<u>Page</u>
43	Asperity contact areas, which are the sliding marks, and some evidence of metal dissolution on sample tested under trial 6 conditions in Table 2.	79
44	Sliding marks at an angle to the rolling direciton on sample tested under trial 4 conditions in Table 2	80
45	Sample from run 59, showing an array of pits generated along the line of contact.	80

1. INTRODUCTION

The corrosion-wear process is defined as material loss by simultaneous occurrence of wear and corrosion. The Navy's demand for corrosion-wear study accrued from the numerous aircraft bearing failures suspected to have arisen from localized corrosion caused by exposure to marine environment.

When corrosion and wear occur separately, they are overcome by a materials engineering approach. For corrosion resistance, the common ferrous engineering materials are alloyed with chromium, which forms a protective chromium-rich oxide; and for wear resistance, heavy-duty bearing steels are alloyed with carbon and some elements forming hard carbides resisting abrasion. But when the corrosion and wear occur simultaneously, the alloying approach described above is not adequate due to the affinity of chromium for carbon to form chromium carbide. Chromium carbide formation depletes the matrix of both chromium and carbon, accelerating both corrosion and wear. Approaches other than the replacement of material, therefore, must be pursued to combat the corrosion of bearings. Study of the corrosion-wear process provides an ideal tool to evolve a possible solution to the bearing problem.

At IITRI under the sponsorship of NADC, the corrosion-wear process was previously studied in two phases using a pin and a disk electrode under sliding contact with full rotational and oscillatory motion. During the first phase of this work, various electrochemical and tribological factors were examined to understand the basic aspects of the corrosion-wear process as well as its control using lubricants and inhibitors. The second phase of the program involved similar investigations, with oscillating motion between the rubbing members to simulate the relative motion between the ball and the racer of Navy aircraft on a ship deck. During this work, various electrochemical (corrosion potential, corrosion current, and polarization behavior) and tribological (coefficient of friction, wear loss) factors were studied to clarify the underlying principles of corrosion-wear.

The present work was initiated based on the understanding generated by these previous IITRI efforts. A triboelectrochemical apparatus designed for

this study incorporated the rolling-sliding type wear as encountered in actual bearings. The effects of rolling-sliding wear on the open-circuit potential, corrosion current density, wear loss, changes in surface morphology, and artifacts were studied in terms of variables such as load, percent sliding, and the use of various inhibitors and lubricant. A set of statistically designed corrosion-wear tests based on a Plackett-Burman matrix was performed to demonstrate the significance and effectiveness of these variables. Results of these efforts are given in this report.

2. PROGRAM OBJECTIVE AND TEST PARAMETERS

2.1 OBJECTIVE AND WORK SCOPE

The main objective of this program was to determine, by an electrochemical polarization technique, the major roles of inhibitors, lubricants, load, sliding, and material properties on corrosion-wear of bearing materials in corrosive electrolytes (seawater environment) using laboratory simulation of rolling-sliding motion. The understanding developed under pure sliding conditions¹⁻² was reassessed under these more realistically simulated rolling-sliding conditions. This study pointed out the direction of corrective efforts that may be taken to significantly reduce the major problems now experienced in Navy aircraft bearing systems.

The work scope was divided into two tasks:

- Task I: Equipment modifications to incorporate rolling-sliding motion
- Task II: Electrochemical studies involving inhibitors and lubricants, analysis of results, and recommendations.

2.2 TEST PARAMETERS

To accomplish the above objectives, the selected test parameters and their ranges for corrosion-wear study under rolling-sliding motion were as follows:

- | | |
|-------------------|--|
| 1. Materials | M50 steel, hardened and tempered |
| 2. Electrolyte | 100 ppm NaCl solution in water |
| 3. Inhibitors | $\text{Na}_2\text{Cr}_2\text{O}_7$, NaNO_2 , and Na_2MoO_4 |
| 4. Sliding | -2.19% and -4.38% |
| 5. Load on sample | 4 lb and 40 lb |
| 6. Shaft rotation | 30 rpm |
| 7. Environment | ambient |
| 8. Lubricant | White Kut 210* (water-soluble lubricant) 0 and 10%. |

*White Kut 210 - trade name by Metal Fluid Products, 7540 N. Linden Avenue, Skokie, Illinois 60076.

3. THEORETICAL CONSIDERATIONS

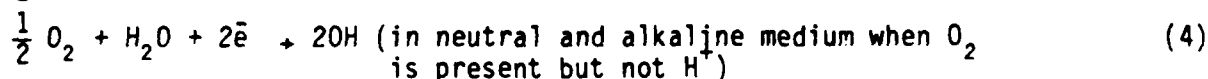
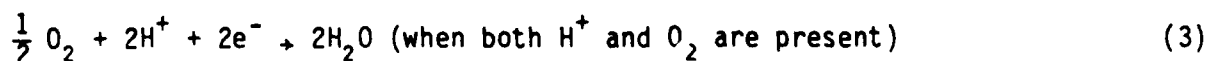
Corrosion-wear is a process occurring between two contacting surfaces exposed to a corroding electrolyte. To understand corrosion-wear, both the simultaneously occurring corrosion and wear processes must be studied. The following paragraphs present various theoretical aspects of corrosion and wear which are pertinent to the corrosion-wear situation.

3.1 CORRODING PROCESSES IN STEEL

When a ferrous-base material is exposed to an aqueous electrolyte, many chemical reactions occur at the metal/electrolyte interface. For corrosion to take place, the anodic and the cathodic processes must occur simultaneously. The dominant anodic reaction is considered to be the one in which iron goes into solution by the reaction:



The electrons generated by the anodic reaction are consumed by as many as all three following cathodic reactions, one of which strongly dominates the others in a specific corroding media:



In a corroding system, the sum total of anodic and cathodic currents remains equal. Thus, at the corrosion potential for a single dominating anodic reaction yielding a net current I_{corr} we can write:

$$I_{\text{corr}} = I_{\text{c}_1}^* + I_{\text{c}_2}^* + I_{\text{c}_3}^* \quad (5)$$

when $I_{\text{c}_i}^*$ is the current associated with the i^{th} cathodic reaction. Under an applied potential, E , the net current I is given by the difference between the total anodic and cathodic currents:

$$I = \pm [I_a - (I_{c1} + I_{c2} + I_{c3})] \quad (6)$$

The rates of both anodic and cathodic reactions follow Tafel behavior, i.e.:

$$E = a + b \log i \quad (7)$$

where E is the electrode potential of the specimen, i is the current density of the electrochemical reaction, and a and b are constants. If E_{corr} represents corrosion potential for which I_{corr} is the corrosion current, then

$$E - E_{\text{corr}} = b \log \frac{I_a}{I_{\text{corr}}} \text{ or } \frac{I_a}{I_{\text{corr}}} = \exp \frac{2.3 (E - E_{\text{corr}})}{b} \quad (8)$$

Since equation 8 is valid for both anodic and cathodic reactions, the net current which is the difference between the anodic and the cathodic currents is given by:³

$$\frac{I}{I_{\text{corr}}} = \pm \left[\exp \frac{2.3 (E - E_{\text{corr}})}{0.0592} - \exp \frac{2.3 (E - E_{\text{corr}})}{-0.1183} \right] \quad (9)$$

When $E - E_{\text{corr}}$ is positive, the left-hand side of the equation dominates; when it is negative, the right-hand side of the equation dominates. Equation 9 is the theoretical foundation for the polarization curves, and governs the Tafel slope often employed for corrosion current calculations.

3.2 ELECTROLYSIS OF NaCl SOLUTION WITH INERT ELECTRODES

Pure water containing dilute electrolytes like NaCl is expected to dissociate to oxygen (at the anode) and hydrogen (at the cathode) when inert electrodes like platinum or graphite are used for electrolysis. The literature indicates that the anodic products are chlorine and oxygen when NaCl concentration is high. Stove and Phillips⁴ give the limits as >12% NaCl for Cl_2 and <6% for O_2 evolution; a mixture of Cl_2 and O_2 forms at intermediate concentration. With carbon electrodes, 50% of the O_2 expected at the anode appears as CO_2 .

The electrode potential for the evolution of oxygen and hydrogen depends on the pH of the solution according to the well-known reactions for water stability. Stirring also plays an important role because, according to

Edwards⁵ and Potter,⁶ the electrolysis of neutral NaCl solution produces no oxygen even when very dilute if it is not stirred; but if the alkaline catholyte reaches the anode region, chlorate, chloride, and oxygen can be produced.

During this program, the electrode potential range for scanning was carefully selected to minimize the dissociation of water.

3.3 IMPORTANT INHIBITORS AND THEIR EFFECTS ON CORROSION

Inhibitors added to the electrolyte prevent or decelerate the corrosion process described earlier. Since both the anodic and the cathodic processes are involved in corrosion, the inhibitors--depending on whether they inhibit the anodic or the cathodic processes--are categorized as anodic or cathodic inhibitors. The anodic inhibitors are more effective and hence are popular. Although many compounds act as anodic inhibitors, the important ones are the nitrites, chromates, dichromates, phosphates, molybdates, and tungstates of sodium and potassium.

Inhibitors such as nitrites, dichromates, and molybdates deter corrosion by the passivation process. In this process a thin adherent coating forms on the metal surface, especially in the microscopic areas dissolving anodically, and hinders the process of oxygen diffusion to the corroding surface. The effectiveness of the inhibitors depends on their concentration and the pH of the solution. For sodium dichromate and molybdate a minimum concentration of 500 ppm is generally considered essential for adequate corrosion prevention, whereas for sodium nitrite 300 ppm is usually enough for severe corrosive environments (500 ppm NaCl solution).

The mechanism by which sodium nitrite functions as an inhibitor is not a subject of complete agreement. Rozenfeld⁷ considers it an anodic inhibitor. Putilova et al.⁸ believe that the inhibition is a result of oxidation of corrosion products (like ferrous or cuprous) to higher salts by nitrite ions, which are deposited on the metal surface and cause a rise in electrode potential. According to Wachter and Smith,⁹ the nitrite functions as an oxidizing agent to produce a thin and tenacious iron oxide film on anodic areas. Cohen¹⁰ suggests the most widely accepted theory that the passive film is $\gamma\text{-Fe}_2\text{O}_3$ with a small amount of $\gamma\text{-Fe}_2\text{O}_3 \cdot \text{H}_2\text{O}$ and the oxide film is formed by

the reaction of nitrite and oxygen with the metal at the liquid/metal interface, with the adsorption of inhibitor as a probable intermediate step.

Chromates (dichromates) and molybdates work in a similar manner, using their strong oxidizing ability. Chromates and molybdates, therefore (and perhaps other oxidizing substances like permanganates), should all be equally effective in corrosion prevention. But performance-wise, chromates are superior to molybdates and others. Thus, the oxidizing theory suggesting rapid oxidation of ferrous to ferric oxide at the metal surface must be supplemented by a secondary mechanism to account for the superiority of the chromates (and dichromates). Cohen and Beck¹¹ propose the following mechanism: Iron corrodes to form ferrous hydroxide. The ferrous ion is then oxidized to a ferric oxide film on the surface by oxygen in the system. The presence of chromate ions helps this oxidation, leaving behind some chromate ions on the oxide skin (as some investigators have indeed found). If the sample has already formed a protective iron oxide film as by preexposure, the function of chromate is to repair the worn places on this film and strengthen and thicken it with ferric and chromic oxide mixtures. An adsorption theory of protection is suggested by Kingsbury.¹² He postulates that a layer of chromate ion is first adsorbed on the metal surface which obstructs the electrode process and at the same time provides a reservoir for oxygen atoms, resulting in superior passivation by the chromate inhibitors.

3.4 WATER-SOLUBLE LUBRICANTS

As mentioned earlier, inhibitors in most cases provide a passive film on the corroding surface. Under wear conditions, when the surfaces rub against each other, the tenacity of these films is questionable. Nevertheless, a fair assumption is that the use of some kind of lubricant can protect the passive film from wear.

While many lubricants are feasible for the protection of the passive films, only the effects of the water-soluble lubricants can be studied in an aqueous electrolytic medium. This is due to the fact that the water-soluble lubricant disintegrates in an aqueous medium to very fine droplets of oil. These oil droplets adhere to the wear-prone surface and protect it. Because of the dispersion of oil, the normal electrolytic processes could take place

together with the diffusion of oxygen from the atmosphere. Needless to say, all water-soluble oils contain additives; thus, selection of these oils should include the ones with a minimum amount of additives.

Corrosion-wear was studied using White Kut 210 soluble oil. This oil, being a general-purpose one, did not contain heavy duty additives like sulfur and chlorine. It did, however, contain sodium sulfonate (13.57%), which served as an emulsifier. No other corrosion inhibitor was present in this oil.

3.5 WEAR

Wear may be defined as the removal of material from solid surfaces as a result of mechanical action. Characteristic of the wear process, the amount of material removed is quite small and the cause is often the rubbing of two surfaces.

3.5.1 Types of Wear

Material can be displaced in three ways from the rubbing surfaces that are inert to their environments. Depending on this mode, the wear is termed as adhesive, abrasive, or surface fatigue.

Adhesive wear is characterized by the interaction of the asperities, causing metal to be transferred from one surface to another, a particularly severe form being known as scuffing. When the localized temperature due to contact exceeds a critical value, adhesive wear takes place.

Abrasive wear may be defined as the damage to a surface by a harder material. This hard material may have been introduced between two rubbing surfaces from outside, or it may be formed in situ by oxidation and other chemical processes, or it may be the material forming the second surface.

Surface fatigue takes place on smooth surfaces wherein the material flakes off due to crack initiation by fatigue stresses. Ball and roller bearings are often subjected to this kind of failure.

3.5.2 Sliding, Rolling, and Rolling-Sliding Motion and Their Associated Wear

3.5.2.1 Sliding Motion.

Sliding, as the name would suggest, describes the relative motion between two bodies in contact with each other in which the contact area corresponding to one of the bodies does not change. The process leads to wear of both the contacting surfaces.

In general, sliding motion gives abrasive type wear. Although no abrasives may be present, the asperities of the two contacting surfaces abrade each other. Thus, it is expected that the material loss due to sliding motion will obey the abrasive-wear laws. The dependence of abrasive wear on distance of sliding (or time) is rather complex. In situations where abrasion always takes place with fresh abrasive paper or fresh abrasive particles, the wear continues at a steady rate.

When the sliding system contains a limited amount of abrasive, however, which is used over and over again as the sliding continues, the wear rate tends to drop off. Mulhearn and Samuels¹³ studied the wear rate of steel as a function of time when steel is abraded on SiC abrasive paper and found that their data fit the form:

$$V = V_{\infty} (1 - e^{-gL}) \quad (10)$$

where V_{∞} is the total volume of metal removed abrasively when the sliding is continued indefinitely and g is a constant. V is the volume of metal removed, and L is the length of the wear path. From the above equation, it is clear that dV/dL or the wear rate approaches zero as L approaches infinity.

Mulhearn and Samuels¹³ explained the eventual dropping off in wear rate as due to blunting of abrasive particles. It could also occur by clogging of the abrasive paper by wear debris. While equation 10 predicts almost zero wear after a very long time, other wear processes may be responsible for material removal. To determine if other material removal processes are active, the weight loss (ΔW) and wear time (t) can be related through an equation:²

$$\Delta W = kt^n \quad (11)$$

$$\text{or, } \log \Delta W = n \log t + \log k$$

where k and n are constants. For abrasive wear, when the wear rate decreases with time, n is less than 1. When other material removal processes are active in addition to abrasive wear, n is greater than 1.

3.5.2.2 Rolling Motion.

Rolling motion is associated with the revolution of one object along another surface. If both surfaces are smooth and the rolling object is a sphere or a cylinder, the material loss is minimal.

Friction and wear loss during rolling has been a subject of extensive study due to the engineering importance of ball and roller bearings. The region of contact between two smooth surfaces depends on the load contact geometry and the elasticity of the material. Similarly, the stress near the contact areas depends on these variables.

During rolling, the region of contact experiences not only fatigue stresses but also some degree of sliding within the contact area. A solution to the two-dimensional contact problem of rolling cylinders was first presented by Carter¹⁴ and discussed in more detail by Poritsky¹⁵ in connection with the action of a locomotive driving wheel. This situation has been presented in Figure 1. The results of their analysis, as presented by Johnson¹⁶ are shown in Figure 2, which gives the slip and lock-in regions under static and dynamic conditions.

In the case of rolling-sliding, the sliding severity is between those of rolling and sliding. In the case of ball and roller bearings, the percent sliding depends on the type of bearing and loading conditions and could go as high as 5%.

3.5.3 Friction During Rolling and Sliding

For bearings, the frictional losses are very important since they are responsible for heat evolution and energy loss. Coefficient of friction is generally expressed as:

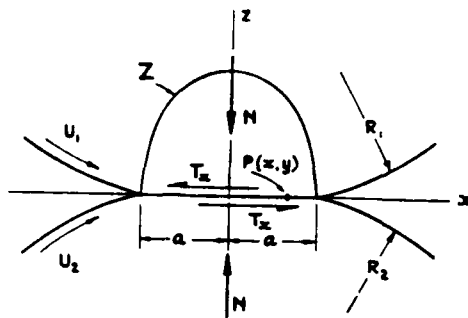


Figure 1. Rolling under the action of a tangential force.¹⁶

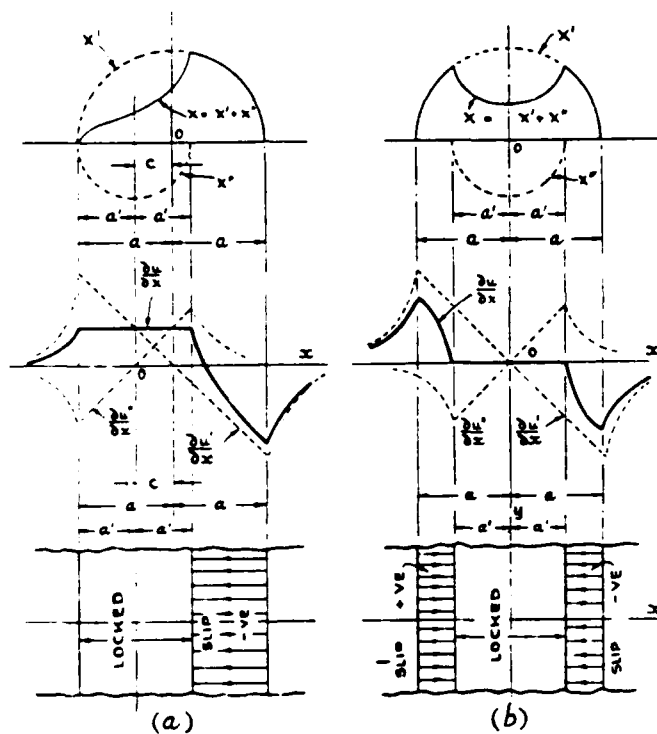


Figure 2. Carter-Poritsky theory of driving wheel; tangential tractions, surface strains, and micro-slip in contact area. (a) Rolling contact and (b) static contact.¹⁵

$$f = F/P \quad (12)$$

where F is the friction resistance (force) and P is the total load over the sliding surface. This quantitative law is generally obeyed; however, exceptions are found with very hard materials like diamond and very soft materials like Teflon. In many such cases the law can be modified to $F = fP^m$ where m varies between $2/3$ and 1 .

The coefficient of friction, and hence the frictional loss, is dependent on the temperature and surface properties. In fact, Spurr¹⁷ proposes a relationship: $f = (\sigma_y/H) \cot \psi$ where σ_y is the yield strength, H is the Meyer's hardness, and $\cot \psi$ is the parameter describing the condition of the surface. Later on, he¹⁸ defined $\cot \psi$ using measurable parameters. Most experiments that he did, however, involved metallic materials with some plasticity. He also¹⁷ correlated the coefficient of friction under static and dynamic conditions with the difference in mechanical properties.

Use of oxides as lubricants has drawn considerable interest in the metalworking industry. Accordingly, many experiments have been conducted to study the frictional properties of oxides at elevated temperature. Hot extrusion¹⁹ and forging tests²⁰ have shown that oxide formed on copper in air at 800°C gives low frictional losses during the metal deformation at that temperature. On the other hand, the oxide formed on 70/30 brass (predominantly ZnO) gives high friction. When both ZnO and CuO were applied in the form of powders, however, they were very effective lubricants during a hot-forging operation.²¹ Other experiments have shown that infusible oxides like CaO and slate can be used effectively as lubricants for hot extrusion tests.²² Hinsley and co-workers²³ studied the frictional properties of many metal oxides at higher temperatures and concluded that the friction could be reduced if a friable oxide was formed.

In summary, one can conclude that the frictional loss between two rubbing surfaces depends not only on the hardness (yield strength) of the material and the surface characteristics but also on the nature and mechanical properties of the oxides present between the two surfaces. It also depends on whether a static or a dynamic condition prevails.

3.5.4 Asperities and Their Interaction²⁴

Asperities on surfaces lead to so-called "surface roughness." The interaction of surfaces is very important in friction and wear during rolling and sliding motion.

If these asperities can be assumed as waves on the metal surfaces, the measure of the surface roughness could be the centerline average (CLA) or the root-mean-square (rms) values of these asperities. Although the CLA and rms values are important for various machined products, other details of asperities like mean tip radius, mean slope of asperities, and bearing area curves are significant in wear studies. The surface profile can usually be described by a Gaussian distribution of coordinates. Thus, the rms value of the surface roughness assumes a very important role.

When a hypothetically smooth surface is forced against a randomly distributed profile, a separation of 3σ (where σ is standard deviation) will produce an interaction of only 1% of the profile. For moderate intensity of loading, a ratio between the real area and the apparent area of contact (η) takes the form

$$\eta = b\epsilon^\nu \quad (13)$$

where ϵ is the relative penetration equal to the actual approach of surfaces under pressure divided by the maximum asperity heights, b is a constant depending on material and surface characteristics, and ν is a constant of value between 2 and 3.

Direct observation of the contact of conformal surfaces has been reported by a number of workers. For example, Jones²⁵ obtained a contact pattern under different normal applied loads and studied the contact pattern by using phase-contrast illumination. Despite a fivefold increase in load, he found no change in the few widely dispersed contact spots. The contact areas of a few spots merely enlarged slightly. Sakurai, cited for a study of the asperities of sliding contacts,²⁴ found that the trailing edges of the asperities were damaged, whereas the leading edges were relatively undisturbed.

3.6 CORROSION-WEAR

Corrosion-wear or corrosive wear occurs in situations where the environment surrounding a sliding surface interacts chemically with it. If the products of reaction (corrosion) are worn off the surface, corrosion-wear has occurred.

When the bare surface of a metal is exposed to an environment with which it can react, there is a rapid initial reaction. As the initial reaction product deposits on the surface of the metal, further reaction kinetics become diffusion-controlled, slowing down the overall reaction. For metals not able to form protective films, the corrosion reaction progresses indefinitely at a constant rate (or may even increase due to pitting, etc.).

The second step of the corrosive wear process consists of the wearing away of the reaction product film, as result of the sliding that takes place. When this occurs, bare surface is exposed and corrosive attack continues.

In most cases, the corrosion products are harder and more brittle than the surfaces on which they form. The layer tends to be reasonably wear-resistant as long as it is thin, but wear becomes possible as soon as a certain thickness of layer is exceeded. *How soon wear does, in fact, occur after the critical thickness is reached is determined by the conditions of the sliding process.* If the layer is brittle, it may be assumed that, at any place on the surface, the total thickness of layer flakes off completely at one time.

In those few cases where the reaction product layer is ductile and softer than the surface on which it forms, there is a high probability that, when wear occurs, only part of the layer will be removed. In that case, the total amount of wear will be far smaller than in the previous case, assuming that the rate of formation of reaction product and the probability of its removal remain the same.

While the above analysis forwarded by Rabinowicz²⁶ is of a fundamental nature, such analysis and the available literature provide very little insight and solution to this important problem. Clearly, the study of corrosion-wear involves the mechanical (wear resistance) properties of the protective layer whose composition and physical properties are often not well understood.

In a corrosion-wear system, the corrosion rate of the substrate is of main concern and is affected by:

- (a) Formation of a passive layer and its permeability to electrolyte and ions
- (b) Thickness and type of the protective layer
- (c) Growth kinetics of the layer--ability of the alloy to re-form a passive layer after its destruction
- (d) Microstructure of the base alloy and the passive layer.

Similarly, the wear characteristics of the substrate are affected by:

- (a) Mechanical properties of the passive layer and the substrate rupture strength, etc.
- (b) Coherency of the layer with respect to the substrate
- (c) Kinetics of the layer growth
- (d) Effect of lubricant--its adherence and change in friction coefficient.

The importance of corrosion-wear in a component varies from application to application. For example, in the case of abrasive wear, the protective layer generated by the corrosion process may not provide any protection due to the abrasive nature of the wear conditions. On the other hand, under softer/milder wear conditions, a protective corrosion product could be deposited on the worn surface which would prevent further corrosion. Lubricants could be used to make this layer even more wear-resistant.

The limited work that has been performed on corrosion-wear indicates that the process could be successfully controlled to minimize material loss under the following conditions:

- (a) Wear and corrosion should occur simultaneously.
- (b) The corrosion process could be minimized by a passivation process.
- (c) The passive layer must be tenacious and impervious under wear conditions.
- (d) The passivated layer could be lubricated to reduce frictional losses.

- (e) Finally, the material loss by the passivated and lubricated surfaces by wear must be less than the material loss by the combined nonpassivated and lubricated corrosion-wear loss.

3.7 PREVIOUS IITRI RESULTS ON CORROSION-WEAR

The initial program, "Wear and Corrosion of Components Under Stress and Subjected to Motion," was studied in two phases. During the first phase, a dynamic corrosion-wear cell was developed. An electrode polarization technique was used to evaluate corrosion behavior of the materials under stress and motion. Bearing steels, Armco iron, and 304 stainless steel were evaluated in various electrolytes containing NaCl with corrosion inhibitors such as dichromates and molybdates. Corrosion current density, open-circuit potential, and wear loss were analyzed both phenomenologically and statistically.

The Phase I study demonstrated that continuous wear affected the corrosion process very significantly when a passive film was formed in air or in solution, but almost negligibly otherwise. Generation of active metal surface by disruption of passive film under wear was mainly responsible for increase in corrosion current and the open-circuit potential shift. However, a small increase in corrosion current and a negligible shift in the open-circuit potential resulted from surface roughening and structural deformation by frictional wear. Analytical scanning electron microscopy (SEM) was used for metallurgical examination of the corrosion-wear surface morphology. Elemental maps of the materials passivated in NaCl solutions with $\text{Na}_2\text{Cr}_2\text{O}_7$ and Na_2MoO_4 showed that deposition of Cr and Mo was higher in the activated wear debris than at general wear scar areas. Surface roughness was measured to obtain additional insight into the observed phenomena.

Also, wear appeared to control the anodic polarization process significantly, but not the cathodic polarization process. A kinetic mechanism occurring in corrosion-wear systems was suggested to explain the phenomenon.

The Phase II program was initiated based on the preliminary studies conducted in Phase I. Sliding wear under corrosive conditions was studied using a specially designed electrochemical cell for oscillatory motion simulating the movement of the aircraft bearings on the ship deck. The test materials

were two bearing steels, M50 and AISI 52100. Along with open-circuit potential, corrosion current density, and wear loss, an additional corrosion-wear parameter--namely, coefficient of friction--was evaluated. All these dependent variables were analyzed statistically in terms of the independent variables such as load, frequency (of oscillation), corrosion inhibitor, and lubricant, as well as run-in time. Corrosion-wear surface morphologies were examined by SEM and energy-dispersive X-ray analysis (EDX), and the surface roughness measurements were analyzed.

The study indicated that the effect of wear on the corrosion process was very marked for alloys that were able to form a passive film. Disruption of the passive films was the principal factor leading to an increase in corrosion rate and wear loss, while surface deformation by increasing load and motion within the range evaluated appeared to be secondary. An increase in load at a constant frequency did not affect the polarization reactions as much as an increase in frequency at a constant load.

The wear phenomenon clearly proved to dominate the anodic polarization process, but not the cathodic polarization process. This understanding of the corrosion-wear mechanism indicated that the stability and repairability of the passive film with a careful selection of corrosion inhibitors will be of paramount importance in these tribological systems.

In the unlubricated system, friction coefficient was observed to be a complex function of tribochemical parameters: the effect of load, motion, and electrolyte composition on friction coefficient depended on the relative effectiveness of each of the competing parameters. However, the friction coefficient of tool steels (52100 and M50) in NaCl solutions tended to increase with the addition of corrosion inhibitors, most significantly by sodium dichromate.²⁷ The addition of a small quantity of water-soluble oil, however, had an overwhelming influence in greatly decreasing the friction coefficient.

All corrosion inhibitors used in this program effectively passivated 52100 and M50 steels under the no-wear condition. Under wear conditions, in 100% sliding motion (with no rolling component present), corrosion inhibitors decreased corrosion activities, but the inhibitors were not always equally

beneficial to wear processes. The extent depended greatly on the type of interface motions (100% sliding vs. rolling-sliding). Actual Naval aircraft components will always suffer a combination of sliding-rolling motion (with rolling motion predominating). Inhibitors added to a lubricant under such surface motion conditions are recommended for evaluation using the "Dynamic Corrosion-Wear Cell" developed in the program and modified to take into consideration the higher resistance of the lubricant.

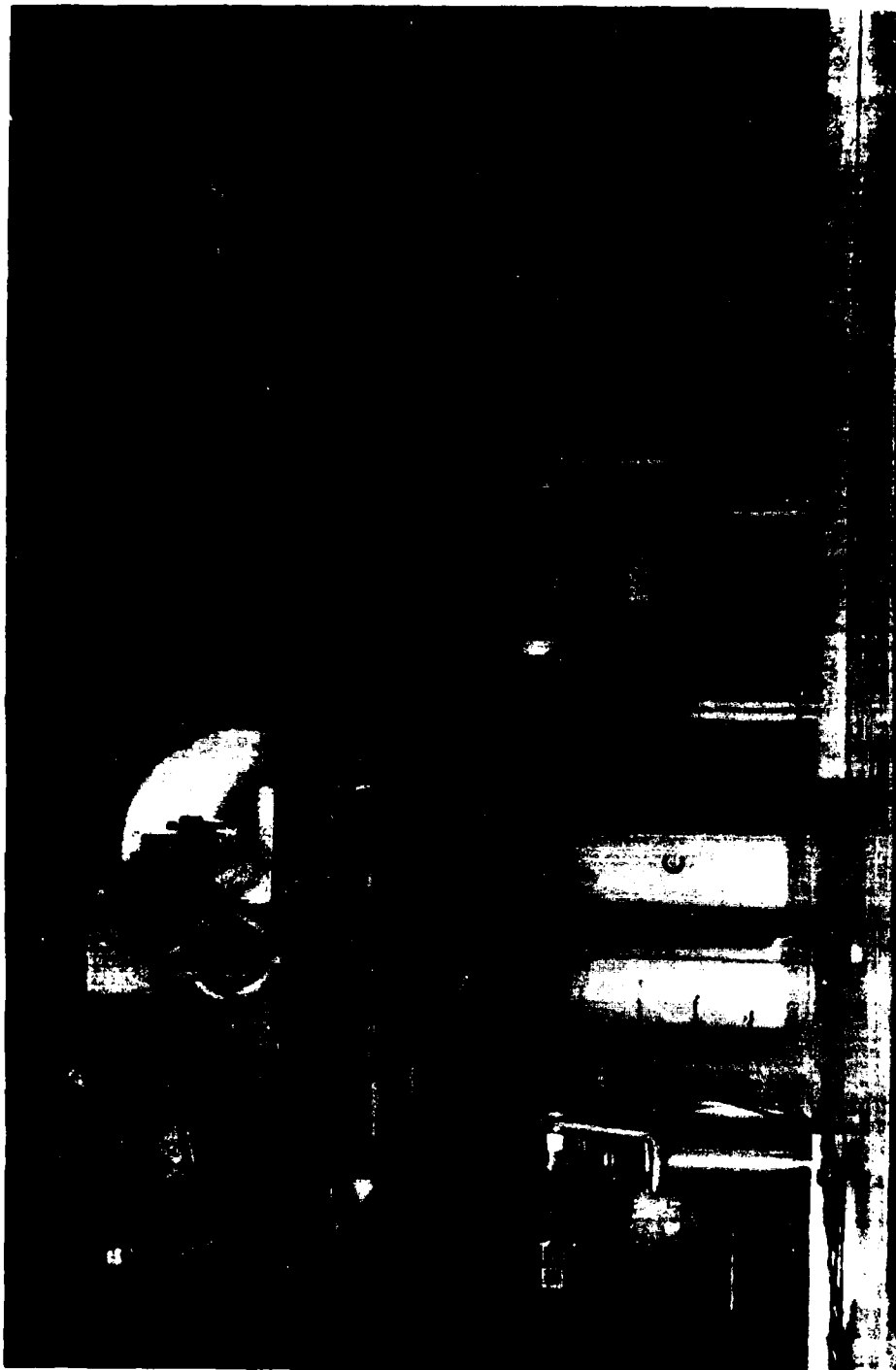
4. TEST APPARATUS

4.1 EQUIPMENT DEVELOPMENT

The equipment design was based on classical rolling contact fatigue equipment used in gear and bearing research. Gear and bearing pressure and motion were simulated by a pair of test elements rolling under load at different peripheral speeds controlled by phasing gears. Instead of operating in oil, the elements performed in an electrolyte to be adjusted with salt, inhibitors, and lubricants. The lower specimen was the test element, loaded with a much larger upper specimen to develop a significant Hertzian contact stress. A salt bridge connection to an electrochemical setup permitted measurement of corrosion current at the contact area while the applied potential was varied.

4.2 THE CORROSION-WEAR TEST APPARATUS FOR ROLLING-SLIDING MOTION

Figure 3 is a photograph of the equipment used in this study. The 1 1/2 in. (nominal) diameter test specimen (A), made of hardened and tempered steel, is loaded through contact with a 5 in. diameter loading disk (B), which is also carburized, hardened, and tempered. The disk is loaded by means of deadweights up to a maximum load of 60 lb. The contact area of the sample and the loading is an ellipse whose major and minor axes depend on the applied stress and the geometry of the contacting rollers. To obtain various degrees of Hertzian contact stresses, the contact radius of the loading disk and the specimen radius can be varied, together with the applied deadweight load. To minimize the deflection of the shafts under higher loads, Teflon supports (C) are provided. A pure rolling condition can be achieved by removing at least one of the phasing gears (D). Under this condition, the contact surface velocities of the two mating members (A and B) remain the same. Since the test specimen (A) drives the loading disk (B), a minimum load must be applied to the loading disk to overcome frictional losses at the bearings (E). When the phasing gears are in position, the contact surface velocities will depend on the diameter ratios of the specimen and the loading disk; thus a predetermined amount of slip can be achieved in the contacting surfaces by changing



Neg. No. 57503

- | | | |
|---------------------------------------|------------------------------|----------------------------|
| A - Sample | F - D.C. motor | M - Mercury pool |
| B - Loading disk | G - Speed controller | N - S.C.E. |
| C - Teflon supports | H - Gear box | O - Salt bridge |
| D - Phasing gears | I - Power transmitting shaft | U - Shaft support bearings |
| E - Support bearings for loading disk | J - Counterelectrodes | V - Solution tank |
| | L - Copper disk contact | |

Figure 3. View of the assembled IITRI corrosion-wear test apparatus.

their diameters. The rotational torque is supplied by a D-C motor (F), whose speed is controlled by a variable-speed controller (G). The rotational speed of the motor is reduced by a flanged worm-drive gear reducer (H) with a 15-to-1 reduction. The rotational torque from the gear box is transmitted to the sample through the shaft (I).

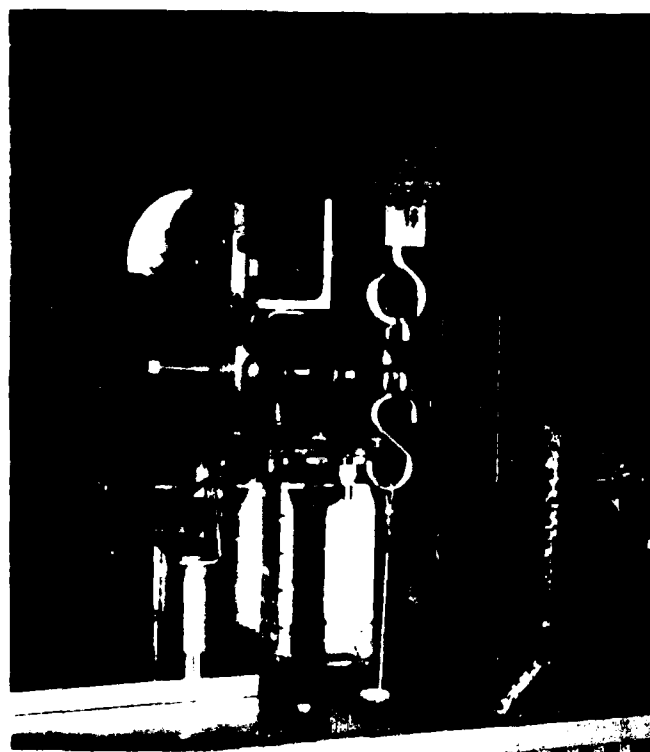
During the polarization measurement, the Plexiglas solution tank (V) was filled with a suitable electrolyte and the sample (A) and the loading disk (B) acted as the working electrode for all the experiments. The sample was then polarized by the platinum counterelectrodes (J). While the platinum counterelectrodes were connected directly to the potentiostat (K), the rotating sample could only be connected to the potentiostat through the rotating copper disk contact (L) in the mercury pool (M). The reference saturated calomel electrode (N), which was used to measure the potential of the working electrode with respect to its own potential, was connected to the polarization cell through the salt bridge (O). The salt bridge was placed very close to the working electrode (sample) to avoid, if possible, the potential gradient set up by the counterelectrode. The open-circuit potential (OCP) of the working electrode was measured using a Keithley 616 digital electrometer. The change in OCP over a long period was recorded by the Gould strip chart recorder, Model No. 105. The polarizing current was provided by a Wenking potentiostat, Model No. 07TS1, whose output was used to construct the potential-current diagrams using a Houston X-Y recorder, Model No. 2000. The controlling voltage was provided to the potentiostat by a Wenking scanning potentiometer, Model No. SMP72.

The specifics of the operating parameters and the capabilities of the corrosion-wear system described above are listed in Table 1.

The test apparatus shown in Figure 3 was modified later to prevent the lateral shift of the loading disk during rotation. This was accomplished by providing the loading arm with an L-shaped support with a roller attached to its end. This modification is shown in Figure 4. In addition to the side support, the following modifications were carried out:

TABLE 1. CAPABILITIES OF THE CORROSION-WEAR TEST EQUIPMENT

1. Load: up to 60 lb (30 lb of deadweight on the 2-to-1 lever arm)
2. Rotational speed: 2 to 110 rpm
3. Liquid volume: 2.8 liters
4. Phasing gear ratio: 3.3 to 1
5. Rolling velocity: 39.2 fpm at 100 rpm
6. Slip: -4% to +4%
7. Nominal sample diameter: 1.5 in.
8. Loading roller diameter: 5 in.
9. Loading roller profile radius: 12.5 to 2 in.
10. Hertzian contact stress: up to 270 ksi



Neg. No. 57645

Figure 4. Side support device for the loading arm of the corrosion-wear test apparatus.

- (a) The Luggin capillary salt bridge was modified to a two-piece structure for ease of placement between the two moving rollers.
- (b) The bearing post closest to the gear box, (H) in Figure 3, was removed to reduce variations in the cell current during sample rotation. This post, being farther away from the loading disk, bore a small amount of load and could be dispensed with.
- (c) A parallel current-carrying path was constructed using the reinforcement rod passing through the center of the shaft. In this path the polarizing current passed from the sample directly to the reinforcing rod and then to the copper disk. The applied pressure made the contact firm between the inner surface of the control hole on the sample and the rod passing through it.

As is evident from the geometry of the experimental setup, the supply of oxygen to the corroding sample comes from the atmosphere through the electrolyte by convection and diffusion. The level of the electrolyte, therefore, must be maintained exactly 1/4 in. above the top surface of the sample. Introduction of the loading disk increases the convective flux of oxygen and other ions accelerating the diffusion-controlled processes. The loading disk not only supplies oxygen to the corroding sample but also consumes some oxygen for its own corrosion processes.

When the loading disk is in contact with the sample, more than about 90% of its surface area is exposed to atmosphere accelerating its own corrosion. Under passivating conditions (when inhibitors are added to the electrolyte), passivation of the loading disk is much faster than that of the sample due to its better proximity to the atmospheric oxygen. When the passive layer breaks down due to the contact between the sample and the loading disk, the loading disk passivates much faster, allowing most of the current to pass through the damaged wear track of the sample.

Two counterelectrodes are situated at equal distances from equivalent points on the sample surface. These counterelectrodes are positive with respect to the sample during cathodic polarization studies and are negative during the anodic polarization studies. Although they are equidistant from the sample, they do not carry equal amounts of current during the corrosion-wear study. The one closer to the damaged (passive layer removed) wear track carries a higher current than the one closer to the passivated wear track.

5. SAMPLE PREPARATION AND TEST PROCEDURES

5.1 MATERIAL

M50 steel, which was the material selected for this program, was not readily available in bar form. Therefore, some preliminary studies were conducted under pure rolling conditions on samples that were remachined from earlier samples. The new material which arrived later and was used for the rolling-sliding experiments had the following composition (in wt%):

0.82 C	4.16 Mo
0.24 Mn	1.01 V
0.18 Si	0.06 Ni
0.015 P	0.03 Cu
0.001 S	0.01 Co
4.16 Cr	0.03 W

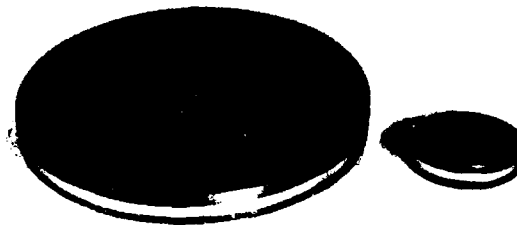
Specimens were made in three different diameters to generate three different degrees of slip: 1.5 in., 1.525 in., and 1.55 in. diameter to generate 0, 2.2, and 4.4% slip, respectively. Prior to final grinding, the specimens were heat treated. Hardness measurement indicated that the specimens had a hardness of HRC 62. The specimens had a fine ground finish at their loading edges.

The loading disks available for the experiment were of 5 in. diameter, and were carburized and hardened. To generate 2.2 and 4.4% slip, the diameters of the loading disks had to be reduced to 4.975 and 4.950 in., respectively. Therefore, the disks were sectioned and were checked for case depth to ascertain whether these disks could undergo the grinding operation and still maintain adequate hardness. The disks were then sent for grinding, after which the hardness at the anticipated contact points was checked and was found to be HRA 82. This value is equivalent to HRC 61.5, which is an acceptable hardness for running experiments.

5.2 SAMPLE PREPARATION

To increase the sensitivity of the corrosion-wear process to changes in electrochemical measurements, the ground and finished samples must be coated with a very thin nonconductive coating that minimizes the surface area in contact with the electrolyte. Various coating processes including waxing were attempted to coat the entire specimen and the loading disk, leaving only the center part of the contacting edges. Of all the attempts made, the Teflon coating was found to be the best. Even 1 mil of Teflon coating provided enough ohmic resistance to carry out the electrochemical analysis. The samples and the loading disks were all coated with 2 mils of Teflon. The coated samples were polished along the contact edges to generate the mirror finish actually encountered in bearings.

The polishing was done manually by using "Q-tips" soaked in diamond paste. The diamond paste containing 15-, 6-, and 3-micron diamonds was applied and rubbed successively to generate a shiny surface. The disks and the samples were then cleaned thoroughly in alcohol and acetone to remove the remaining oils and diamond particles. The coated and polished sample and disk are shown in Figure 5.



Neq. No. 57644

Figure 5. Teflon-coated M50 sample and the loading disk.

5.3 THE PLACKETT-BURMAN MATRIX

To determine the most significant variable influencing the corrosion-wear process and minimize the number of test runs, a statistical test design is required. A Plackett-Burman test matrix is an effective design to test the variables and, therefore, was selected here. Table 2 shows the designed test matrix used for the statistical corrosion-wear tests. In this test design, a set of six independently controlled variables were varied at two levels each. These variables were load, percent slip (or rolling-sliding ratio), lubricants, and three different inhibitors studied in earlier programs. The test was conducted exclusively with M50 steel in 100 ppm NaCl solution at room temperature. The 16-run, 6-variable test matrix shown in Table 2 is in accordance with the proposal submitted for this program.

5.4 SELECTION OF LOAD

The effect of contact stress on the corrosion-wear system under pure sliding conditions has been established through earlier programs. Increasing stress (load) increases the wear effects on the corroding system by decreasing the open-circuit potential (OCP) and increasing the corrosion current density (I_{corr}) and current densities at other overpotentials. Similar effects are anticipated under rolling-sliding condition. Since the scope of the program did not permit studying a complete load-effect pattern, only two load levels were chosen for investigation.

The maximum contact shear stress is proportional to the cube root of the applied load. An order-of-magnitude increase in the applied load, therefore, only increases the contact stress by a factor of 2.15. Since the apparatus can only take up to 60 lb (27.22 kg) of load, 4 lb (1.81 kg) and 40 lb (18.15 kg) loads were selected for study. These two load levels were generated by the application of 2 lb (0.907 kg) and 20 lb (9.07 kg) of load on the weight pan. The contact radii of the sample and the loading disk are important factors in the development of contact stresses, sharper radii developing higher stresses. In the present case, the sample edge must be flat to maintain a stable equilibrium between the loading disk and the sample. Thus, attempts were made to reduce the contact radius of the loading disk to generate higher levels of contact stress. The 12 1/2 in. (317.5 mm) contact radius of the

TABLE 2. SIXTEEN-TEST STATISTICAL DESIGN AND TEST MATRIX

Trial	Mean	A	B	C	D	E	F	G	H	I	J	K	L	M	N	O	Run No.	Y
1	+	+	-	-	-	+	-	-	+	+	-	+	-	+	+	+		
2	+	+	+	-	-	-	+	-	-	+	+	-	+	-	+	+		
3	+	+	+	+	-	-	-	+	-	-	+	+	-	+	-	+		
4	+	+	+	+	+	-	-	-	+	-	-	+	+	-	+	-		
5	+	-	+	+	+	+	-	-	-	+	-	-	+	+	-	+		
6	+	+	-	+	+	+	+	-	-	-	+	-	-	+	+	-		
7	+	-	+	-	+	+	+	+	-	-	-	+	-	-	+	+		
8	+	+	-	+	-	+	+	+	+	-	-	-	+	-	-	+		
9	+	+	+	-	+	-	+	+	+	+	-	-	-	+	-	-		
10	+	-	+	+	-	+	-	+	+	+	+	-	-	-	+	-		
11	+	-	-	+	+	-	+	-	+	+	+	+	-	-	-	+		
12	+	+	-	-	+	+	-	+	-	+	+	+	+	-	-	-		
13	+	-	+	-	-	+	+	-	+	-	+	+	+	+	-	-		
14	+	-	-	+	-	-	+	+	-	+	-	+	+	+	+	-		
15	+	-	-	-	+	-	-	+	+	-	+	-	+	+	+	+		
16	+	-	-	-	-	-	-	-	-	-	-	-	-	-	-	-		

Six assigned variables and their levels:

	Variable	(+)	(-)
A	Slip (%)	-4.38	-2.19
B	Load (lb)	40	4
C	NaNO ₂ (ppm)	500	0
D	Na ₂ Cr ₂ O ₇ (ppm)	500	0
E	Na ₂ MoO ₄ (ppm)	500	0
F	Lubricant (%)	10	0

Observations:

Y = Open-Circuit Potential
or I_{corr}

Parameters G to O are used for statistical analysis.

disks was ground down to 2 in. (50.8 mm) on all the loading disks used in this study. This procedure not only increased the contact stress to 109 ksi (4 lb load) and 235 ksi (40 lb load) but also created more clearance between the sample and the edge of loading disk away from the contact line. This is an essential feature for avoiding contact between the specimen coating and the loading disk.

5.5 SELECTION OF INHIBITORS AND LUBRICANT

A 100 ppm sodium chloride solution was the main electrolyte in previous programs and was therefore the choice recommended for this study. Very pure distilled, deionized water was used in this program. The inhibitors studied were sodium molybdate (Na_2MoO_4), sodium dichromate ($\text{Na}_2\text{Cr}_2\text{O}_7$), and sodium nitrite (NaNO_2). Their upper concentration limits are in line with the previous experiments--500 ppm of each.

The lubricant in this study was the previously selected water-soluble White Kut 210 oil. Fresh oil was procured for this program, and two levels (0 and 10% by volume) of the oil were used to study its effects.

5.6 SELECTION OF ROLLING-SLIDING RATIO

The system has been designed so that if the sum total of the specimens and the loading roller diameter is maintained at 6.5 in., the ratio of the revolutions per minute of the sample shaft and the loading shaft always remains at 10/3 for all combinations of roller and specimens. On the other hand, the surface velocities of the sample and the loading disk will change with different diameter combinations along the contact line. The rolling velocity is defined as the sum of the velocities of the two contacting surfaces:

$$V_{\text{rolling}} = \frac{V_1 + V_2}{2} \quad (14)$$

where V_2 (upper disk velocity) is usually kept larger than V_1 (lower specimen surface velocity). The sliding velocity is given by $V_2 - V_1$ and the percent slip is

$$\frac{V_2 - V_1}{V_1} \times 100 \quad (15)$$

In this study the two levels of slip were obtained by combining 1.525 in. diameter specimens with a 4.975 in. diameter loading disk and by combining 1.55 in. diameter specimens with a 4.95 in. loading disk. The corresponding percent slip values are -2.19 and -4.38%.

For pure rolling (with 0% sliding), the phasing gears could be removed and both the specimen and the loading disk may be allowed to roll under an applied load. Results of such experiments were given in a quarterly report (IITRI-M06140-3).

The electrical connections and the recording procedures remained essentially the same as depicted earlier (IITRI-M06140-3). To eliminate the effects of many variables, values of some variables were fixed at the following levels for all the experiments:

- (1) shaft speed: 30 rpm
- (2) scan rate: always started at -0.8 volt (which is approximately 400 mV below the OCP in pure NaCl solution) and scanned upwards at a rate of 12 mV/min (2 mV each step and 6 steps/min) to +0.70 volt
- (3) level of electrolyte: maintained at 6.35 mm (0.25 in.) above the top of the specimen
- (4) test temperature: RT
- (5) contact radii of the specimen and the loading disk: fixed at infinity and 2 in., respectively
- (6) stirring: it was assumed that the specimen revolution would provide enough stirring for sample corrosion, and no extra stirring was employed.

The sample was mounted on the shaft with two thin natural latex rubber gaskets to prevent any leakage of electrolyte to the center of the shaft. Before the experiment, the pH and the temperature were noted and the sample was allowed to rotate in the electrolyte for about 4 h during which time the OCP had approximately stabilized to a suitable limit for experimentation. Each run lasted for approximately 2 h. Each sample and the electrolyte were used only once. At the end of each experiment, the cell was washed with distilled water before initiation of the next experiment.

6. RESULTS AND DISCUSSION

Altogether, 67 runs were carried out in different electrolytes containing sodium chloride, often with inhibitors and lubricants, under varying loads and percent sliding in rolling-sliding situations. Both phenomenological and statistical analyses were conducted to determine the effects of inhibitors, load, percent sliding, and lubricant on corrosion current, open-circuit potential, and morphology of the wear track. The complete data on important runs are given in the Appendix.

In the following sections, the results presented in the Appendix are discussed in terms of

- specimen history
- electrochemical behavior
- appearance of wear track.

The studies under rolling-sliding motion followed a statistically designed test matrix and were analyzed both phenomenologically and statistically.

Two groups of samples were used: The first group consisted of previously tested samples, which had been surface ground for the present study followed by the application of primer and paint for marking. The second group of samples was freshly prepared, heat treated, and marked by a thin Teflon coating.

6.1 RESULTS WITH THE FIRST GROUP OF SAMPLES

The first 32 runs were made with the first group of samples, which had a ground surface finish. Details of these runs have been provided in a previous report (IITRI-M06140-3). Since these runs were conducted on a separate group of samples with a developmental coating process, these results are not discussed here in greater detail. The results, however, have served the following basic purposes:

- (1) Checking the reproducibility of the apparatus
- (2) Demonstrating effect of load on the electrochemical behavior under rolling motion
- (3) Indicating behavior of inhibitors under rolling motion.

The first few runs were carried out (runs 1 through 7) to check the reproducibility of the polarization behavior in the newly built cell using 100 ppm NaCl as the electrolyte. During this period the upper loading disk was not inserted into the electrolyte. The results were found to be quite reproducible within the limits of the variables studied. The polarization diagrams obtained during this study have been reported previously (IITRI-M06140-2 and M06140-3).

In addition to checking the reproducibility of the experimental setup, the scan rate was studied at 2 rpm and 30 rpm levels to observe the effects of such a variation. Under fast scan conditions, a large shift (by about 350 mV) in the potential for zero current was observed towards the more active direction when the shaft rotated at 2 rpm. Such a difference was not observed under 30 rpm rotation. Since the shift at low rpm was associated with reduction in cathodic current, inadequate convection was suspected to be responsible for this behavior and therefore a shaft revolution of 30 rpm was adopted for studying the corrosion-wear behavior during the rest of this program.

6.1.1 Behavior of Open-Circuit Potential

The steady-state open-circuit potentials (OCP) or the rest potentials of M50 steel were reached either by the gradual shift towards the noble direction (in the presence of inhibitors) or by the gradual shift in the more active direction (in the absence of inhibitors). A stronger inhibitor tends to push the OCP farther towards the noble direction. The steady-state open-circuit potential was reached within about 5 to 6 h of immersion, after which the potential scans were performed.

Table 3, listing the OCP values obtained, shows that with increase in inhibitor concentration of both NaNO_2 and Na_2MoO_4 , the OCP shifted towards the more noble direction. Of the three inhibitors studied in this program, NaNO_2 was found to be the strongest passivator, followed by the sodium dichromate.

TABLE 3. EFFECT OF INHIBITORS AND CONTACT STRESS ON THE OPEN-CIRCUIT POTENTIAL(OCP)

Test Condition	OCP* for Given Electrolyte, volts						
	100 ppm NaCl	100 ppm NaCl + NaNO ₂	100 ppm NaCl + Na ₂ Cr ₂ O ₇	100 ppm NaCl + Na ₂ MoO ₄	100 ppm NaCl	100 ppm NaCl	100 ppm NaCl
	50 ppm	50 ppm	500 ppm	500 ppm	500 ppm	500 ppm	500 ppm
1. Sample in solution, but not the loading disk	-0.320	-0.17	-0.15	-0.13	-0.210	-0.28	-0.25
2. Both sample and loading disk in solution but not electrically connected				-0.12	-0.08		-0.20
3. Both sample and loading disk in solution and electrically connected without any contact	--	--	--	-0.02	-0.11	--	-0.14
4. 4 lb (1.815 kg) load on sample	--	--	--	-0.08	-0.07	--	-0.22
5. 40 lb (18.15 kg) load on sample	--	--	--	-0.14	-0.17	--	-0.29

*All negative with respect to saturated calomel electrode (SCE).

Increasing the Hertzian stress shifted the OCP in the more active direction, suggesting a reduction in passivating capability of the inhibitors. The sample treated with sodium dichromate under 4 lb load seems to deviate from this trend. This sample was exposed to the electrolyte for more than 15 h and was heavily corroded prior to experimentation. The loading disk was also heavily corroded due to longer exposure.

In the case of test condition 1 (Table 3), the variation of OCP is readily justified. With increase in the addition of inhibitors, the corrosion process decreases, increasing the OCP. On a weight-to-weight basis, NaNO_2 seems to be more effective than the other two inhibitors studied, each inhibitor acting in its unique way to reduce corrosion.

When the loading disk is inserted into the solution but not in contact, the convection increases, raising the corrosion current for some of the inhibitors. This behavior can be explained with the aid of Figure 6,²⁸ which illustrates how an increase in corrosion current would raise the OCP. However, if the passivation is high and need for oxygen is low, increase in convection has little effect on the OCP and corrosion current; such is the case with NaNO_2 . On the other hand, for $\text{Na}_2\text{Cr}_2\text{O}_7$ inhibitor, a large increase in OCP suggests its greater need for oxygen to provide a passive layer superior to that provided by Na_2MoO_4 .

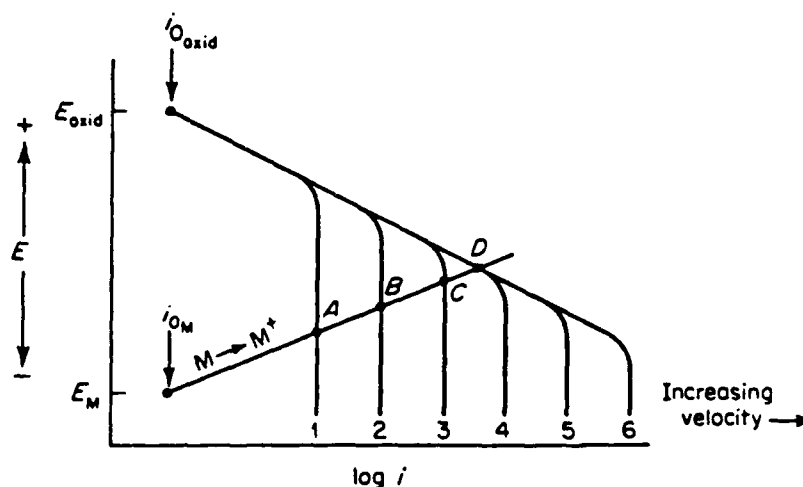
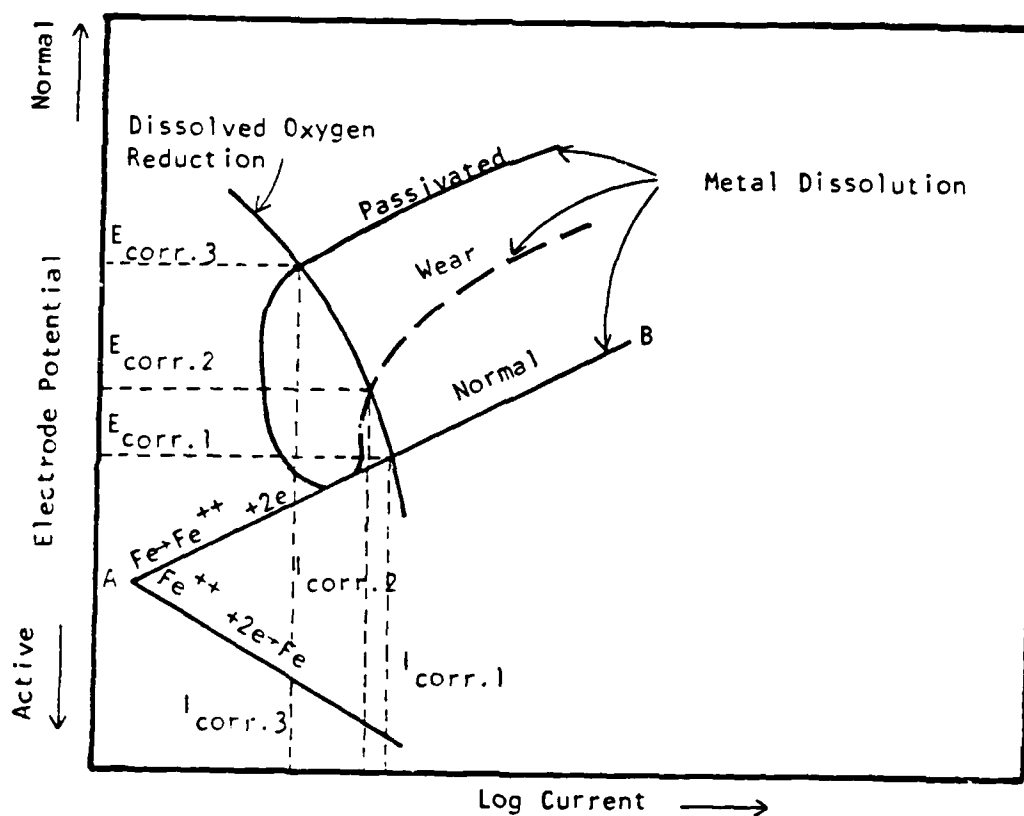


Figure 6. Effect of velocity on the electrochemical behavior of a normal metal corroding with a diffusion-controlled cathodic process.²⁸

When the loading disk is connected with the sample, a different situation occurs. The loading disk being exposed to the atmosphere is passivated more than the sample (assuming that the need for electrolyte is not critical compared to the need for oxygen) with fewer areas of anodic processes. Upon electrical contact, the cathodic areas increase considerably shifting the oxygen reduction curve to the right. Such a shift (see Figure 7) will increase the OCP, as reflected in the case of NaNO_2 and Na_2MoO_4 . On the other



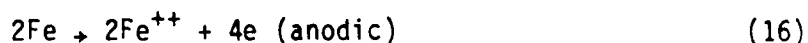
- $I_{\text{corr.1}}$ and $E_{\text{corr.1}}$ - correspond to anodic polarization in pure NaCl solution
- $I_{\text{corr.3}}$ and $E_{\text{corr.3}}$ - correspond to anodic polarization in pure NaCl solution + passivating additives
- $I_{\text{corr.2}}$ and $E_{\text{corr.2}}$ - correspond to anodic polarization in pure NaCl solution + passivating additives under corrosion-wear conditions

Figure 7. Schematic of the effects of passivating electrolyte and wear on anodic polarization of steel.

hand, in the case of $\text{Na}_2\text{Cr}_2\text{O}_7$, a decrease in OCP occurs upon the completion of the electrical contact (with no contact with the sample). This is probably due to the fact that a portion of the oxygen available to the sample is not available to the loading disk itself because of the passivation process. Such behavior is logical when passivation requires a great amount of the dissolved oxygen.

Of the two theories explaining the superiority of chromate inhibitors (discussed in Section 3.3), the adsorption theory--which postulates the adsorption of chromate ions in anodic areas, inhibiting the electrolytic process and providing a reservoir for oxygen--implies no dependence on the availability of oxygen in the electrolyte. On the other hand, the more popular theory proposed by Bregman²⁹ and similar to Cohen and Beck¹¹--which suggests that the chromate ions aid in formation and repair of the iron oxide layer--seems more appropriate to the observations of this study. In the absence of oxygen, degradation of the passive layer formed by the chromate takes place, so that the protective properties approach those of the passive layer formed by molybdate.

The destruction of the passive layer by rolling motion as observed in these experiments by a corresponding drop in OCP can be explained with the aid of Figure 7. The shift of the OCP towards the more noble direction is often encountered in passivating inhibitors and is due to the upward shift of the anodic oxidation curve, as shown in Figure 7. The presence of the passivator changes the oxidation kinetics so that, upon rupture of the passive film, the anodic current rises suddenly to the unprotected level (line AB in Figure 7). The average current of the system will, however, remain in between, as shown by the thick dashed line. The corrosion potential of the corroding system is given by the equilibrium condition where the total anodic and cathodic currents (I_{corr}) remain equal. Graphically, these points are represented by the points of intersection of the anodic and cathodic polarization curves governed by the reactions



and

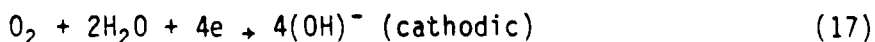


Figure 7 demonstrates that if the anodic polarization pattern of the steel in a given inhibitor is similar to the one shown, rupture of the oxide film will cause a sharp drop in E_{corr} (or OCP) with relatively little change in the corrosion current density (I_{corr}).

Downward shift of OCP has been observed in all cases with increase in contact load, as evident from Table 3. Even under severe contact stresses (40 lb load), NaNO_2 was found to be the most effective inhibitor of the three inhibitors studied, due to its higher corrosion potential.

6.1.2 Effect of Working Electrode Area on Polarization Behavior

The effect of working electrode area was varied by marking areas on the sample and by introducing the electrically connected loading disk into the electrolyte and holding it slightly above the top of the sample. The purpose of this test was to see if the counterelectrodes had enough capacity for handling larger currents.

Little change in current density was found with inhibitors like NaNO_2 and Na_2MoO_4 when the working electrode area was approximately increased to two or four times the marked sample with 1/6 in. opening. On the other hand, $\text{Na}_2\text{Cr}_2\text{O}_7$ showed an increase in anodic current with increase in the area of working electrode, the cathodic part suffering little change. This increase in working electrode area was due to the introduction of the electrically connected top loading disk into the electrolyte.

Since the passivation kinetics of M50 steel by $\text{Na}_2\text{Cr}_2\text{O}_7$ inhibitor is affected by the introduction of the top loading disk into the electrolyte and is largely unaffected by the other two inhibitors studied, it was concluded that the size of the counterelectrodes was adequate for the program.

6.1.3 Polarization Behavior Under Dynamic Corrosion-Wear Conditions

Increase in the concentration of inhibitors increased passivation in all inhibitors. This was reflected by a detectable amount of reduction in the anodic polarization current. The cathodic part of the polarization diagram remains almost unchanged.

Upon the application of contact load during the rolling motion, the anodic current increases keeping the cathodic part unaffected. The increase

in anodic current depends on the inhibitor used. Figure 8 shows a set of polarization curves for an electrolyte containing Na_2MoO_4 as inhibitor. The shift of OCP and the changes in anodic current with increasing load are evident from Figure 8.

6.2 RESULTS WITH THE SECOND GROUP OF SAMPLES

6.2.1 Statistically Designed Tests

The experiments with the second group (fresh samples) started with the evaluation of the effects of the six important corrosion-wear variables according to a statistically designed test matrix. The test matrix design was carried out according to procedures laid out by Plackett and Burman.³⁰ Table 2 shows the test matrix design, together with the six variables studied.

The statistical design adopted here allows the statistical evaluation of the effects of all six variables and, at the same time, permits the phenomenological analysis of any single variable under eight different test conditions.

6.2.1.1 Statistical Analysis

A sixteen-test, six-variable Plackett-Burman test matrix was designed for this study. The six variables (A through F in Table 2) are the assigned variables, and the remaining variables (G through O in Table 2) are the unassigned variables used for determining the experimental error. The six assigned variables had two levels and were indicated by + (higher level) and - (lower level) in Table 2. Altogether, 24 runs with eight replications were carried out, details and results of which are given in the Appendix. The dependent variables in this study were the open-circuit potential (OCP) and the corrosion current density (I_{corr}).

The computation procedure for determining the factor effect for a 12-run Plackett-Burman test is described in the literature.³¹ The significance ratios for the present six-variable matrix will be different from those found in the cited literature,³¹ but can be obtained from standard references. The significant ratios for a six-variable matrix are 1.383, 1.833, 2.262, and 3.707 at 80%, 90%, 95%, and 99% confidence levels.

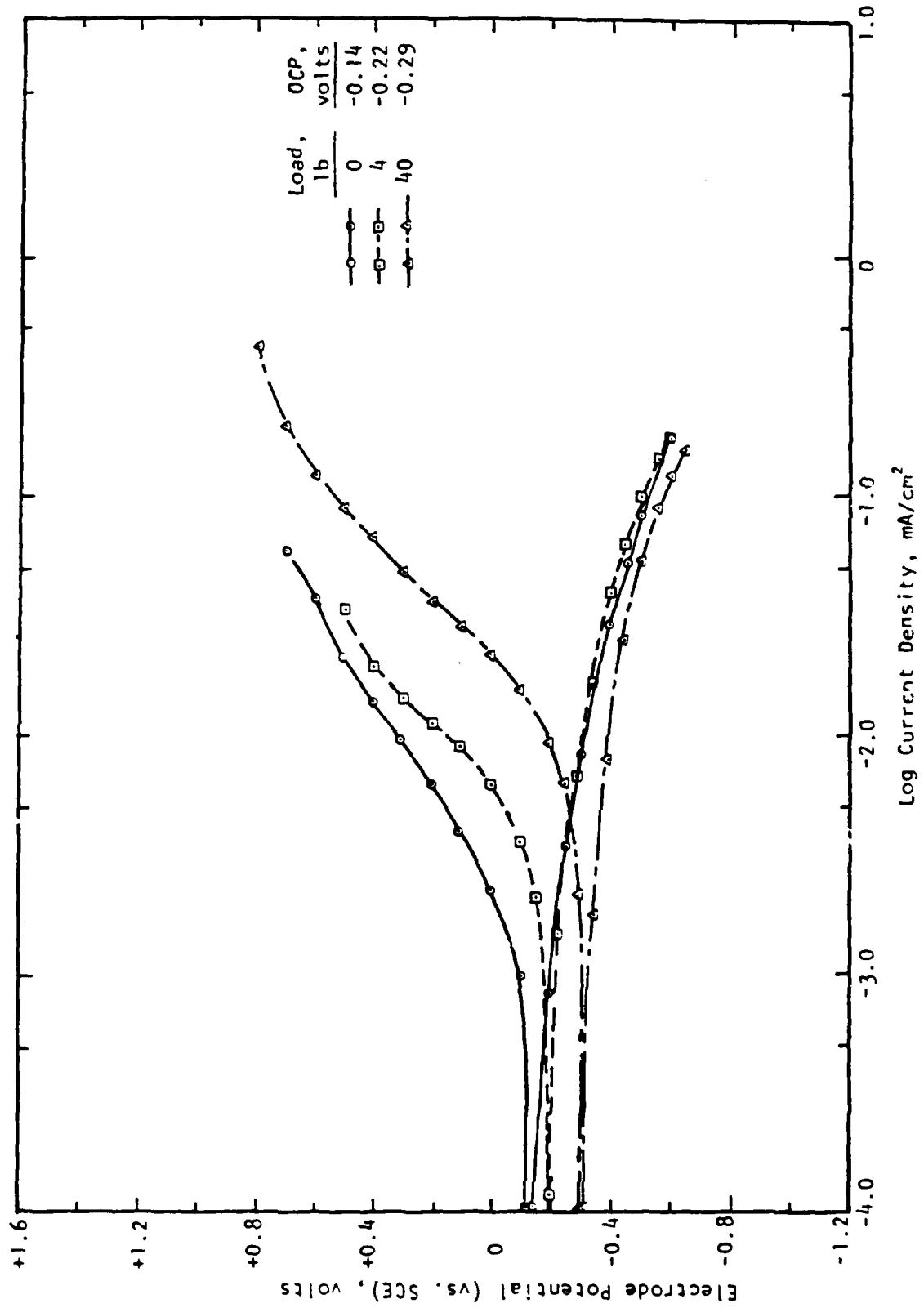


Figure 8. Effect of load on the polarization behavior of M50 steel in a solution containing 100 ppm NaCl and 500 ppm Na₂MoO₄.

(a) Open-Circuit Potential. Table 4 summarizes the results of statistical analysis of the open-circuit potential. Using unassigned variables, the significant effect (S_{FE}) was calculated to be 35.9. The minimum factor effect was 49.7, 65.9, 81.2, and 133.1 at 80%, 90%, 95%, and 99% confidence levels, respectively. At each confidence level, any assigned variable with an absolute factor effect value greater than the minimum factor effect would be considered to be statistically significant for the OCP. This analysis indicated that the presence of $\text{Na}_2\text{Cr}_2\text{O}_7$ (variable D) and percent sliding (variable A) affected the OCP significantly. At higher levels of confidence, the percent sliding was not a significant factor.

If the numerical values of "effect" of each variable are compared, the effect of $\text{Na}_2\text{Cr}_2\text{O}_7$ on the open-circuit potential is observed to be the most prominent over all other factors. The OCP, in general, is more cathodic without $\text{Na}_2\text{Cr}_2\text{O}_7$. An increase in OCP in the anodic direction due to the presence of $\text{Na}_2\text{Cr}_2\text{O}_7$ can be attributed to fast oxygen reduction in cathodic areas.

The other two inhibitors, NaNO_2 and Na_2MoO_4 , show the shift of OCP towards the more noble direction moderately. From the "effect" numbers, it is apparent that their effectiveness is nearly equal. On the other hand, the load and the water-soluble oil seem to have very little effect on the OCP changes during corrosion-wear.

The polarization curves for the 16 tests with replications were given in earlier reports (IITRI M06140-4 and M06140-5) and are presented again here in Figures 9 through 16. The replication tests show close reproducibility of results. The S_{FE} in Table 4 representing the magnitude of experimental error seems high. An important point to remember is that this statistical analysis does not take into account the interaction factors among the additives to the electrolyte and a large part of S_{FE} seems to be attributable to interaction effects.

The effect of load and percent sliding in this program seems to be straightforward; while the change in load levels has little effect on the OCP, increase in percent sliding shifts the OCP in the noble direction of the electrode potential. Such behavior is expected if increase in percent sliding

TABLE 4. RESULTS OF STATISTICAL ANALYSIS FOR OPEN-CIRCUIT POTENTIAL (OCP)

Trial	Mean	Assigned Variables								Unassigned Variables								Y (OCP), mV	Run No.
		A	B	C	D	E	F	G	H	I	J	K	L	M	N	O			
1	+	+	-	-	-	+	-	-	+	+	-	+	-	+	+	+	-199	37	
2	+	+	-	-	-	+	+	-	-	+	+	-	+	-	+	+	-275	40	
3	+	+	+	-	-	-	-	+	-	-	+	+	-	+	-	+	-322	38,42	
4	+	+	+	+	+	-	-	-	+	-	-	+	+	-	+	-	-052	41,55	
5	+	-	+	+	+	+	-	-	-	+	-	-	+	+	-	+	-005	36,43	
6	+	+	-	+	+	+	+	-	-	-	+	-	-	+	+	-	-141	48	
7	+	-	+	+	+	+	+	+	-	-	-	+	-	-	+	+	-170	50,51	
8	+	+	-	+	-	+	+	+	+	-	-	-	+	-	-	+	-243	53,54	
9	+	+	+	-	+	+	+	+	+	+	-	-	-	+	-	-	-145	49	
10	+	-	+	+	-	+	-	+	+	+	+	-	-	-	+	-	-377	35,58	
11	+	-	-	+	+	-	+	-	+	+	+	+	-	-	-	+	-139	46	
12	+	+	-	+	+	+	-	+	-	+	+	+	+	-	-	-	-078	47	
13	+	-	+	-	+	+	+	-	+	-	+	+	+	+	-	-	-322	44,52	
14	+	-	-	+	-	-	+	+	-	+	-	+	+	+	+	-	-250	45	
15	+	-	-	-	+	-	-	+	+	-	+	-	+	+	+	+	-246	33	
16	+	-	-	-	-	-	-	-	-	-	-	-	-	-	-	-	-345	34	
Sum +	-3309	-1455	-1668	-1529	-976	-1535	-1685	-1831	-1723	-1468	-1900	-1532	-1471	-1630	-1710	-1599			
Sum -	0	-1854	-1641	-1780	-2333	-1774	-1624	-1478	-1586	-1841	-1409	-1777	-1838	-1679	-1599	-1710			
Overall	-3309	-3309	-3309	-3309	-3309	-3309	-3309	-3309	-3309	-3309	-3309	-3309	-3309	-3309	-3309	-3309			
Sum																			
Diff.	-3309	399	-27	251	1357	239	-61	-353	-137	373	-491	245	367	49	-111	111			
Effect	-206.8	49.9	-3.4	31.4	169.6	29.9	-7.6	-44.1	-17.1	46.6	-61.4	30.6	45.8	6.1	-13.9	13.9			

S_{FE} = 35.9

Significant Factors

(MIN) 1.383 x 35.9 = 49.7 (80% confidence level)
 1.833 x 35.9 = 65.9 (90% confidence level)
 2.262 x 35.9 = 81.2 (95% confidence level)
 2.707 x 35.9 = 97.1 (99% confidence level)

D, A
D
D
D

increases the kinetics of the passivation process. In fact, the increase in interfacial temperature during sliding has been shown to be very high and is capable of inhibiting many chemical reactions.³²

(b) Corrosion Current Density. Table 5 summarizes the results of statistical analysis of the corrosion current density. The I_{corr} determination, which uses linear analysis technique, has been explained in detail in IITRI report M06140-3. The statistical analysis showed that the significant factor effect (S_{FE}) is 253. The minimum factor effect was 350, 464, and 572, at 80%, 90%, and 95% confidence levels, respectively.

At 80% confidence level, the load, $\text{Na}_2\text{Cr}_2\text{O}_7$, and lubricating oil were found to be most effective; at 90% confidence level, only $\text{Na}_2\text{Cr}_2\text{O}_7$ is the most effective variable. At confidence levels higher than 90%, none of the factors appear to have any statistical significance in affecting I_{corr} .

Both $\text{Na}_2\text{Cr}_2\text{O}_7$ and the lubricating oil tend to reduce the corrosion current density with increasing levels. While the inhibiting behavior of $\text{Na}_2\text{Cr}_2\text{O}_7$ is well known, the inhibition properties of the lubricating oil seem to originate from the emulsifier (sodium sulfonate) added to the oil. The action of the lubricating oil appears to be twofold--inducing passivation and reducing the cathodic reaction at cathodic sites. These two effects act in such a way that the corrosion current is reduced without appreciable change in the OCP. An increase in load will increase the corrosion current, causing an increase in the area of contact. Since the current density is calculated over the total sample area exposed to the electrolyte, increase in contact area will increase the current density on a passivated surface.

Studying the statistical effects (Table 5) of the other parameters, it can be seen that an increase in percent sliding decreases the corrosion current. This behavior again suggests an increase in passivation kinetics due to an instantaneous increase in temperature of the contacting surfaces upon increase in percent sliding. Additions of NaNO_2 and Na_2MoO_4 increased the corrosion current. Although some experimental error may be involved, the effect cannot be ignored since both NaNO_2 and Na_2MoO_4 (two inhibitors often acting in a similar fashion) show the same behavior. Interaction with other inhibitors is probably responsible for this effect. The illustration of

TABLE 5. RESULTS OF STATISTICAL ANALYSIS FOR CORROSION CURRENT DENSITY (i_{corr})

Trial	Mean	Assigned Variables								Unassigned Variables								(I_{corr}) , $\mu A/mm^2$	Run No.
		A	B	C	D	E	F	G	H	I	J	K	L	M	N	O			
1	+	+	-	-	-	+	-	-	+	+	-	+	-	+	+	+	292	37	
2	+	+	-	-	-	+	-	-	-	+	+	-	+	-	+	+	291	40	
3	+	+	+	-	-	-	+	-	-	-	+	+	-	+	-	+	1465	38,42	
4	+	+	+	+	-	-	-	+	+	-	-	+	+	-	+	-	55	41,55	
5	+	+	+	+	+	+	-	-	-	+	-	-	+	+	+	+	109	36,43	
6	+	+	+	+	+	+	+	-	-	-	+	-	-	+	+	-	130	48	
7	+	-	-	+	+	+	+	-	-	-	-	+	-	-	+	+	158	50,51	
8	+	+	-	-	+	+	+	+	+	-	-	-	+	-	-	+	71	53,54	
9	+	+	+	+	-	+	+	+	+	+	-	-	-	+	-	-	164	49	
10	+	-	+	+	-	+	+	+	+	+	+	-	-	-	+	-	2230	35,58	
11	+	-	-	+	+	-	+	-	+	+	+	+	-	-	-	+	110	46	
12	+	+	-	+	+	+	-	+	-	+	+	+	+	-	-	-	99	47	
13	+	-	+	-	+	+	-	+	+	-	+	+	+	+	-	-	245	44,52	
14	+	-	+	-	-	-	+	+	-	+	-	+	+	+	+	-	141	45	
15	+	-	-	-	+	-	+	+	+	-	+	-	+	+	+	+	146	33	
16	+	-	-	-	-	-	-	-	-	-	-	-	-	-	-	-	482	34	
Sum +	6188	2567	4717	4311	971	3334	1310	4474	3313	3436	4716	2565	1157	2692	3443	2642			
Sum -	0	3621	1471	1877	5217	2854	4878	1714	2875	2752	1472	3623	5031	3496	2745	3546			
Overall	6188	6188	6188	6188	6188	6188	6188	6188	6188	6188	6188	6188	6188	6188	6188	6188			
Sum																			
Diff.	6188	-1054	3246	2434	-4246	480	-3568	2760	438	684	3244	-1058	-3874	-804	698	-904			

Significant Factors

 $S_{FE} = 253$

(MIN) $1.383 \times 253 = 350$ (80% confidence level)
 $1.833 \times 253 = 464$ (90% confidence level)
 $2.262 \times 253 = 572$ (95% confidence level)

B,D,F

0

-

anomalous inhibitive behavior of $\text{Na}_2\text{Cr}_2\text{O}_7$ in the next section suggests this as a strong possibility.

6.2.1.2 Effect of Sodium Dichromate Additions on the Polarization Behavior under Various Test Conditions

Individual polarization curves for the test matrix were reported in quarterly reports IITRI-M06140-3 and IITRI-M06140-4. Here Figures 9 through 16 present these polarization diagrams in pairs to explain the effectiveness of the most important factor (as the results of the statistical analysis indicate) under various corrosion-wear conditions. Careful examination of these figures indicates that the test environments influencing the effectiveness of $\text{Na}_2\text{Cr}_2\text{O}_7$ can be divided into two broad categories: the presence and the absence of the lubricating oil. Addition of $\text{Na}_2\text{Cr}_2\text{O}_7$ in the absence of lubricating oil brings about dramatic changes in the polarization behavior, open-circuit potential, and corrosion current density. The presence of 10% lubricating oil somewhat mitigates these effects.

(a) Effectiveness of $\text{Na}_2\text{Cr}_2\text{O}_7$ in the Absence of Lubricating Oil. Figure 9 shows the changes in the polarization behavior of the sample under 4 lb load and -2.2% sliding tested in NaCl solution upon the addition of $\text{Na}_2\text{Cr}_2\text{O}_7$. It is evident from the polarization diagram that addition of $\text{Na}_2\text{Cr}_2\text{O}_7$ increases the OCP considerably toward the nobler direction of the electrode potential. It also reduces the anodic and cathodic currents during polarization. Upon addition of 500 ppm Na_2MoO_4 to the solution (Figure 10), a small degree of passivation behavior is observed (more pronounced upon addition of $\text{Na}_2\text{Cr}_2\text{O}_7$) but similar shifts in OCP and current density curves are induced upon dichromate addition.

The addition of NaNO_2 to the solution increased the effectiveness of $\text{Na}_2\text{Cr}_2\text{O}_7$ dramatically. As Figure 11 indicates, large increase in electrode potential towards the noble direction, together with sharp decrease in corrosion current, is observed upon dichromate addition. Similar strong effectiveness of $\text{Na}_2\text{Cr}_2\text{O}_7$ has been observed in the presence of both 500 ppm NaNO_2 and Na_2MoO_4 under high load and low sliding conditions (Figure 12).

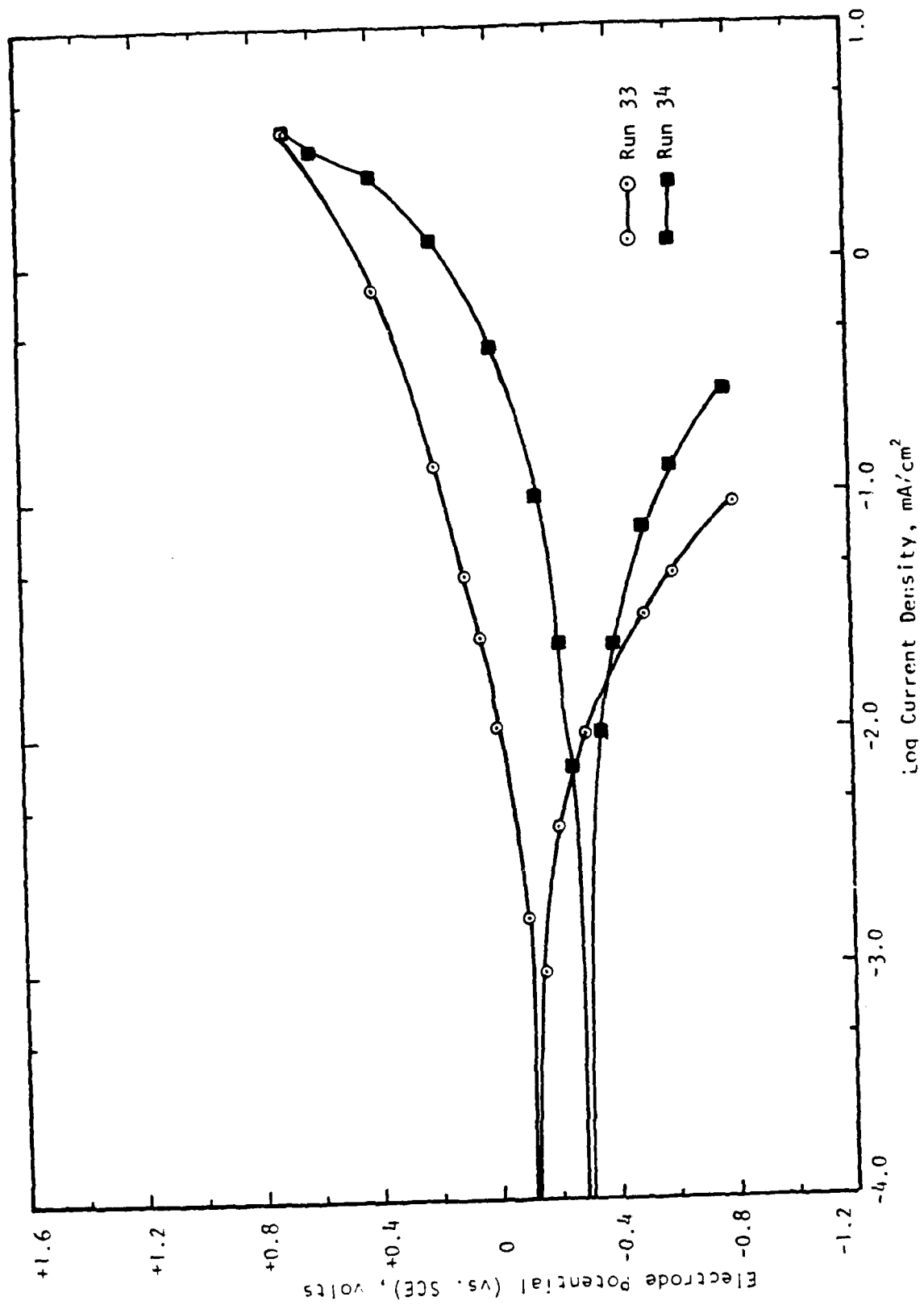


Figure 9. Polarization behavior of M50 steel with (run 33, trial 15 conditions in Table 2) and without (run 34, trial 16 conditions in Table 2) the addition of $\text{Na}_2\text{Cr}_2\text{O}_7$. Load = 4 lb; sliding = -2.19%.

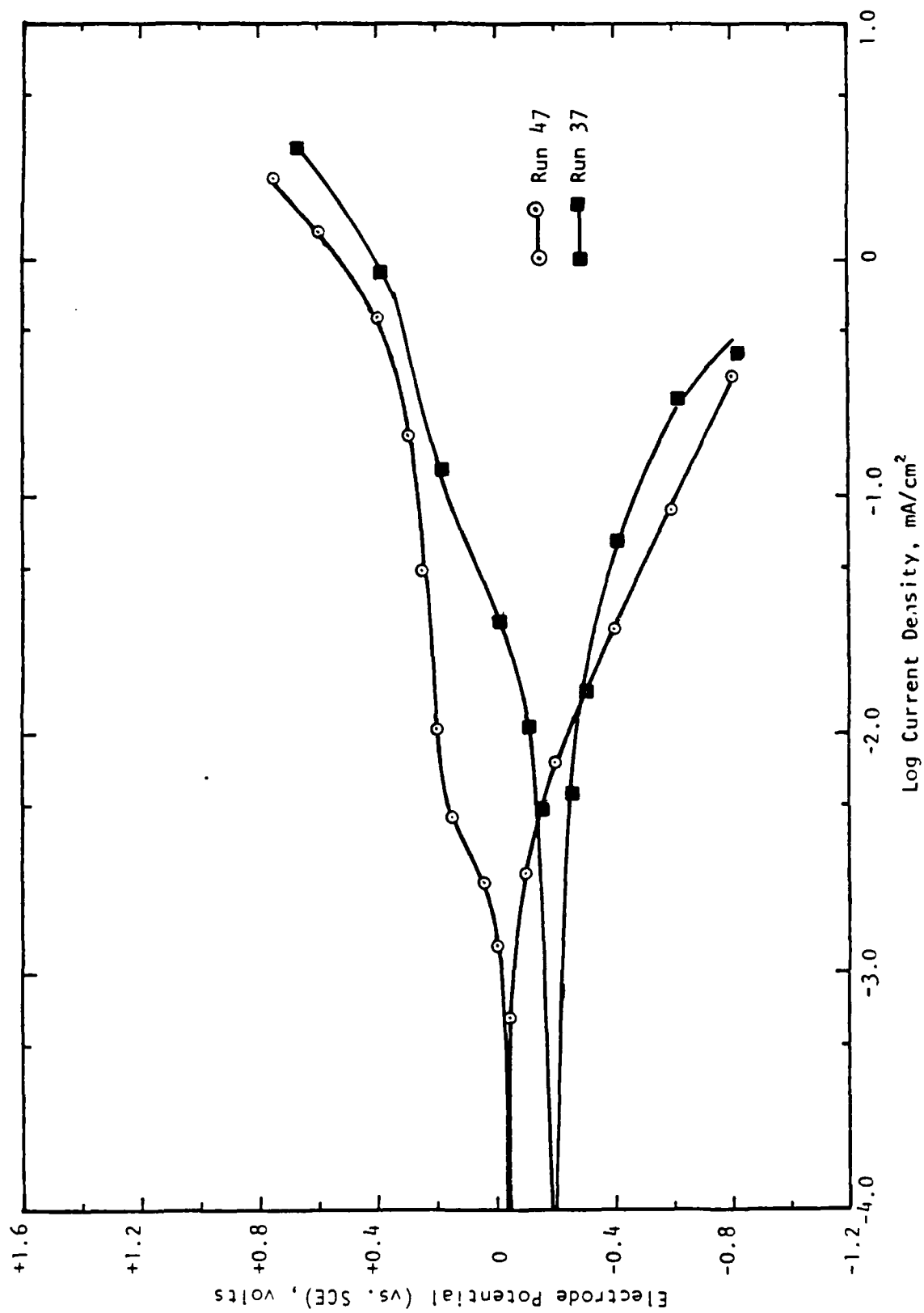


Figure 10. Polarization behavior of M50 steel with (run 47, trial 12 conditions in Table 2) and without (run 37, trial 1 conditions in Table 2) the addition of $\text{Na}_2\text{Cr}_2\text{O}_7$. Load = 4 lb; sliding = -4.38%; Na_2MoO_4 = 500 ppm.

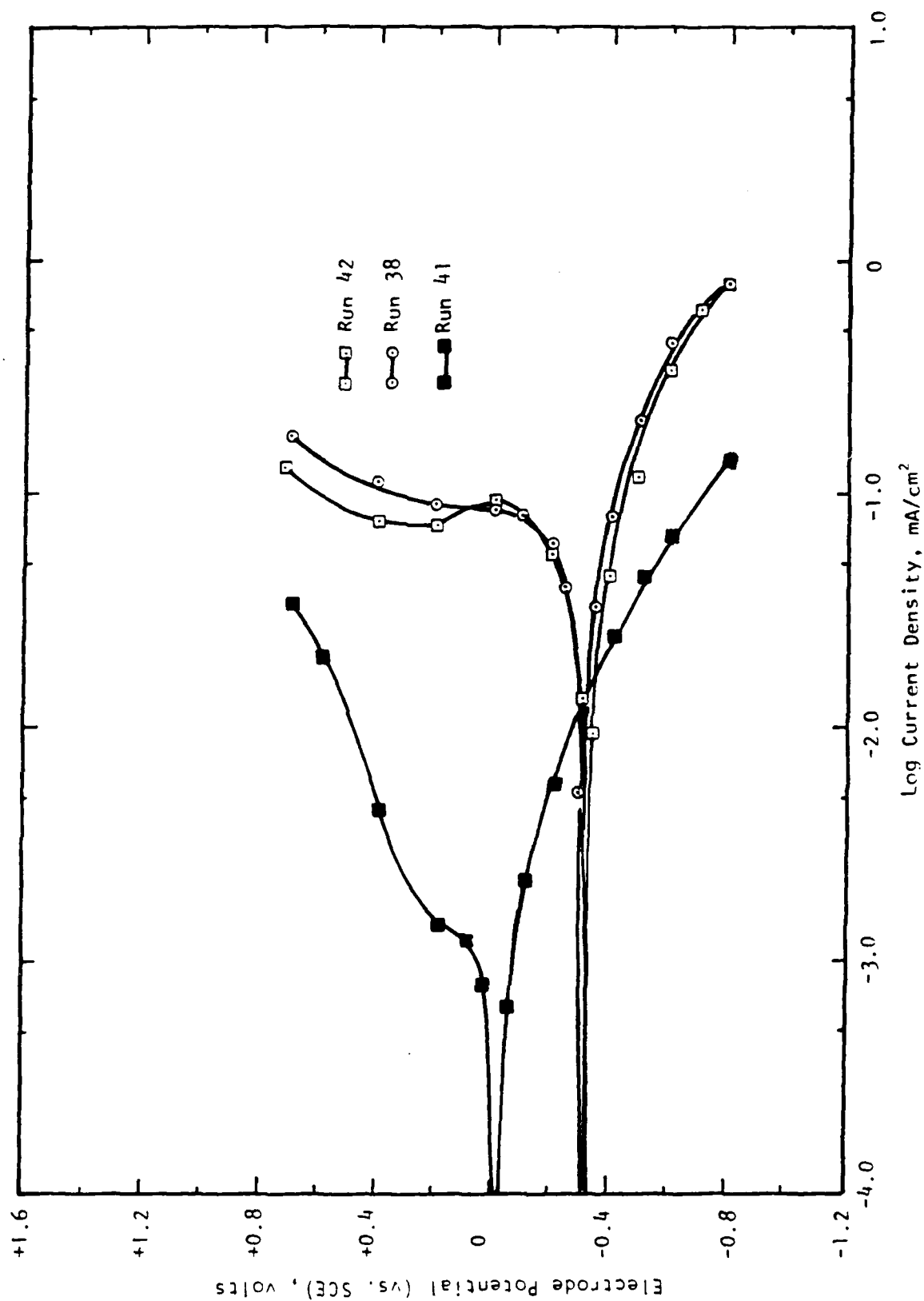


Figure 11. Polarization behavior of M50 steel with (run 41, trial 4 conditions in Table 2) and without (runs 38 and 42, trial 3 conditions in Table 2) dichromate addition. Load = 40 lb; sliding = -4.38%; $\text{NaNO}_2 = 500 \text{ ppm}$.

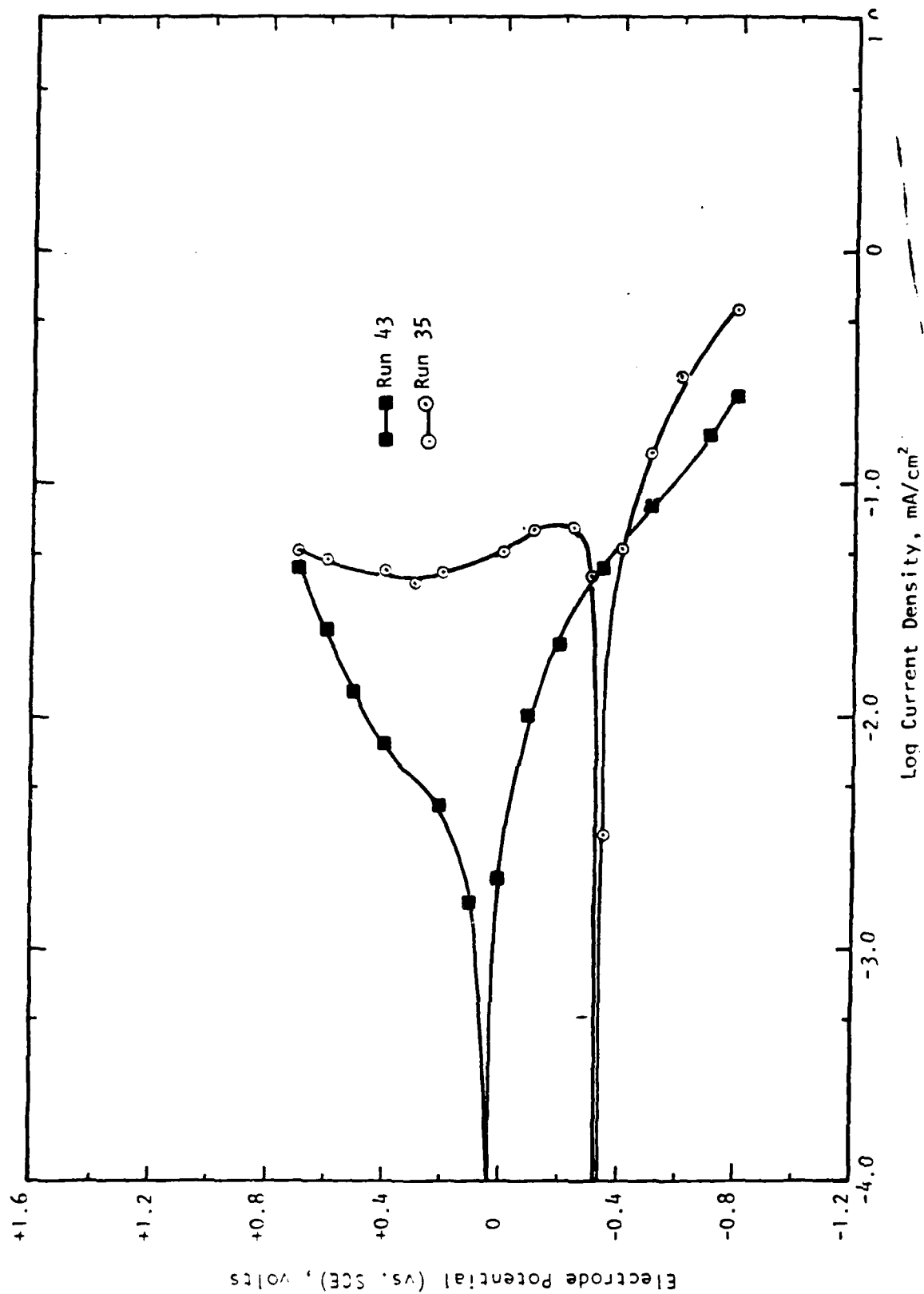


Figure 12. Polarization behavior of M50 steel with (run 43, trial 5 conditions in Table 2) and without (run 35, trial 10 conditions in Table 2) dichromate addition. Load = 40 lb; sliding = -2.19%; NaNO_2 and Na_2MoO_4 = 500 ppm each.

(b) Effectiveness of $\text{Na}_2\text{Cr}_2\text{O}_7$ in the Presence of Lubricating Oil

Although the inhibiting power of the dichromate is felt in the presence of lubricating oil in solution with the electrolyte, its effectiveness is not as dramatic as discussed above. Figures 13 through 16 indicate that, unlike in the absence of lubricating oil, the effectiveness decreases with the presence of NaNO_2 and the soluble oil.

Figure 13 shows the effectiveness of the dichromate in the absence of other inhibitors. A rise of about 100 mV occurs in the OCP with corresponding decrease in corrosion current upon addition of dichromate. Addition of 500 ppm of NaNO_2 (Figure 14) decreases even this little effectiveness that exists with the dichromate addition. Figures 15 and 16 show the results upon addition of dichromate in the presence of other inhibitors like Na_2MoO_4 and a mixture of NaNO_2 and Na_2MoO_4 , respectively. A slight change in polarization behavior is observed in these cases upon dichromate addition.

A current density peak between +0.4 and +0.8 V is observed in all polarization diagrams with electrolytes containing lubricating oil and either NaNO_2 or Na_2MoO_4 or both. The occurrence of this peak cannot be explained without special experimentation.

6.2.2 Tests Under Pure Rolling Conditions

With the availability of the fresh batch of samples, some tests were carried out to study the effect of contact load on the electrochemical behavior of M50 steel under pure rolling motion of the polished surfaces. Determining the action of the inhibitors and the lubricant was the object in these tests, the results of which are discussed below.

6.2.2.1 Polarization Behavior in the Mixture of Sodium Chloride and Sodium Nitrite Solution

Figure 17 presents the polarization behavior of M50 steel in an electrolyte containing 100 ppm sodium chloride and 500 ppm NaNO_2 under 4 lb and 40 lb (runs 56 and 57, respectively) and the corresponding I_{corr} and OCP values are shown in Table 6. For comparison, sliding motion has been introduced, and as evident from Figure 17 and Table 6, both increase in load and introduction of sliding raise corrosion current density significantly and decrease OCP towards the reactive side of electrode potential. This type of behavior is expected

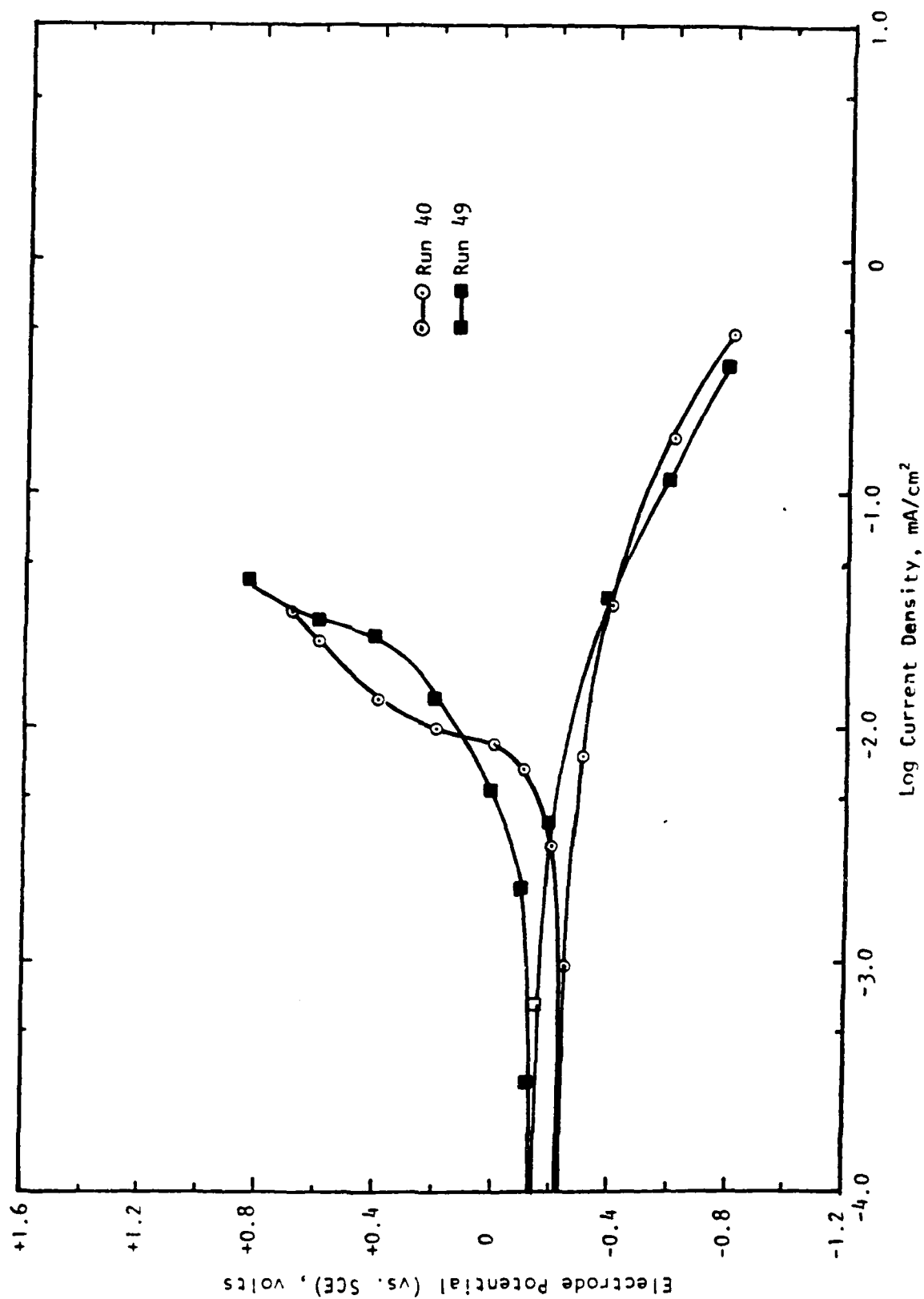


Figure 13. Polarization behavior with (run 49, trial 9 conditions in Table 2) and without (run 40, trial 2 conditions in Table 2) dichromate addition. Load = 40 lb; sliding = -4.38%; lubricant (10%).

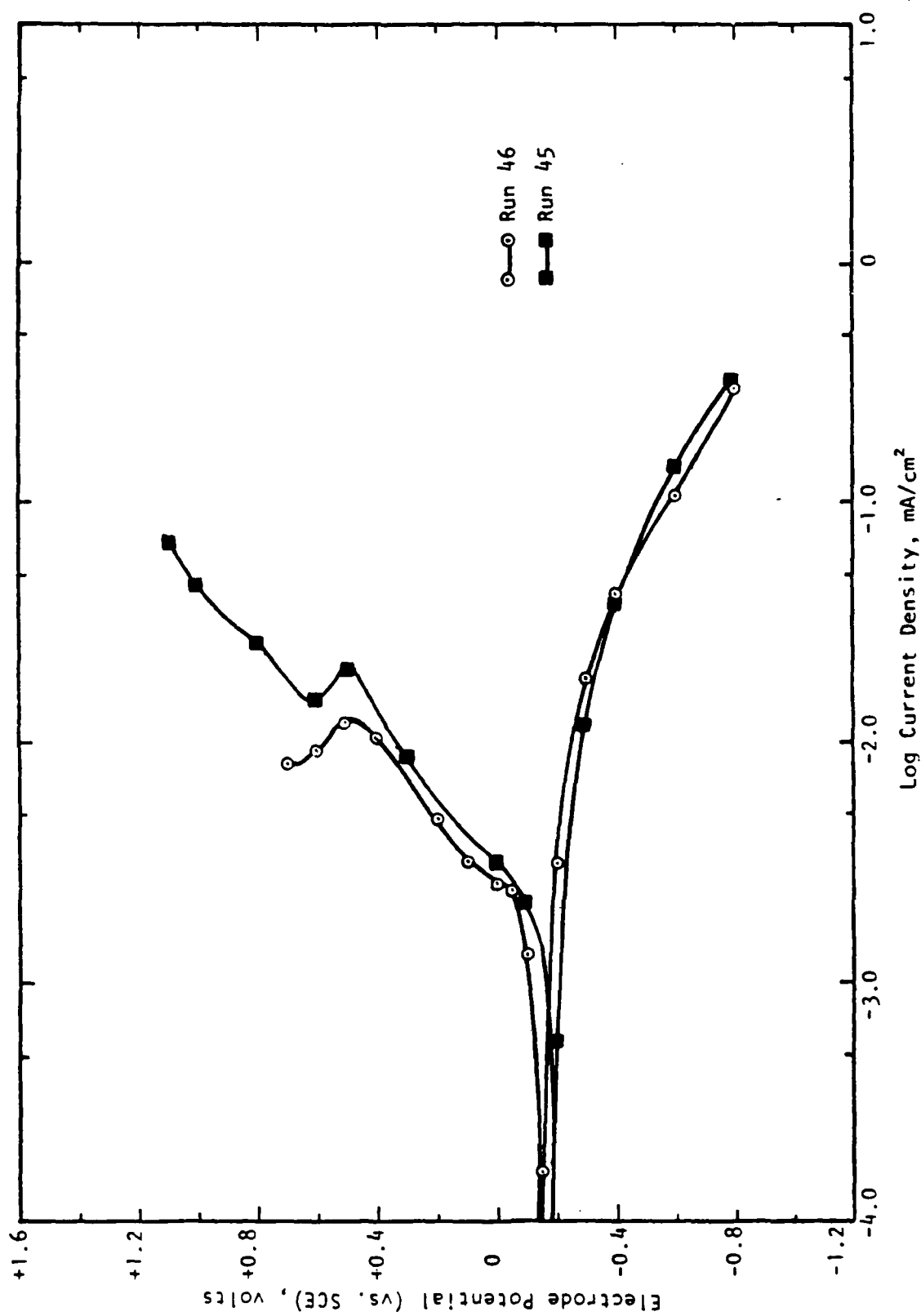


Figure 14. Polarization behavior of M50 steel with (run 46, trial 11 conditions in Table 2) and without (run 45, trial 14 conditions in Table 2) dichromate addition. Load = 40 lb; sliding = -2.19%; NaNO_2 = 500 ppm; lubricant (10%).

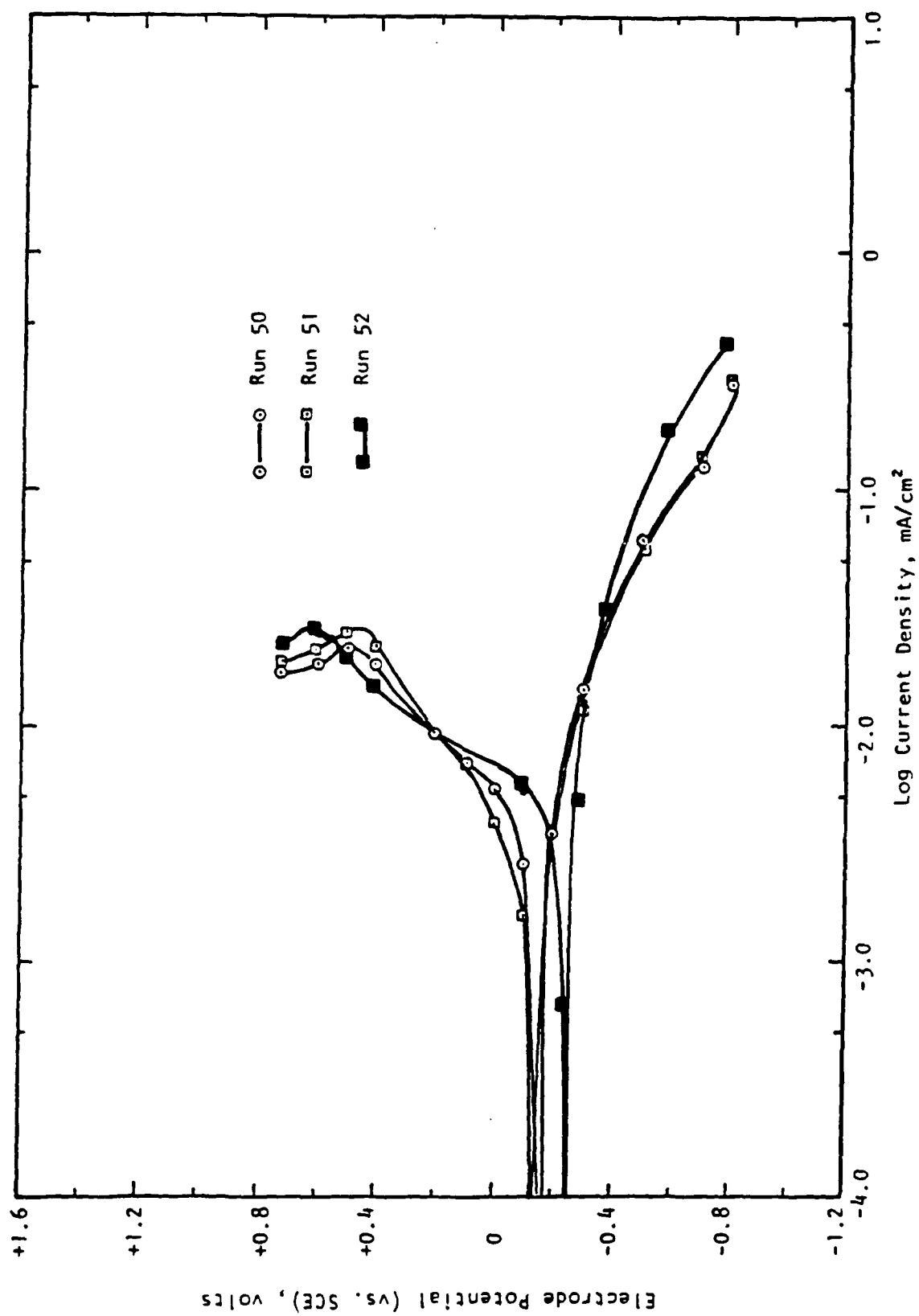


Figure 15. Polarization behavior of M50 steel with (runs 50 and 51, trial 7 conditions in Table 2) and without (run 52, trial 13 conditions in Table 2) dichromate additions. Load = 40 lb; sliding = -2.19%; Na_2MoO_4 = 500 ppm; lubricant (10%).

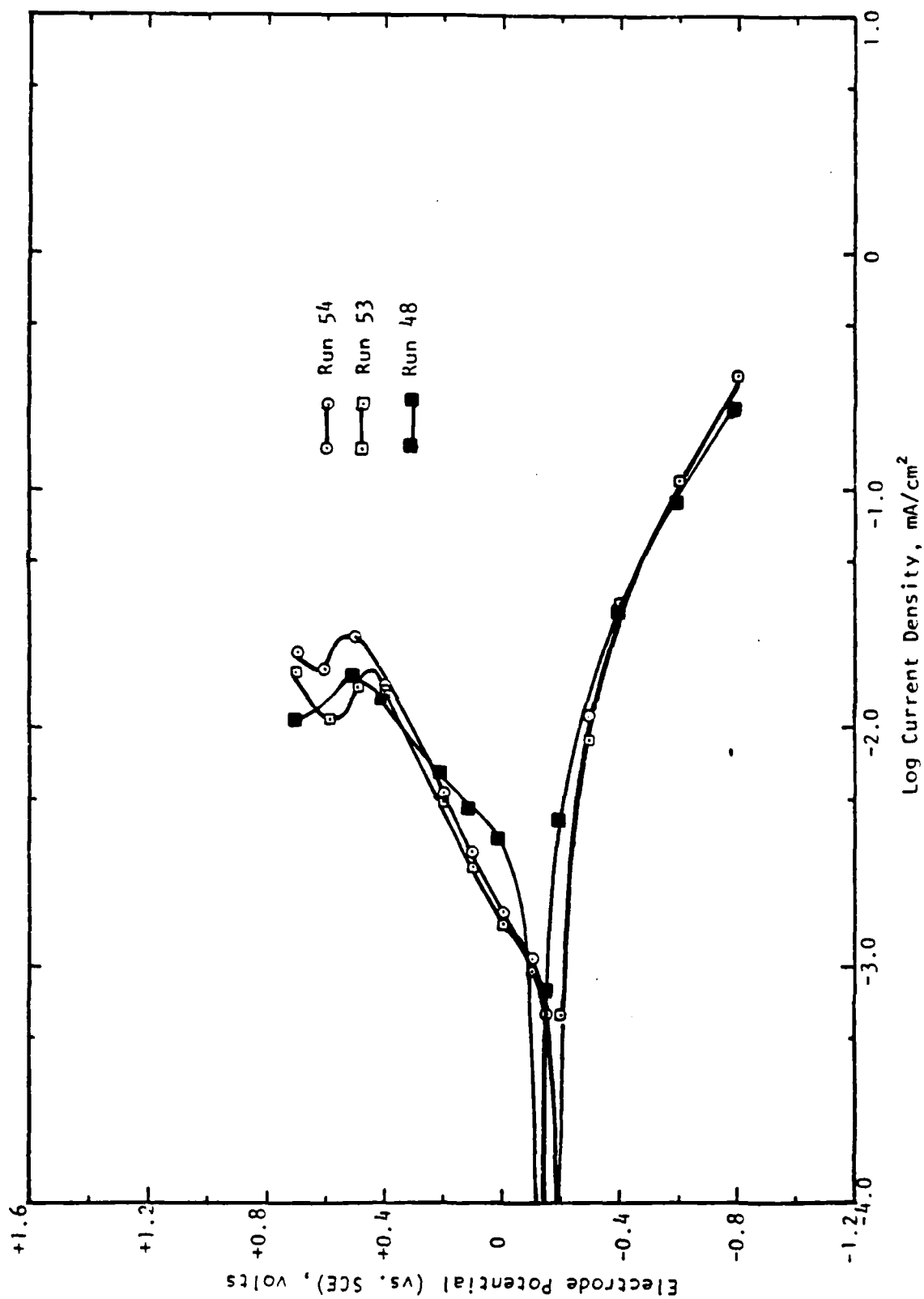


Figure 16. Polarization behavior of M50 steel with (run 48, trial 6 conditions in Table 2) and without (runs 53 and 54, trial 8 conditions in Table 2) dichromate additions. Load = 40 lb; sliding = -4.38%; NaNO_2 and Na_2MoO_4 = 500 ppm each; lubricant (10%).

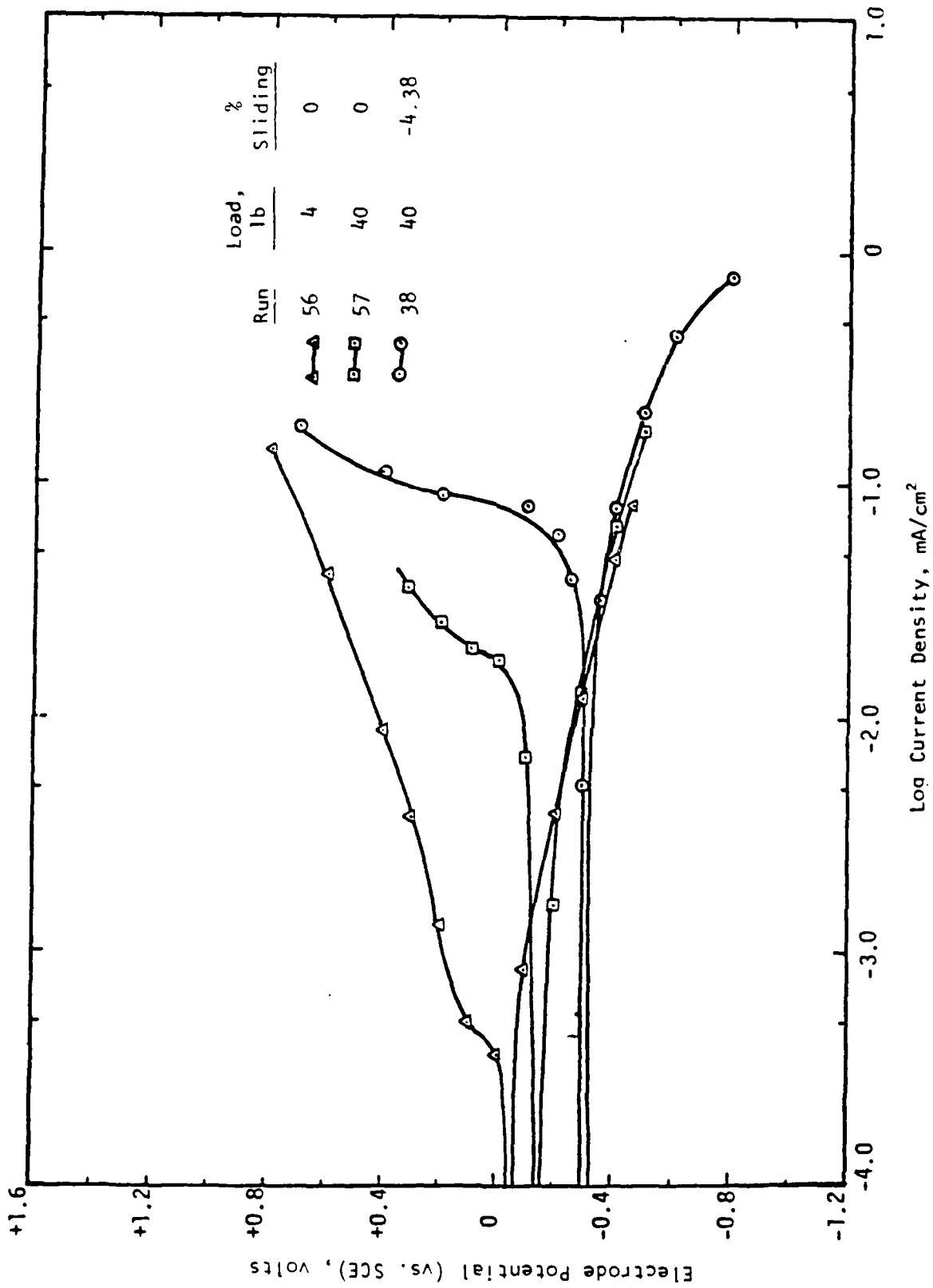


Figure 17. Effect of load and sliding on the polarization behavior of M50 steel under pure rolling and rolling-sliding motion in electrolyte containing 100 ppm NaCl and 500 ppm NaNO_2 .

TABLE 6. EFFECT OF LOAD AND SLIDING ON OCP AND I_{corr} IN THE PRESENCE OF NITRITE INHIBITOR

Run No.	Load, lb	Sliding, %	OCP, volts	I_{corr} , mA/cm ²
56	4	0	-0.08	2.84×10^{-4}
57	40	0	-0.14	2.56×10^{-3}
38	40	-4.38	-0.31	1.63×10^{-2}

Inhibitor: 500 ppm NaNO_2 .

because, with increase in load, the anodic current increases as the passivated anodic regions open up due to friction caused by both rolling and sliding motion. The cathodic behavior remains unchanged during increase in load and introduction of sliding.

6.2.2.2 Polarization Behavior in a Mixture of Sodium Chloride and Sodium Dichromate

Polarization behavior in an electrolyte containing 100 ppm NaCl and 500 ppm $\text{Na}_2\text{Cr}_2\text{O}_7$ was studied by varying the contact load on the specimen. Figure 18 shows the results, and Table 7 gives the corresponding OCP and I_{corr} values.

During this study, run 60 was carried out after run 59 with increase in load (to 40 lb) using the old disk but with a new sample. This resulted in an increased I_{corr} and decrease in OCP close to -0.24 V as shown for run 62. The results of run 60 are not reported because the disk was not changed. Upon

TABLE 7. EFFECT OF LOAD AND SLIDING ON OCP AND I_{corr} IN THE PRESENCE OF DICHROMATE INHIBITOR

Run No.	Load, lb	Sliding, %	OCP, volts	I_{corr} , mA/cm ²
59	4	0	-0.21	1.32×10^{-3}
62	40	0	-0.24	0.92×10^{-3}
33	4	-2.19	-0.246	1.46×10^{-3}

Inhibitor: 500 ppm $\text{Na}_2\text{Cr}_2\text{O}_7$.

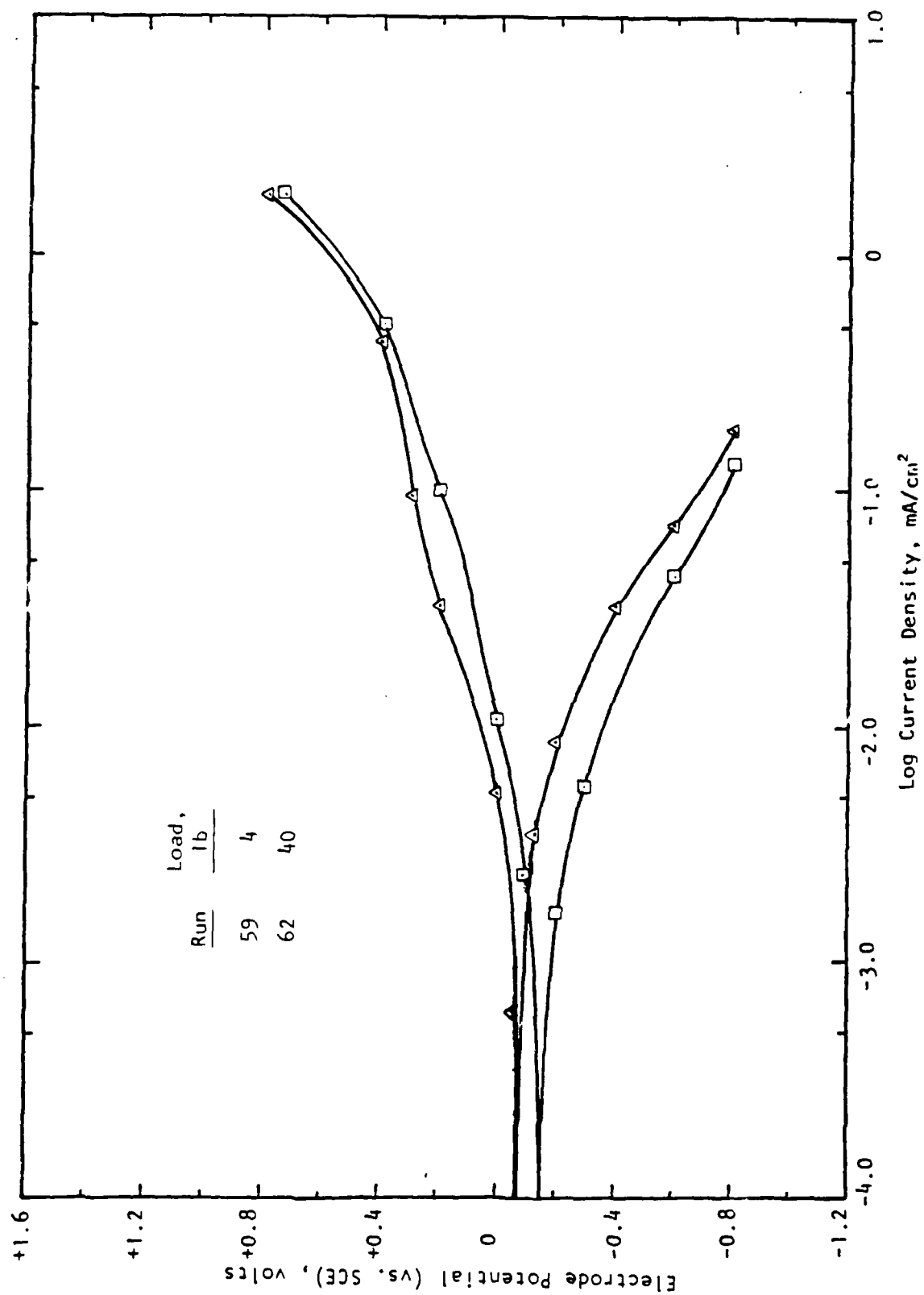


Figure 18. Effect of load on the polarization behavior under rolling motion in electrolyte containing 100 ppm NaCl and 500 ppm $\text{Na}_2\text{Cr}_2\text{O}_7$.

introducing a fresh sample and disk (run 62), the OCP was reduced to -0.24 V and I_{corr} decreased. Similar inconsistencies were reported for the ground-finished first-batch samples earlier. Figure 18 indicates marginal change in the polarization diagrams between the 4 lb and 40 lb load runs. A slight difference also exists between the results of runs 59 and 33, when the introduction of 2.2% sliding in run 33 caused a drop of 36 mV in OCP.

6.2.2.3 Polarization Behavior in the Presence of Lubricating Oil

Polarization behavior of M50 steel in the electrolyte containing 100 ppm NaCl and 10% water-soluble oil is presented in Figure 19. Studying the samples in the presence of lubricant was found to be important earlier because of the passivating nature of the lubricant used. Table 8 lists the OCP values and the corrosion current densities for M50 steel under rolling and rolling-sliding motion.

Little difference in corrosion current was observed upon increasing the load from 4 lb to 40 lb, but the OCP fell by 120 mV. Introduction of 4.38% sliding under 40 lb load caused a significant increase in I_{corr} with simultaneous decrease in OCP towards the more active side of the electrode potential. The strong passivation properties of the lubricating oil are suspected to be due to the large amount (13%) of emulsifier (sodium sulfonate) it contained.

TABLE 8. EFFECT OF LOAD AND SLIDING ON THE OCP AND I_{corr} IN THE PRESENCE OF A LUBRICANT

Run No.	Load, lb	Sliding, %	OCP, volts	I_{corr} , mA/cm ²
63	4	0	-0.10	3.59×10^{-4}
65	40	0	-0.22	4.1×10^{-4}
67	40	-4.38	-0.28	1.41×10^{-3}

Lubricant: 10% White-Kut 20.

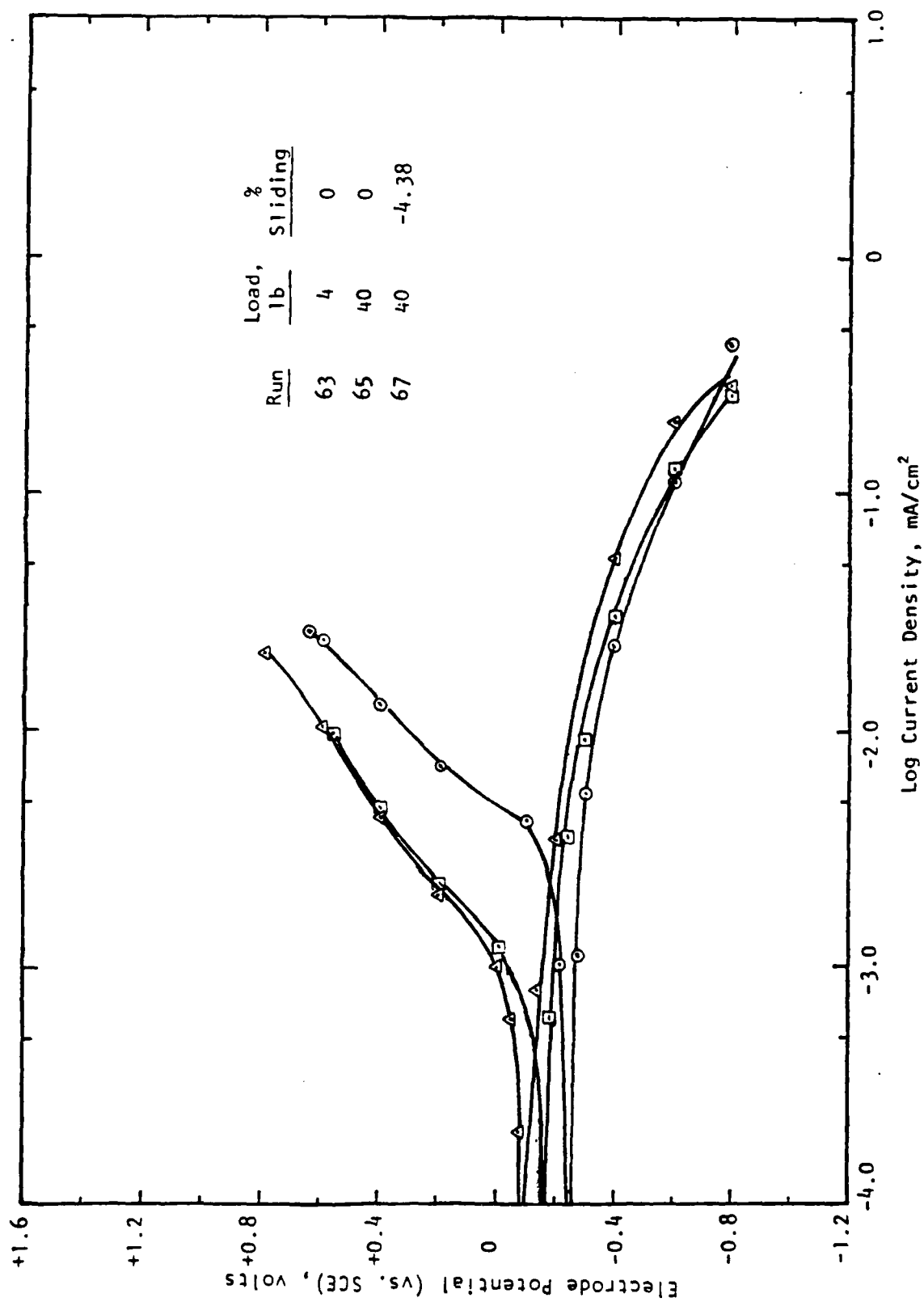


Figure 19. Effect of load and sliding on the polarization behavior under rolling and rolling-sliding motion in electrolyte containing 100 ppm NaCl and 10% lubricant.

The effect of Na_2MoO_4 on the electrochemical behavior under pure sliding motion was not studied since it was similar to that of NaNO_2 .

As a point to be noted, the study of the statistical effects of various assigned variables showed that an increase in percent sliding increased the OCP and reduced I_{corr} (though these changes were not significant); similarly, increase in load increased I_{corr} with little change in OCP. These results were the overall effects of many interacting species and inhibitors and, therefore, are expected to generate different conclusions than the study carried out adding a single inhibitor or a lubricant to the base NaCl solution as studied in this section.

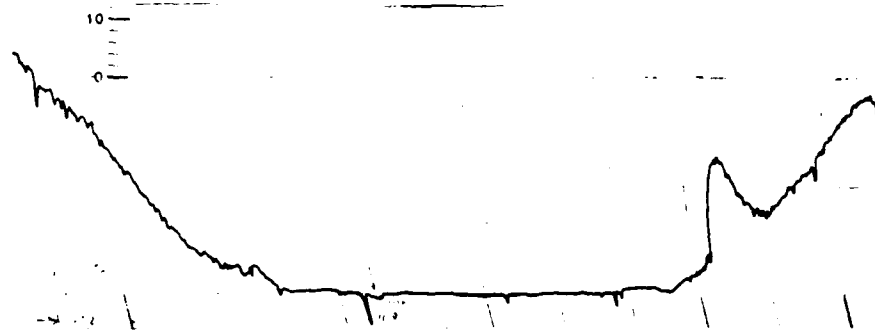
6.3 WEAR LOSS DETERMINED BY SURFACE ROUGHNESS MEASUREMENTS

Of the two rotating disk members, the smaller disk (sample) was selected for wear loss measurements since it was likely to wear more than the larger disk. Accordingly, five equally spaced locations along the disk edge were selected for surface roughness measurements using a profilometer and a Proficorder. These locations were marked with pencil, and the surface roughness across the disk edge was measured before and after the corrosion-wear tests.

Surface roughness measurements were carried out only across the metallic areas exposed to the electrolyte which constituted one-third the total edge area, the remaining two-thirds being coated with Teflon. Figures 20 and 21 show representative results. As seen from these figures, the stylus of the measuring instrument moved through the worn (by polishing) Teflon coating to the exposed metal and back to the Teflon coating again. The metallic portion of the disk edge was not exactly flat but was slightly concave due to polishing.

The surface roughness of the polished samples was $3 \mu\text{in.}^*$ whereas the as-ground samples had a roughness of $13 \mu\text{in.}^*$ both being the rms values. The difference in the profile geometry before and after the corrosion-wear test is expected to yield the wear loss due to simultaneous corrosion and wear.

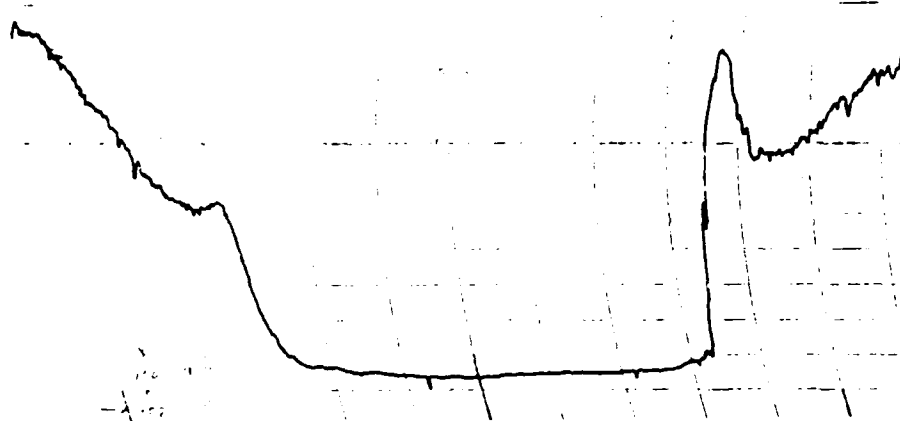
* $39.4 \mu\text{in.} = 1 \mu\text{m.}$



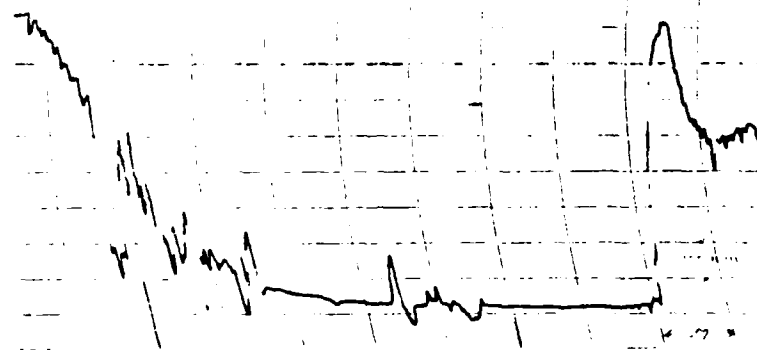
(a) Location A. before



(b) Location A. after

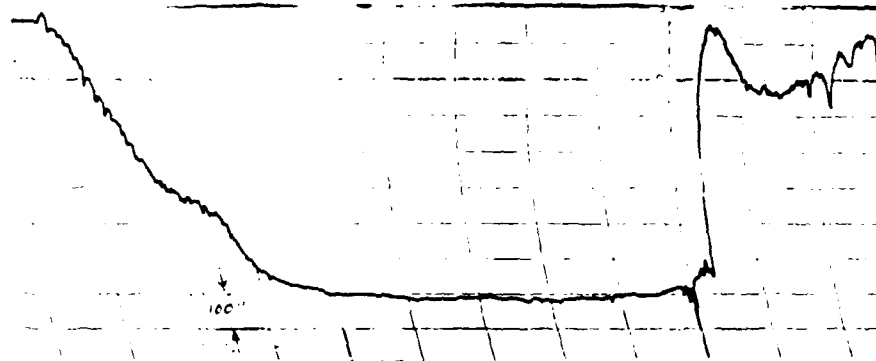


(c) Location B, before

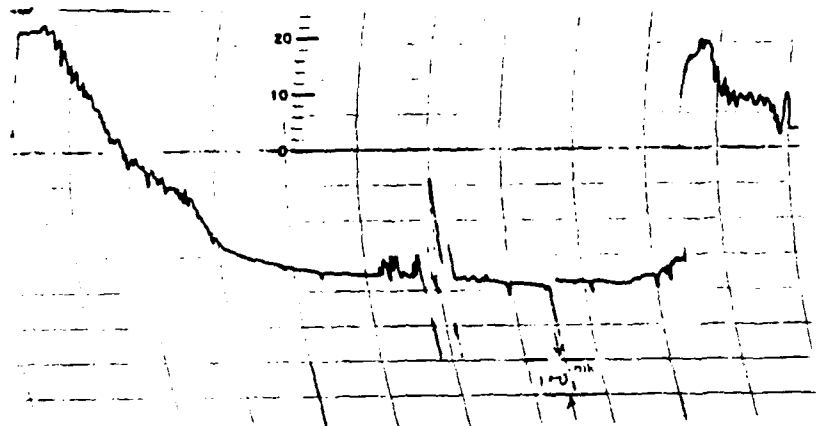


(d) Location B, after

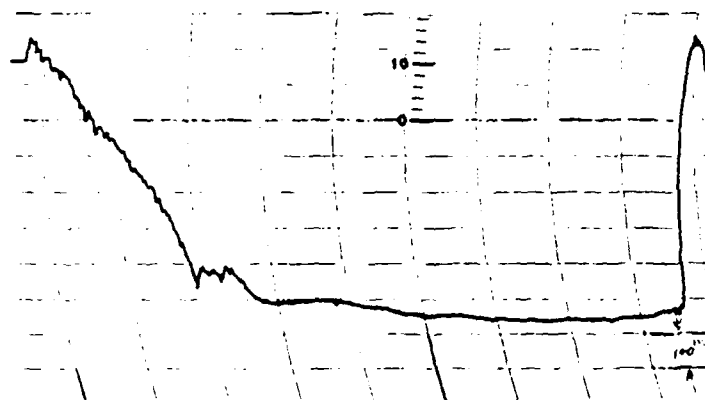
Figure 20. Difference between the surface profiles of the region around the wear track prior to and after the corrosion-wear tests. Samples tested in $\text{Na}_2\text{Cr}_2\text{O}_7$ (500 ppm) solution under 4 lb load in rolling motion. (Locations A through E represent different locations along the sample edge.)



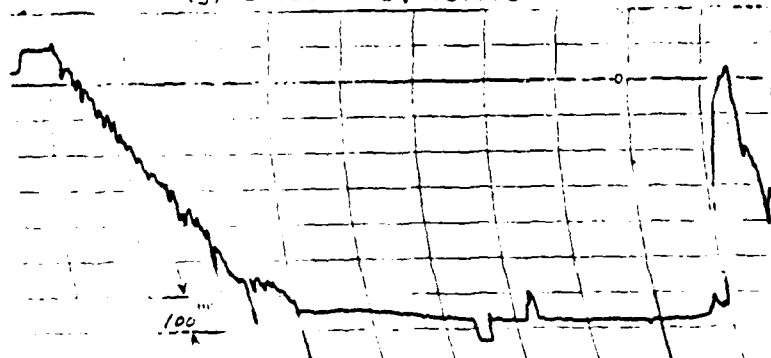
(e) Location C, before



(f) Location C, after

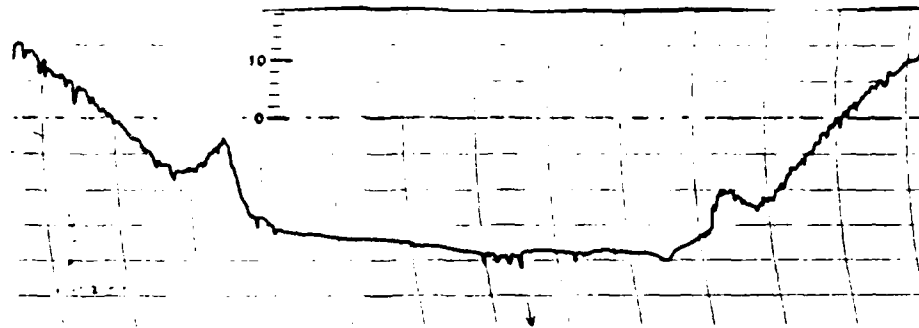


(g) Location D, before

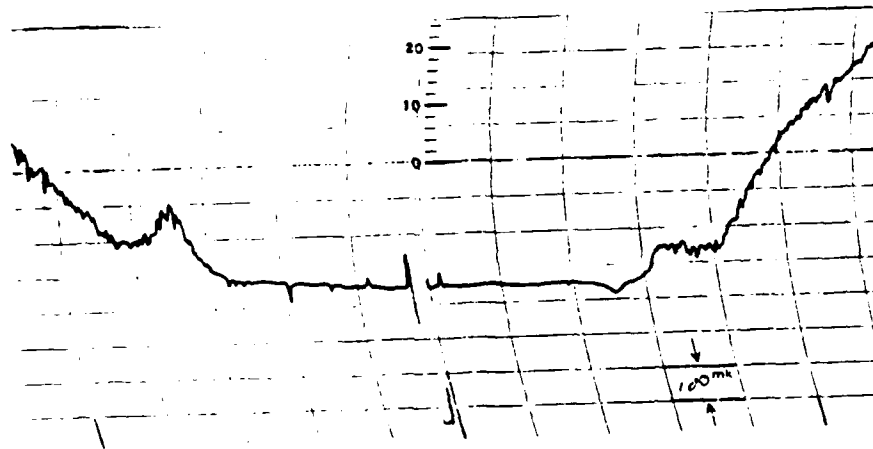


(h) Location D, after

Figure 20 (continued)



(i) Location E, before



(j) Location E, after

Figure 20 (continued)

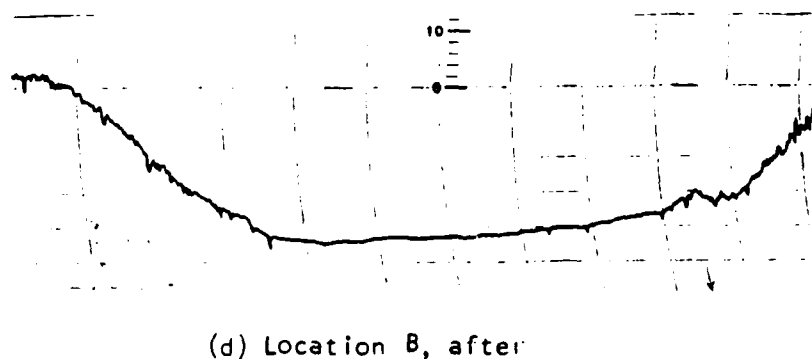
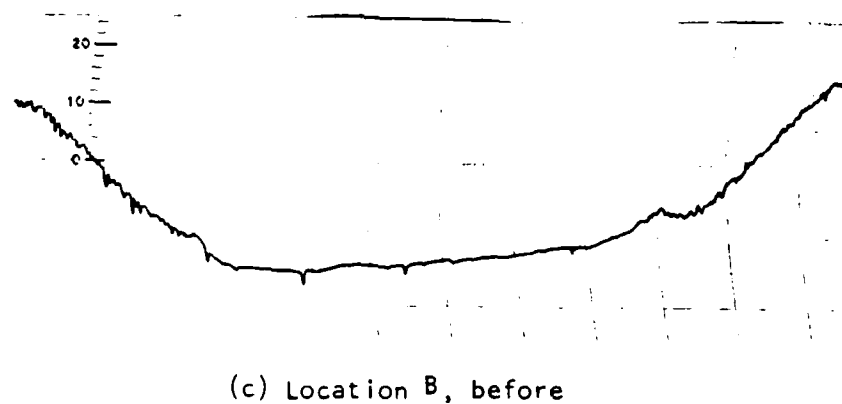
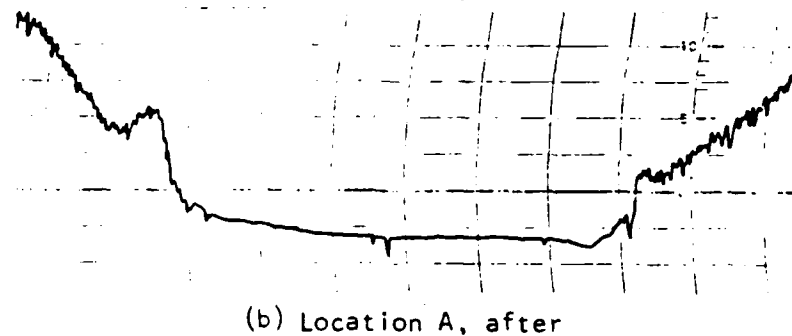
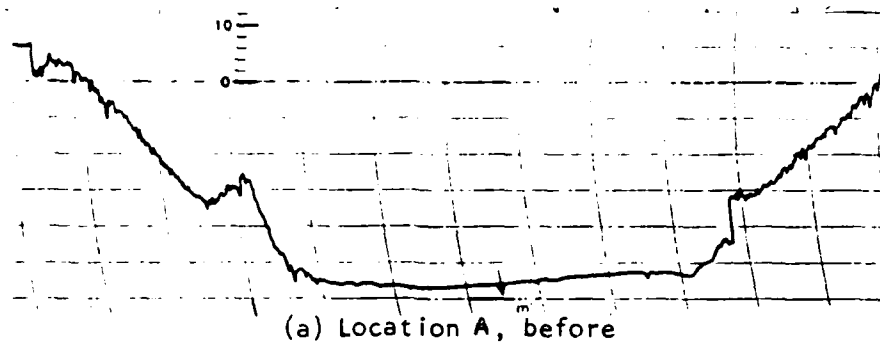
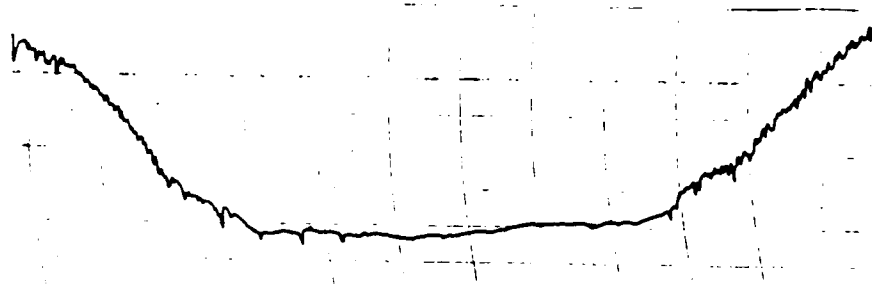


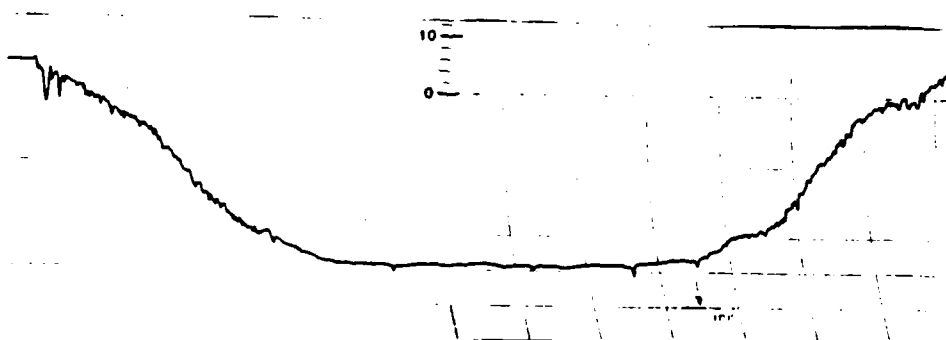
Figure 21. Difference between the surface profiles of the region around the wear track prior to and after the corrosion-wear test. Sample tested in 10% water-soluble oil (with NaCl) under 40 lb load in rolling motion. (Locations A through E represent various locations along the sample edge.)



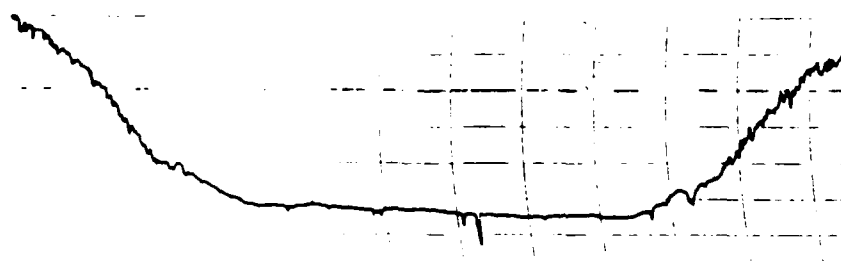
(e) Location C, before



(f) Location C, after

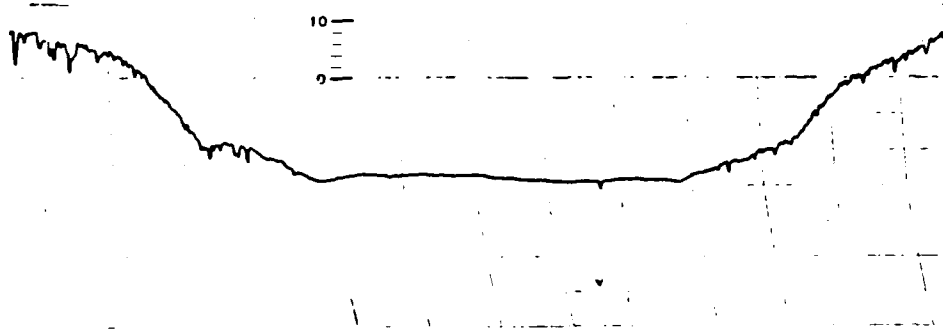


(g) Location D, before

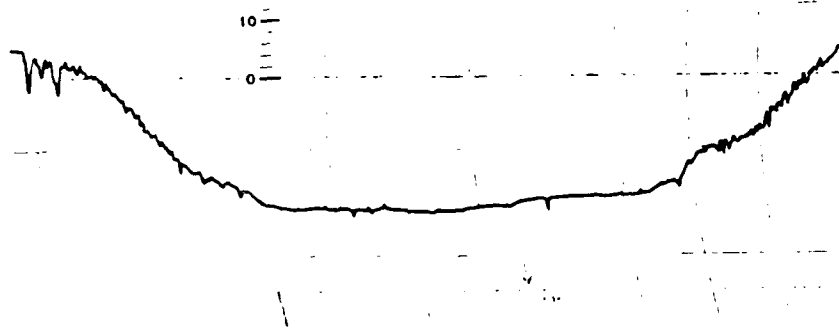


(h) Location D, after

Figure 21 (continued)



(i) Location E, before



(j) Location E, after

Figure 21 (continued)

The pairs of profiles cited above (Figures 20 and 21) show little difference in results before and after testing. A small perturbation observed for the sample under 4 lb load (Figure 20) is due to severe pitting on the sample along the line of contact and the presence of corrosion products inside the cracks. Many other runs carried out in similar manner did not show enough wear along their wear track for accurate evaluation.

Thus, the technique used here may be the only viable one for the quantitative evaluation of material removal by the simultaneously occurring corrosion and wear processes, but longer exposure times are essential to generate significant wear.

6.4 STUDY OF WEAR TRACKS

6.4.1 Studies Under the Optical Microscope

Of the 24 test runs made according to the statistical test matrix, 16 samples were selected to be studied under a binocular microscope after they were tested. During this study, general observations of the corroded surfaces, together with the measurement of track width, were made. Table 9 gives the track widths and a brief general description of the corroded surface, and Figures 22 to 37 are macrophotographs of the worn samples.

6.4.2 Studies Under the Scanning Electron Microscope

Optical microscopy indicated a variety of surface appearance types among the tested samples. To observe the samples in greater detail, scanning electron microscopy was carried out. A limited number of samples were selected for this purpose. Only samples with trial numbers 10, 3, 14, 6, and 4 (see Table 2) were examined. The reasons for selecting these will be evident from the following discussion. In addition, some pitted samples under pure rolling motion were studied, and all these results are presented here.

TABLE 9. RESULTS OF OPTICAL MICROSCOPY OF CORRODED SURFACES

Trial No. (Refer to Table 2)	Run No. (Fig No.)	Width of Wear Track, mm	Description of the Corroded Surface
1	37 (22)	1.10	Heavy corrosion all over, even within the wear track.
2	40 (23)	1.48	The wear track is stained with a whitish tinge. At some locations the white stain is turned dark brown, giving a burnt appearance. Sample is bright away from the track width. Sample grinding marks (very light) are present at places other than the track region.
3	42 (24)	1.20	The wear track is very dark and discontinuous.
4	55 (25)	a	Extremely light contact area. The whole surface is bright with some preexisting sample grinding marks.
5	43 (26)	1.05	The wear track here was bounded by two tarnished lines about 0.1-0.2 mm wide. Between these lines some fine pits are seen along with some sliding marks, which are all at an angle of about 20° to the rolling direction.
6	48 (27)	0.82	The wear track is tarnished (appears as dense, thick, white clouds). Spotty marks are seen at an angle of 30° to the rolling direction.
7	51 (28)	1.05	Light stain on the wear track. Sliding marks at an angle of 65°.
8	54 (29)	0.66	Very light stain on the wear track, a little milkier than the sample for trial 4 experiments.
9	49 (30)	1.50	Wear track is stained, sliding marks are at 50° to rolling direction.
10	35 (31)	1.05	The wear track lies between a lighter and a darker stained ring. The area in between is stained, yet shiny.
11	46 (32)	0.82	Track is all stained; small pits seem to be present in the track.
12	47 (33)	1.05 ^b	Heavy rust but not as in trial 5, 15, or 16; track boundary is not clearly defined.

TABLE 9 (continued)

Trial No. (Refer to Table 2)	Run No. (Fig. No.)	Width of Wear Track, mm	Description of the Corroded Surface
13	52 (34)	0.99	Stained area at the center. Sliding marks are at 65° to rolling direction.
14	45 (35)	0.77	Sample has a unique appearance. The stained area (wear track) is white with a crystalline appearance, and at the center a few distinct black spots are present.
15	33 (36)	1.65	Surface corrosion; wear track is rusted more on one side.
16	34 (37)	0.66	Pits and rusts all over; the wear track (rustier) is seen clearly.

^aCould not be measured.

^bThe boundaries are not distinct.



Neg. No. 57816

15X

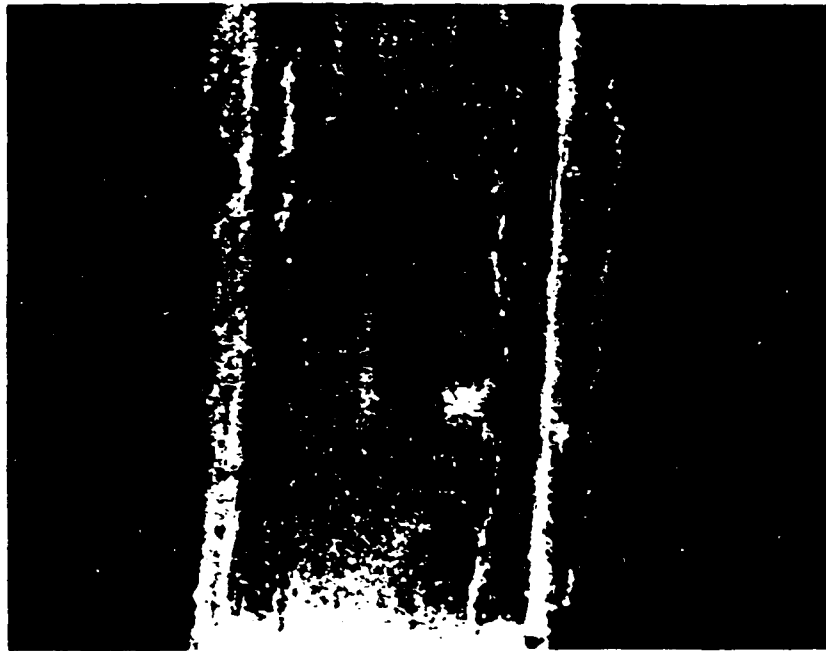
Figure 22. Appearance of the wear track when sample was tested under the trial 1 conditions in Table 2. Heavy corrosion is seen all over, and more pits have nucleated in the wear track.



Neg. No. 57818

15X

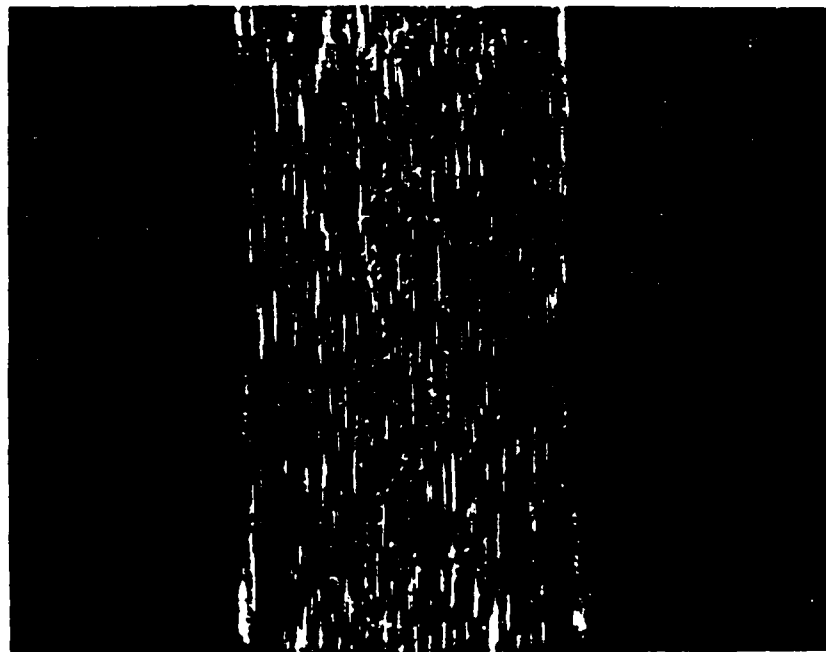
Figure 23. Appearance of the wear track when sample was tested under the trial 2 conditions in Table 2. The vertical lines are some of the pre-existing grinding marks. The wear track is on the left side of the shiny area. The track width is large here due to high load and -4.3% sliding. Parallel white lines, termed "sliding marks," are seen at an angle of about 60°-65° to the rolling direction.



Neg. No. 57820

15X

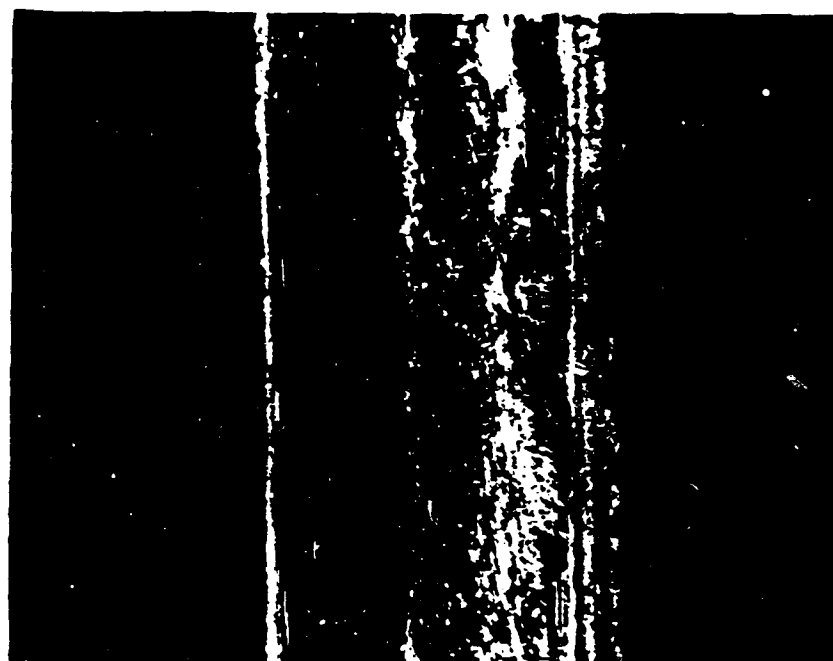
Figure 24. Appearance of the wear track when sample was tested under trial 3 conditions in Table 2. A discontinuous wear track is visible. Numerous sliding marks (appearing as fine lines inside the track) are along the rolling direction.



Neg. No. 57819

15X

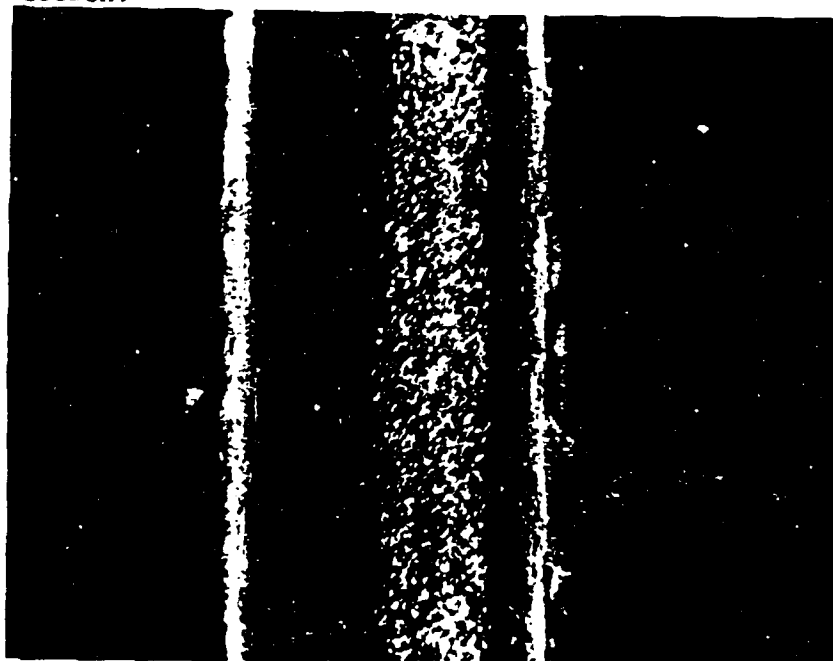
Figure 25. Appearance of the wear track when sample was tested under trial 4 conditions in Table 2. The whole sample surface is bright with no wear track. Some fine white dots are seen at the center of the sample which suggest the contact path.



Neg. No. 57821

15X

Figure 26. Appearance of the wear track when sample was tested under the trial 5 conditions in Table 2. The two tarnished lines (appearing white in the photo) contain the wear track on one side of the uncoated region. Very fine sliding marks are seen inside making a low angle to the rolling direction.



Neg. No. 57822

15X

Figure 27. Appearance of the wear track when sample was tested under the trial 6 conditions in Table 2. Wear track is on one side, appearing whitish and filled with spotty marks. These marks seem to align at an acute angle to the rolling direction.

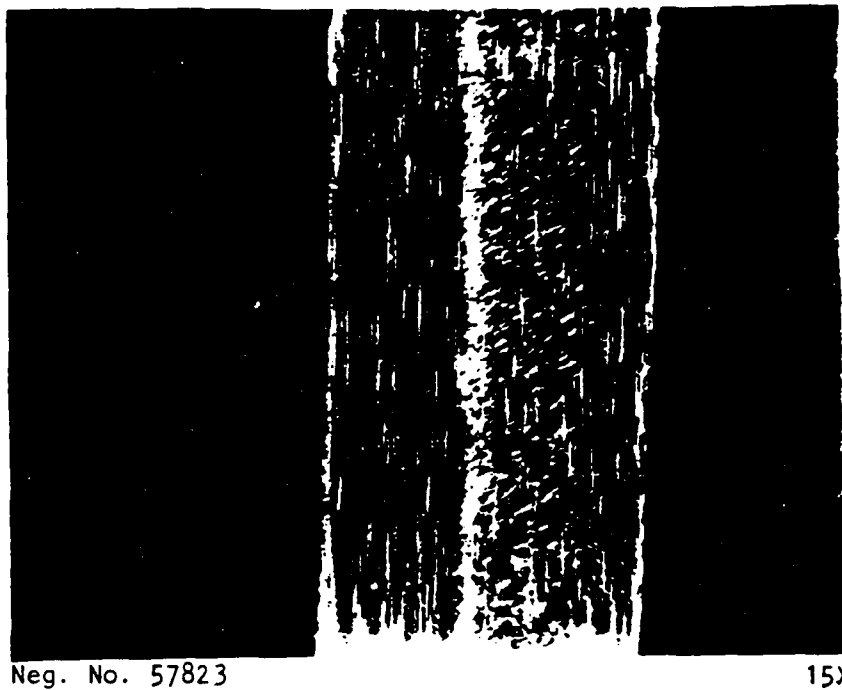


Figure 28. Appearance of the wear track when sample was tested under the trial 7 conditions in Table 2. Wear track is slightly to one side. Whitish wear marks are seen at an angle of about 65° to the rolling direction. Grinding marks on sample surface prior to polishing are seen even inside the wear marks.

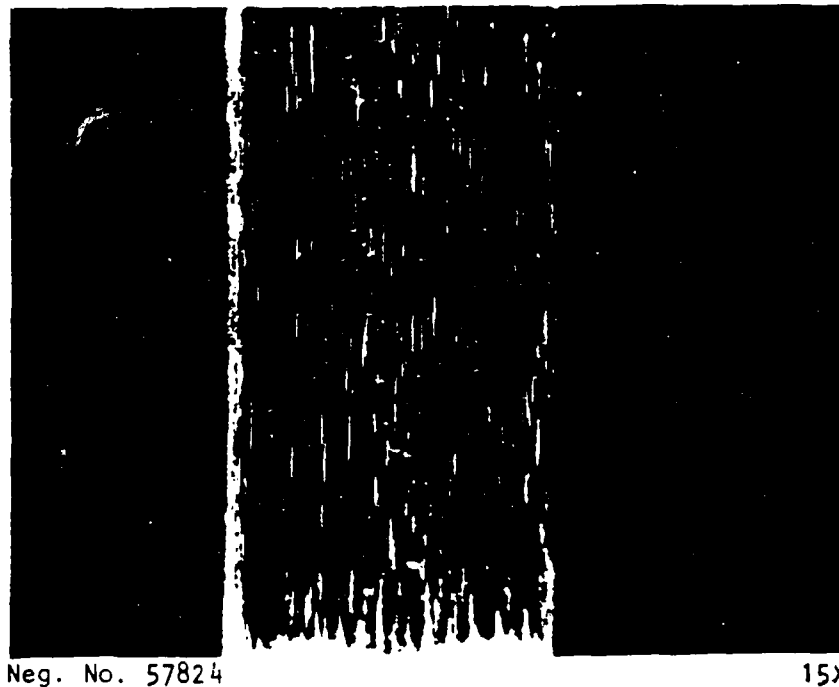
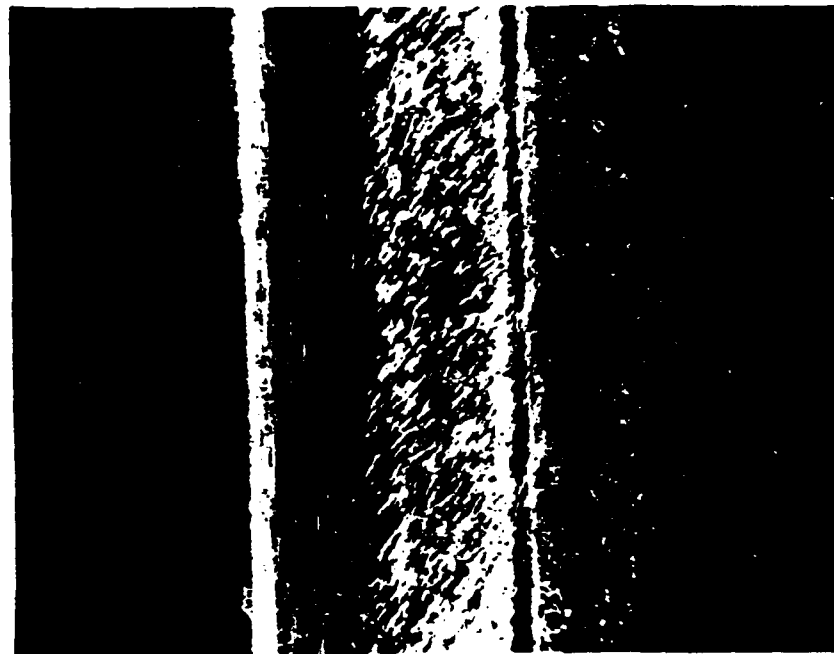


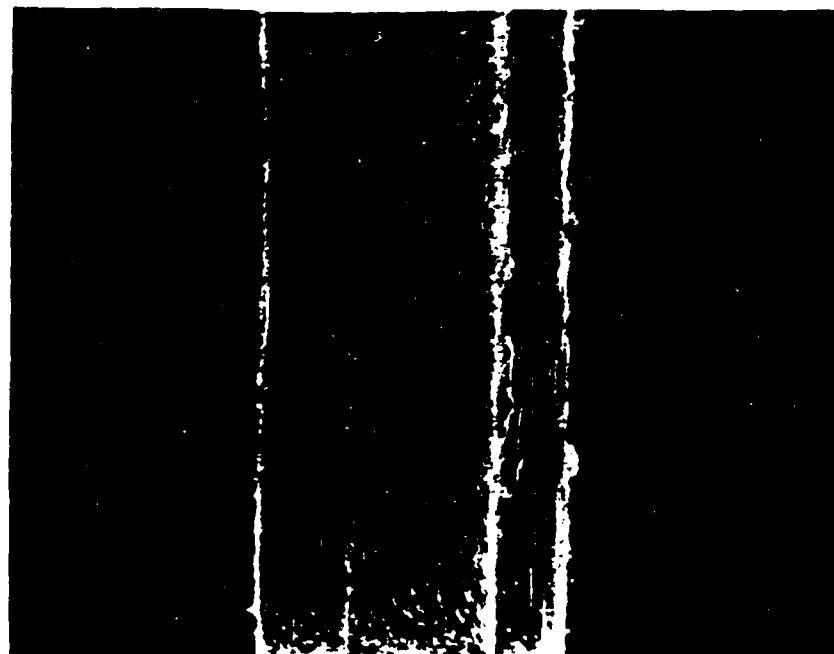
Figure 29. Appearance of the wear track when sample was tested under the trial 8 conditions in Table 2. Wear track is indicated by a very light stain and an array of light dots. Preexisting surface grinding marks on the samples are seen parallel to rolling direction.



Neg. No. 57825

15X

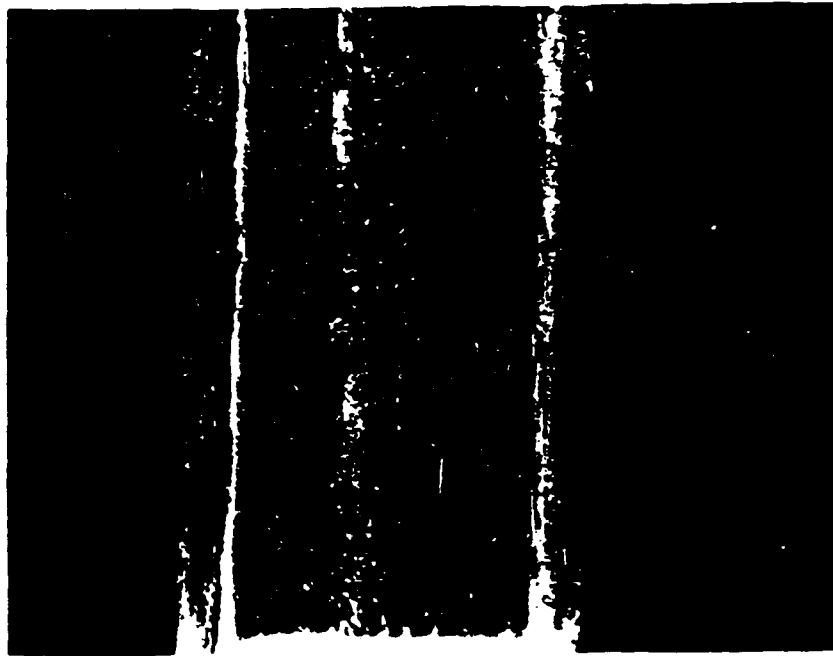
Figure 30. Appearance of the wear track when sample was tested under the trial 9 conditions in Table 2. Wear track is to one side. Sliding marks are seen at an angle of 50° to the rolling direction.



Neg. No. 57826

15X

Figure 31. Appearance of the wear track when sample was tested under the trial 10 conditions in Table 2. The wear track is a little wider, probably due to some axial shift during rotation. The replicate sample had a narrower track but both the wear tracks appeared the same--stained.



Neg. No. 57827

15X

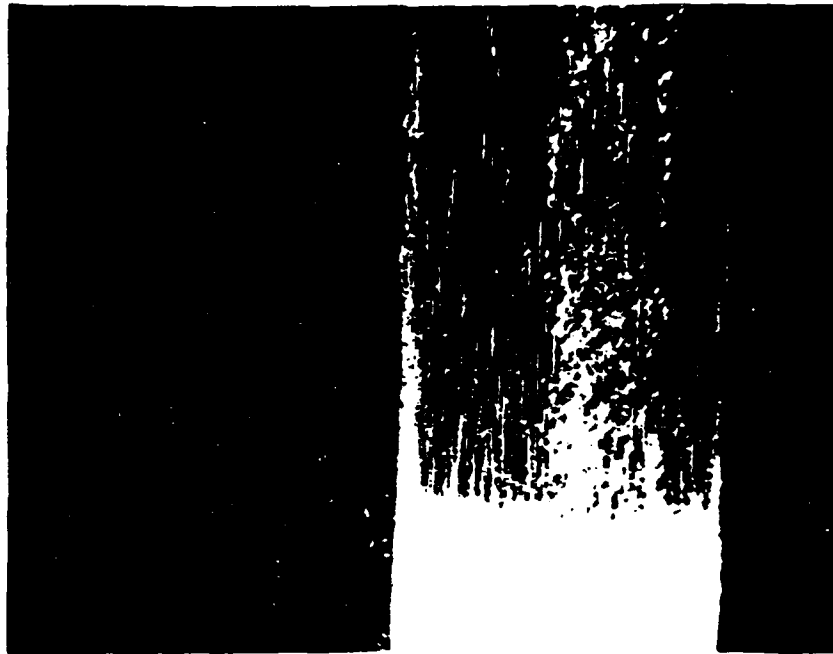
Figure 32. Appearance of the wear track when the sample was tested under the trial 11 conditions in Table 2. Whitish line (brownish on sample) is the wear track with small white dots. Very little corrosion in the wear track.



Neg. No. 57828

15X

Figure 33. Appearance of the wear track when the sample was tested under the trial 12 conditions in Table 2. Heavy rust deposit is seen on the wear track but shiny areas away from it.



Neg. No. 57829

15X

Figure 34. Appearance of the wear track when sample was tested under the trial 13 conditions in Table 2. Stained and exhibiting sliding marks.



Neg. No. 57830

15X

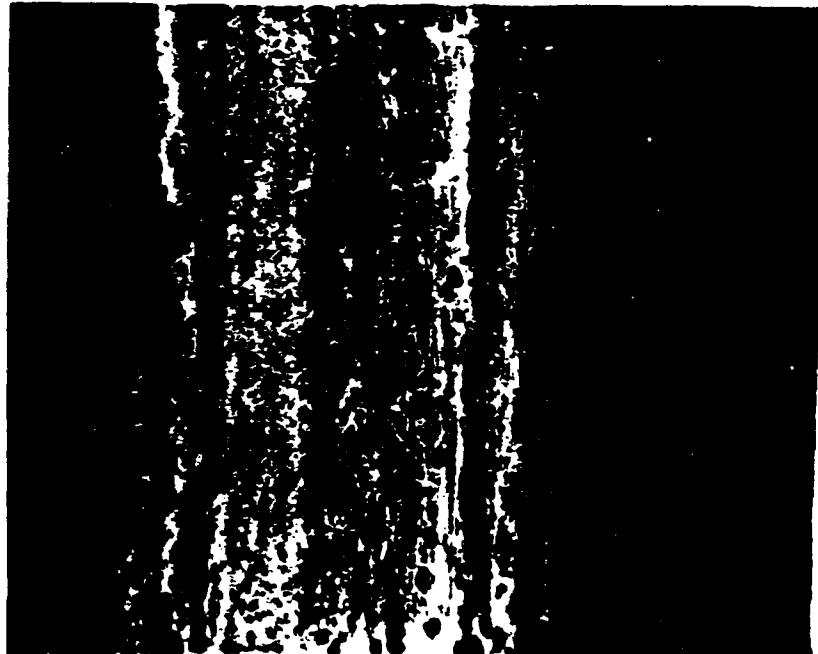
Figure 35. Surface appearance when sample was tested under the trial 14 conditions in Table 2. Fine black and white dots are seen in the wear track giving a crystalline appearance.



Neg. No. 57831

15X

Figure 36. Surface appearance when sample was tested under the trial 15 conditions in Table 2. Corrosion product is seen all over the sample more on the wear track which is seen left of center.



Neg. No. 57832

15X

Figure 37. Surface appearance when sample was tested under trial 16 conditions in Table 2 with no inhibitor in electrolyte. Many corrosion pits all over the sample. Finer ones are on the wear track (towards the left of center).

Figure 38 shows the appearance of the surface away from the wear track for a sample from trial 10 (Table 2). It shows some preexisting grinding marks and some surface voids. The surface is very clean with no rust spots or pits. Examination of the wear track, however, indicates a completely smooth surface of rolling-sliding with almost no features to record on the SEM. This sample had the highest corrosion current density of all the samples in the test matrix.

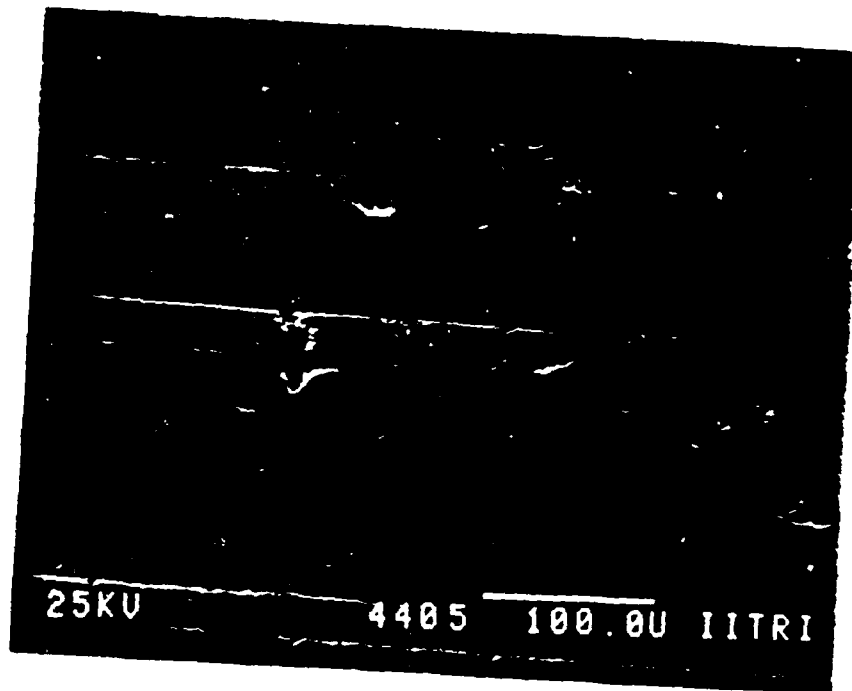
Both samples subjected to trial 3 conditions had alternate shiny and dull areas along the contact line. While the shiny areas had the morphology seen in Figure 39, the dull areas had fine pits lined up in a direction perpendicular to the rolling direction as shown in Figure 40, as is evident in Figure 24.

Figures 39 and 40 show the surface morphologies of samples tested according to trial 3 conditions, yielding moderately high corrosion current density. Trial 14 (Table 2) was associated with corrosion conditions that yielded moderately low corrosion current density. These and similar samples with moderately low corrosion current density showed extensive pitting and accumulation of corrosion products on the wear track. Figures 41 and 42 show features on the wear track and away from it. Numerous pits on the wear track (Figure 41) apparently gave the crystalline appearance on the contact surface of samples from run 45 under the optical microscope.

Figures 43 and 44 show the wear track appearance for test conditions yielding very low current densities. Low current density results in very little metal dissolution and thus preserves the sliding and grinding marks.

While the surface morphologies of different samples can be explained through the observed current density, the optical microscope observation of some light lines, termed "sliding marks," cannot be explained without extensive investigation. The occurrence of these lines is probably associated with the addition of lubricant to the electrolyte and may be the asperity contact areas.

Even under very light loads and pure rolling motion (4 lb) in the presence of inhibitors like NaNO_2 and $\text{Na}_2\text{Cr}_2\text{O}_7$, pits can originate along the line of contact. Figure 45 illustrates such a situation on a sample with smooth surface under 4 lb contact load and pure rolling motion. Earlier (in report



480X

Figure 38. Surface morphology away from the wear track for a sample tested under corrosion-wear conditions of trial 10 in Table 2.



1000X

Figure 39. Sample surface when the sample was tested under the trial 3 conditions in Table 2. Uneven metal dissolution and pitting in some locations.

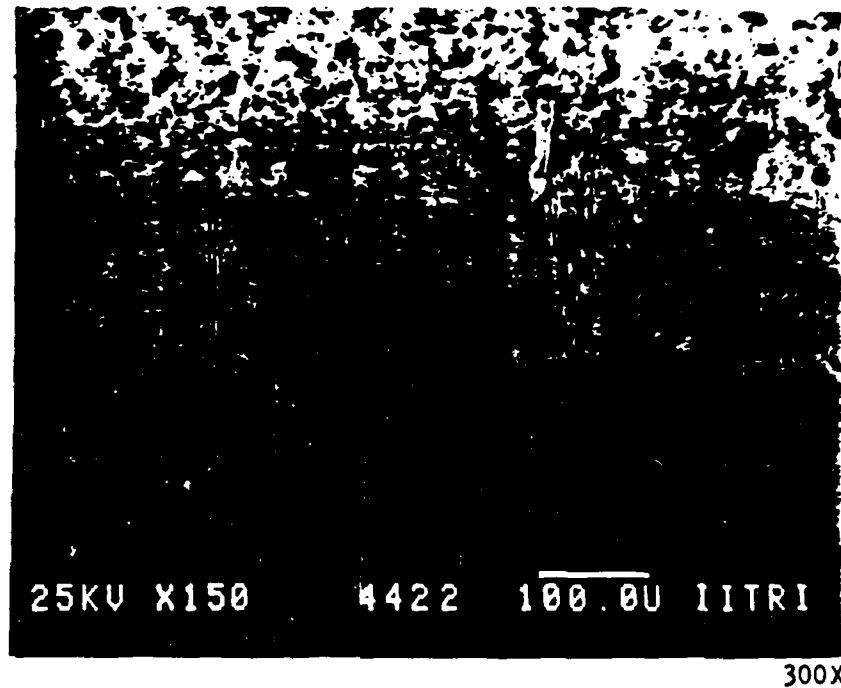


Figure 40. Wear pattern of M50 steel with same load and electrolyte as in Figure 39 but showing the dull areas on the wear track. Note the array of pits along the axis of sample rotation and perpendicular to the line of rolling-sliding. These pits are seen in areas where localized slip (sliding) occurs during testing.

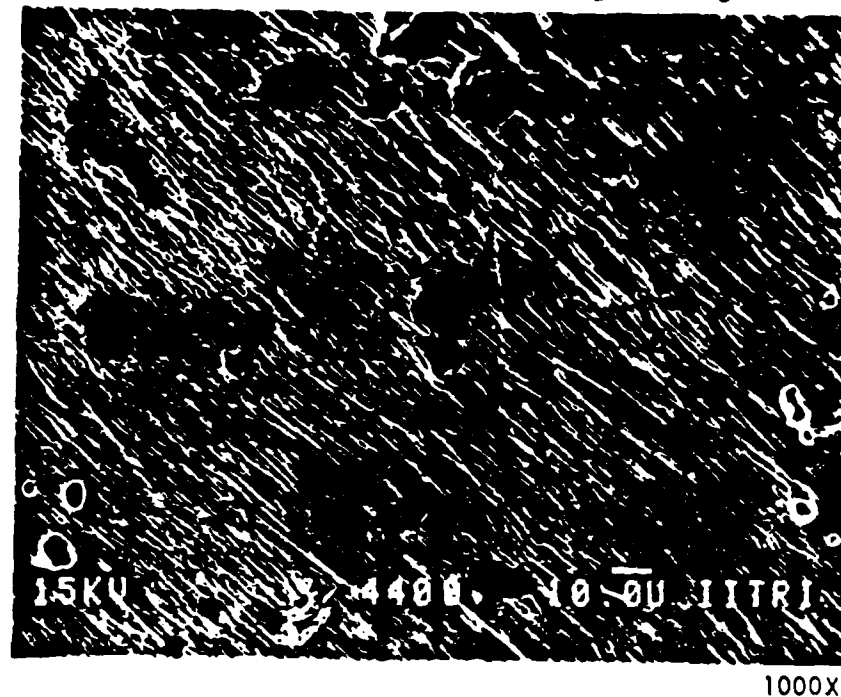


Figure 41. Features on the wear track of a sample tested under the trial 14 conditions in Table 2. Pit formation and wear marks are evident.

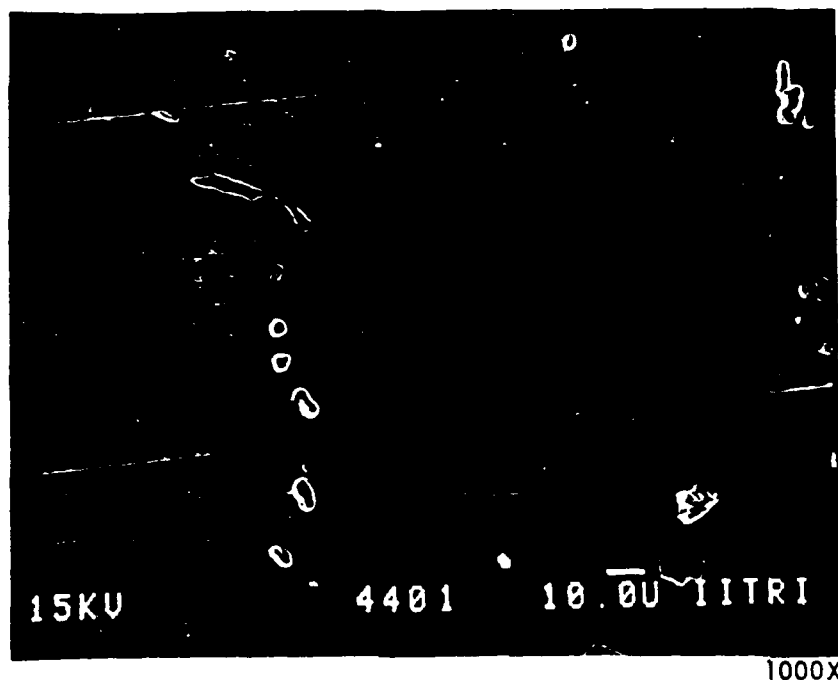


Figure 42. Features of area away from the wear track (same sample as Figure 41). Here the surface appears to be smooth, with some pits formed by metal dissolution.

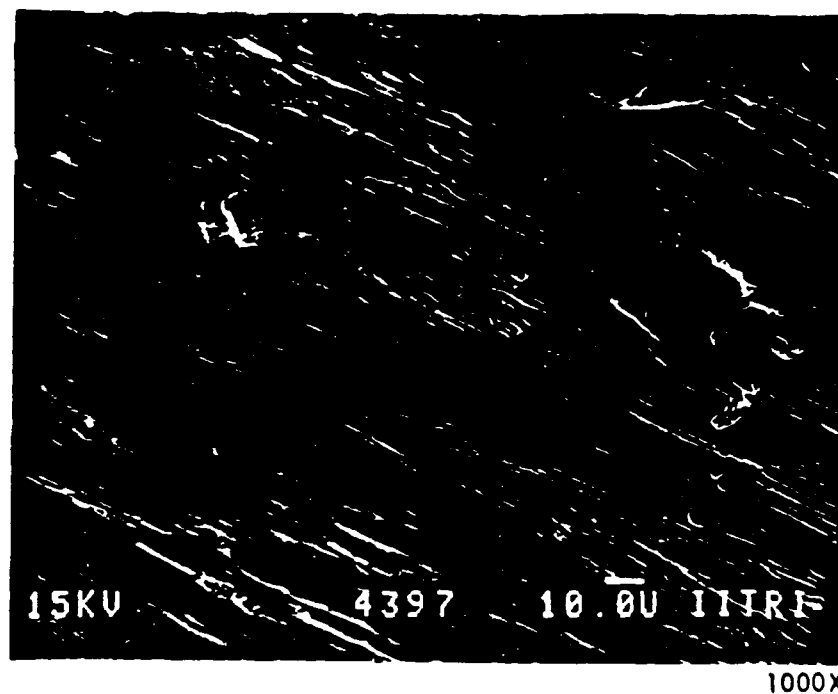


Figure 43. Asperity contact areas, which are the sliding marks, and some evidence of metal dissolution on sample tested under trial 6 conditions in Table 2.

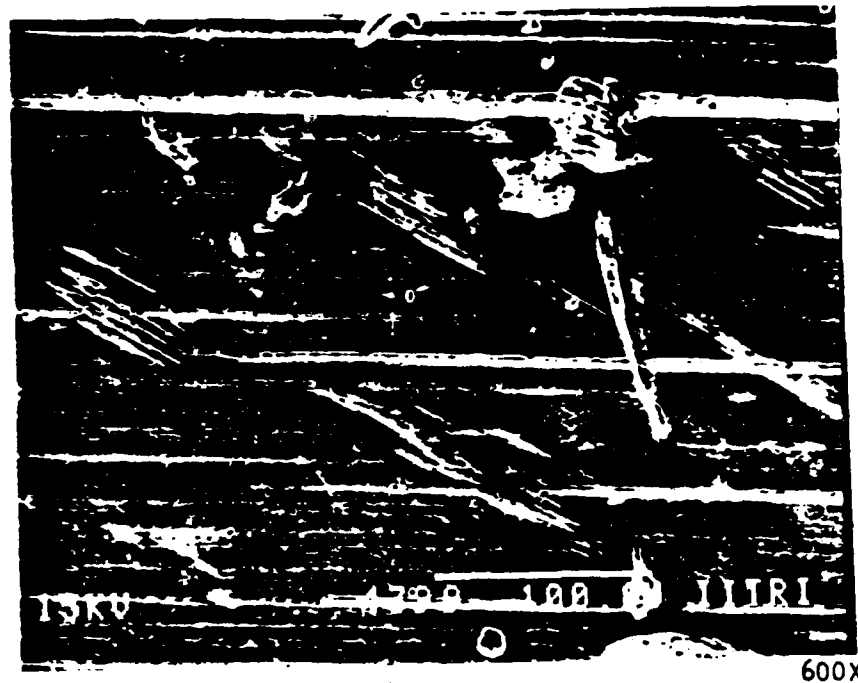


Figure 44. Sliding marks at an angle to the rolling direction on sample tested under the trial 4 conditions in Table 2. Preexisting grinding marks are seen along the rolling direction.

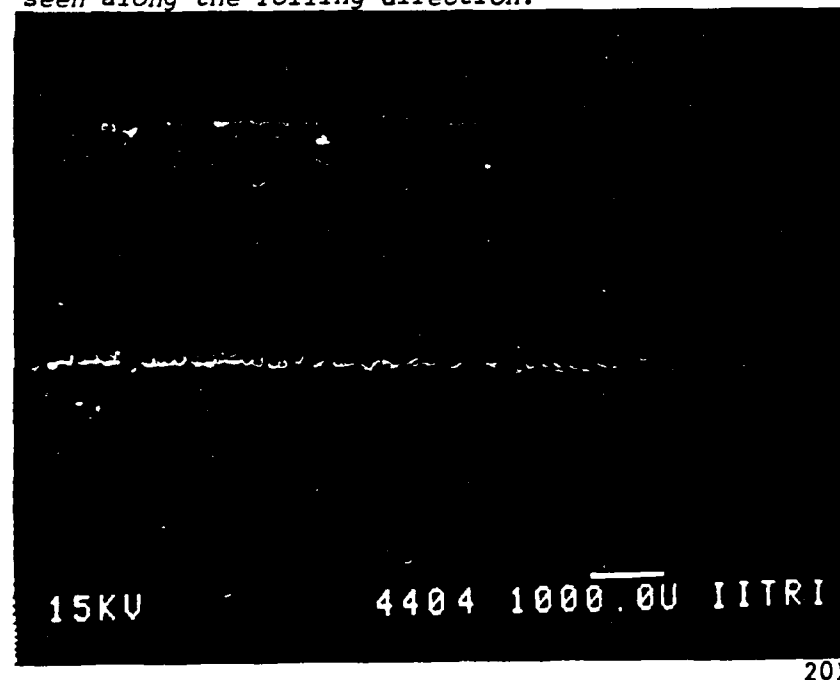


Figure 45. Sample from run 59, showing an array of pits generated along the line of contact. 500 ppm $\text{Na}_2\text{Cr}_2\text{O}_7$ was added to electrolyte for sample under 4 lb load in rolling motion.

No. IITRI-M06140-4), the surface of a ground-finish sample tested in an electrolyte containing 500 ppm NaNO_2 was shown. The difference between Figure 45 and the earlier sample is that the smooth-surfaced sample immersed in $\text{Na}_2\text{Cr}_2\text{O}_7$ inhibitor (Figure 45) had many more pits than the sample with a ground finish and tested in 100 ppm NaCl solution containing 500 ppm NaNO_2 , probably because the ground-finish sample had fewer asperity contacts with the loading disk.

7. CONCLUSIONS

The critical and extensive tests carried out in this program have advanced the understanding of the corrosion-wear phenomenon occurring in load-bearing components in the naval environment. It was demonstrated again with rolling and rolling-sliding motion that the IITRI-designed "dynamic corrosion-wear cell" is a versatile tool capable of monitoring simultaneously occurring corrosion and wear in any electrolyte system by the polarization technique.

In agreement with other prior IITRI corrosion-wear studies, wear proved to control the anodic polarization process significantly, but rarely the cathodic polarization process. This understanding of the corrosion-wear mechanism indicates that the stability and repairability of the passive film with critically selected corrosion inhibitors will be of paramount importance in these tribological systems.

Even under rolling conditions, the effect of wear was significant in the removal of the passive film as indicated by an increase in corrosion current and often a decrease in OCP. Damage of the passive film occurred only along the line of rolling contact, initiating a series of pit nucleations. An increase in load increased the contact area between the rolling surfaces, thereby inducing an increase in overall corrosion current density and a consequent drop in OCP.

Of all the inhibitors and lubricants studied in this program, NaNO_2 is the most suitable under pure rolling and light loading conditions and $\text{Na}_2\text{Cr}_2\text{O}_7$ is perhaps the least preferred mainly because of its unpredictability in the passivation process and generation of a less tenacious passive film (compared to NaNO_2 under identical rolling conditions).

Results from the statistical analyses of the tests based on a Plackett-Burman matrix indicated that there is more than one variable exerting significant influence on the triboelectrochemical parameters. The significant variables at confidence levels of 80% or more are as follows (in descending order):

<u>Parameters Being Affected</u>	<u>Variables</u>
Open-circuit potential	Sodium dichromate, and percent sliding
Corrosion current density	Sodium dichromate, lubricant, and contact stress

Of all these variables, sodium dichromate was found to be the most powerful one affecting both I_{corr} and OCP. Individual polarization diagrams indicate that the influence of sodium dichromate is most dramatic when lubricant is absent and NaNO_2 and/or Na_2MoO_4 is present. A combination of $\text{Na}_2\text{Cr}_2\text{O}_7$ and NaNO_2 was found to be most effective in the absence of the lubricant.

Evaluation of tested samples by optical microscopy revealed many unique surface morphologies; very smooth surfaces were seen under very high corrosion currents, whereas surface damage due to wear was retained under very low corrosion currents. Test conditions inducing intermediate values of corrosion current showed deposition of corrosion products on the surface and the nucleation of pits. While the pits nucleated along the rolling direction under pure rolling motion, the introduction of small amounts of sliding helped nucleate these pits in a direction perpendicular to the rolling direction.

AD-A189 603

CORROSION-WEAR PROCESS UNDER ROLLING-SLIDING MOTION(U)
IIT RESEARCH INST CHICAGO IL 8 PANDA AUG 87
IITRI-M06140-6 NADC-87151-60 N62669-85-C-0265

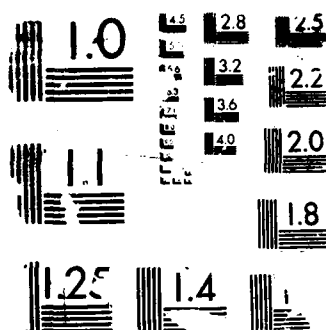
2/2

UNCLASSIFIED

F/G 13/9

NL





RESOLUTION TEST CHART

8. RECOMMENDATIONS FOR FUTURE RESEARCH

One conclusion of this study is that a considerable reduction in the aggressiveness of corrosive environments could be achieved by the use of inhibitors and lubricants under the milder and yet more realistic rolling-sliding condition. While some combination of inhibitors and test conditions resulted in an almost shiny bearing surface at the end of testing, some other conditions resulted in pitting to a serious degree. Since the occurrence of these pits is of prime importance in bearing failures in naval aircraft, their origin and growth under the rolling and rolling-sliding contact wear track should be carried out in the future. The IITRI-designed experimental setup could be used for such a study. The effects of materials parameters such as inclusions, their distribution, hardness and heat treatment, and retained austenite should also be studied so that parameters can be optimized for minimum pit formation.

During the study, the dramatic effect of the combination inhibitors in reducing corrosion was well demonstrated. Although the program included some of the well-known inhibitors, many more inhibitors and lubricants remain to be evaluated. Further studies with other lubricants and inhibitors (especially the new inhibitor DNBM and some cathodic inhibitors) can be initiated.

Wear rates under rolling-sliding conditions are very low, and longer exposures are needed for their more accurate and quantitative determination. To study the interplay of corrosion and wear and to understand the synergism of the two processes, additional experiments with prolonged exposure to the corrosion-wear environment are needed so that the material loss due to wear and corrosion can be evaluated separately.

The presence of a passivated layer between the two rolling surfaces undergoing rolling-sliding motion will change the coefficient of friction between the rolling and sliding surfaces by generating a composite of the passivated layer backed by a metal substrate. The coefficient of friction under dynamic conditions would not only depend on the thickness and physico-mechanical properties of the passivated layer, but also on the size and shape

of associated asperities. The influence of inhibitors and lubricants on this coefficient of friction under rolling and rolling-sliding motion is another aspect of corrosion-wear research worth pursuing.

In summary, IITRI suggests that future corrosion-wear studies take the following directions:

- Study of the nucleation and growth of corrosion pits under wear conditions incorporating rolling and rolling-sliding motion.
- Evaluation of more combination inhibitors.
- Frictional measurements under rolling-sliding conditions in the presence of combination inhibitors and lubricants.

REFERENCES

1. K. Y. Kim and S. Bhattacharyya, "Wear and Corrosion of Components Under Stress and Subjected to Motion," Interim Report, NADC-79137-60, Naval Air Development Center, Warminster, Pa., February 1982.
2. K. Y. Kim and S. Bhattacharyya, "Wear and Corrosion of Components Under Stress and Subjected to Motion," Final Report NADC 79137-60, Naval Air Development Center, Warminster, Pa., March 1984.
3. C. Wagner and W. Trand, *Z. Elektrochem.*, **44**, 391 (1938).
4. J. D. Stove and K. A. Phillips, A Modern Approach to Chemistry, Heinemann, 1963.
5. R. W. Edwards, *Sch. Sci. Rev.* **52**, 155 (September 1970).
6. E. C. Potter, Electrochemistry, Cleaver-Hume, 1956, p. 342.
7. I. L. Rozenfeld, "Mechanism for Protecting Iron from Corrosion with Sodium Nitrite," *Doklady Akad. Nauk SSSR*, **78**(3), 523 (May 1951).
8. I. N. Putilova et al., Metallic Corrosion Inhibitors, Pergamon Press, New York, 1960.
9. A. Wachter and S. S. Smith, "Preventing Internal Corrosion of Pipelines," *Ind. Eng. Chem.*, **35**, 358 (1943).
10. M. Cohen, "An Electron Diffraction Study of Films Formed by Sodium Nitrite Solution in Iron," *J. Phys. Chem.*, **56**, 451 (April 1952).
11. M. Cohen and A. F. Beck, "Passivity of Iron in Chromate Solutions," *Z. Elektrochem.*, **62**, 696 (1958).
12. A. H. Kingsbury, "Passivation of Iron and Steel in Chromate Solutions," *J. Australian Inst. Metals*, **4**, 12 (May 1959).
13. T. O. Mulhearn and L. E. Samuels, "The Abrasion of Metals: A Model of the Process," *Wear*, **5**, 478 (1962).
14. F. W. Carter, *Proc. Roy. Soc. London*, **A112**, 151 (1926).
15. H. Poritsky, *J. Appl. Mechanics*, **72**, 191 (1950).
16. K. L. Johnson, Rolling Contact Phenomena, Joseph B. Bidwell (Ed.), Elsevier Publishing Co., Amsterdam/New York, 1961, p. 6.
17. R. T. Spurr, "The Static and Dynamic Friction of Metals," *Wear*, **19**, 61 (1972).

18. R. T. Spurr, "The Equation for the Friction of Metals," *Wear*, **40**, 389 (1976).
19. A. T. Male, *J. Inst. Metals*, **93**, 288 (1964-1965).
20. *Ibid.*, p. 489.
21. A. T. Male, Friction and Lubrication in Metal Processing, ASME, New York, 1966, p. 200.
22. J. A. Rogers and G. W. Rowe, *J. Inst. Metals*, **95**, 257 (1967).
23. C. F. Hinsley, A. T. Male, and G. W. Rowe, *Wear*, **2**, 233 (1968).
24. F. T. Barell, *Treatise in Mater. Sci. Technol.*, **13**, 2 (1979).
25. M. H. Jones, *ASLE Trans.*, preprint No. 76-LC-2B-3, 1976.
26. E. Rabinowicz, Friction and Wear of Materials, John Wiley and Sons, New York, 1965, p. 186.
27. K. Y. Kim and S. Bhattacharyya, Quarterly Progress Report No. IITRI-M06060-14 for Naval Air Development Center, March 1982.
28. M. G. Fontana and N. D. Greene, Corrosion Engineering, McGraw-Hill Book Company, New York, 1978, p. 328.
29. J. I. Bregman, Corrosion Inhibitors, The Macmillan Company, New York, 1963, p. 97.
30. R.L. Plackett and J. P. Burman, *Biometrika*, **33**, 305 (1946).
31. J. W. Dini and H. R. Johnson, "Use of Strategy of Experimentation in Gold Plating Studies," *Plating and Surface Finishing*, **68**(2), 52 (1981).
32. J. Heidemeyer, *Wear*, **66**, 379 (1981).

APPENDIX

**LIST OF VARIABLES AND THE OBSERVED OPEN-CIRCUIT POTENTIAL
AND CORROSION CURRENT DENSITY VALUES IN RUNS PERFORMED**

NADC-87151-60

Run No.	Trial No. in Table 2	% Slip	Load on Sample, lb	Inhibitor			Lubri-cant, ^a %	pH	OCP, volts	I _{corr} , mA/cm ²	Comments
				NaNO ₂ , ppm	Na ₂ Cr ₂ O ₇ , ppm	Na ₂ MoO ₄ , ppm					
33	15	-2.19	4	10	500	0	0	5.5	-0.246	1.46 x 10 ⁻³	
34	16	-2.19	4	0	0	0	0	7.1	-0.345	4.82 x 10 ⁻³	
35	10	-2.19	40	500	0	500	0	7.5	-0.377	2.23 x 10 ⁻²	
36	5	-2.19	40	500	500	500	0	5.8	-0.007	1.26 x 10 ⁻³	
37	1	-4.38	4	0	0	500	0	6.8	-0.199	2.92 x 10 ⁻³	
38	3	-4.38	40	500	0	0	0	7.6	-0.310	1.63 x 10 ⁻²	
39	4	-4.38	40	500	500	0	0	5.6	+0.17	--	Not reported
40	2	-4.38	40	0	0	0	10	9.7	-0.275	2.91 x 10 ⁻³	
41	4	-4.38	40	500	500	0	0	5.6	-0.052	0.451 x 10 ⁻³	Repeat of run 39
42	3	-4.38	40	500	0	0	0	7.7	-0.335	1.30 x 10 ⁻²	Repeat of run 38
43	5	-2.19	40	500	500	500	0	5.8	-0.003	1.09 x 10 ⁻³	Repeat of run 36
44	13	-2.18	40	0	0	500	10	9.7	-0.345	2.61 x 10 ⁻³	
45	14	-2.18	4	500	0	0	10	9.7	-0.250	1.41 x 10 ⁻³	
46	11	-2.18	40	500	500	0	10	7.8	-0.139	1.10 x 10 ⁻³	
47	12	-4.38	4	0	500	500	0	6.3	-0.078	0.99 x 10 ⁻³	
48	6	-4.38	4	500	500	500	10	7.8	-0.141	1.30 x 10 ⁻³	
49	9	-4.38	40	0	500	0	10	8.0	-0.145	1.64 x 10 ⁻³	
50	7	-2.19	40	0	500	500	10	8.0	-0.178	1.78 x 10 ⁻³	
51	7	-2.19	40	0	500	500	10	7.9	-0.162	1.38 x 10 ⁻³	Repeat of run 50
52	13	-2.18	40	0	0	500	10	9.6	-0.300	2.29 x 10 ⁻³	Repeat of run 44
53	8	-4.38	4	500	0	500	10	9.3	-0.238	0.62 x 10 ⁻³	
54	8	-4.38	4	500	0	500	10	9.4	-0.248	0.80 x 10 ⁻³	Repeat of run 53
55	4	-4.38	40	500	500	0	0	5.6	+0.40	6.49 x 10 ⁻⁴	Repeat of run 39
56	--	0.0	4	500	0	0	0	6.7	-0.08	2.84 x 10 ⁻⁴	
57	--	0.0	40	500	0	0	0	6.7	-0.14	2.56 x 10 ⁻³	
58	10	-2.19	40	500	0	500	0	7.5	-0.350	2.32 x 10 ⁻²	Repeat of run 35
59	--	0.0	4	0	500	0	0	5.45	-0.21	1.32 x 10 ⁻³	
60	--								--	--	Not reported
61	--	0.0	40	0	500	0	0	5.45	--	--	Not reported
62	--								-0.24	0.92 x 10 ⁻³	
63	--	0.0	4	0	0	0	10	9.8	-0.10	3.59 x 10 ⁻⁴	
64	--								--	--	Not reported
65	--	0.0	40	0	0	0	10	9.8	-0.22	4.1 x 10 ⁻⁴	
66	--	0.0	40	0	0	0	10	9.8	--	--	Not reported
67	--	-4.38	40	0	0	0	10	9.8	-0.28	1.41 x 10 ⁻³	

^aWhite Kut 210.

END

DATE

3-88

DTIC